

DISSERTATION

ON THE DYNAMICS OF PRECIPITATING STRATOCUMULUS

Submitted by

Bjorn Stevens

Department of Atmospheric Science

In partial fulfillment of the requirements

for the degree of Doctor of Philosophy

Colorado State University

Fort Collins, Colorado

Fall 1996

COLORADO STATE UNIVERSITY


September 9, 1996

WE HEREBY RECOMMEND THAT THE DISSERTATION PREPARED UNDER OUR SUPERVISION BY BJORN STEVENS ENTITLED ON THE DYNAMICS OF PRECIPITATING STRATOCUMULUS BE ACCEPTED AS FULFILLING IN PART REQUIREMENTS FOR THE DEGREE OF DOCTOR OF PHILOSOPHY.

Committee on Graduate Work



Committee Member: Gerhard H. Dangelmayr



Committee Member: Sonia M. Kreidenweis



Committee Member: Chin-Hoh Moeng



Committee Member: David A. Randall



Committee Member: Wayne H. Schubert



Adviser: William R. Cotton



Department Head: Stephen K. Cox

ABSTRACT OF DISSERTATION

ON THE DYNAMICS OF PRECIPITATING STRATOCUMULUS

An explicit representation of the liquid-water-drop size spectrum is coupled to two- and three-dimensional boundary layer models for the purposes of studying the dynamics of precipitating stratocumulus. A number of hypotheses regarding the effect that precipitation has on boundary layer structure are explored.

The use of the three dimensional model to do large-eddy simulation (LES) of the stratocumulus topped boundary layer suggests that the hypothesis that precipitation unambiguously leads to shallower clouds and shallower boundary layers is incorrect. Comparisons of LES with and without drizzle also indicate that the tendency of drizzle to generate internal stratification within the boundary layer need not result in the boundary layer becoming decoupled. Fluxes may actually become stronger, although more intermittent, in response to the moistening and cooling of the sub-cloud layer relative to both the cloud and surface—although precipitation forming in clouds initially un-coupled to the surface may lead to solutions with a different character.

Overall we find that the primary consequence of drizzle resides in its tendency to stabilize the sub-cloud layer with respect to the cloud layer. The dynamical consequences of this are the reduction in the buoyancy flux, smaller values of vertical velocity variance but larger skewness, and a decline in entrainment rates. Consequently, precipitation affects cloud structure indirectly by reducing cloud top entrainment rates. Drizzle also directly modifies cloud structure by partitioning the boundary layer into a cooler-moister sub-cloud layer and a warmer-drier cloud-layer. This leads to reduced values of cloud liquid water relative to what is expected for a well mixed layer. Depending on the nature of

the cloud-top thermodynamic jumps the indirect and direct effects of drizzle on cloud structure, may either cooperate or compete. Changes in boundary layer structure due to precipitation tend to have a forced character which approaches an equilibrium balance between turbulent transport and drizzle on the eddy turn-over time-scale. The simulated boundary layer relaxes back to a state characteristic of non-precipitating boundary layers on a time-scale of a few hours after the cessation of precipitation.

A number of hypotheses are formed and discussed on the basis of two dimensional integrations, one of which is that the more cumulus-like dynamics characteristic of strongly precipitating boundary layers favors up-scale growth in the characteristic horizontal size of convecting elements. Such up-scale growth is not seen in non-precipitating solutions. Also the dynamics of mixed layer models are analyzed and found to predict the wrong sensitivity of surface fluxes to precipitation. A new two layer model is proposed which attempts to correct this short-coming.

Bjorn Stevens
Department of Atmospheric Science
Colorado State University
Fort Collins, Colorado 80523
Fall 1996

ACKNOWLEDGEMENTS

Life tends to be more cooperative than we give it credit for. The work presented herein benefitted greatly from numerous interactions with colleagues, mentors, friends, and family.

My committee members have taught me more than they realize. In particular the contributions from my advisor Bill Cotton, my honorary advisor Chin-Hoh Moeng, and David Randall are hard to overstate. In addition to his intellectual support, Bill Cotton has also been a tremendous source of support, friendship and encouragement over the years and I am forever grateful for the many opportunities he has provided me. Numerous stimulating interactions with Wayne Schubert, and Sonia Kreidenweis have also nurtured my intellectual skills. I thank Gerhard Dangelmayr for agreeing to take on the difficult task of being an outside committee member. Although not on my committee, the advice and encouragement of Dick Johnson, Mike Montgomery, and Bob Walko has been indispensable. Over the years I have worked very closely with Graham Feingold, the fruits of this collaboration are evident throughout this work. In addition the contributions of Brenda Thompson, Abby Hodges, Connie Uliasz and Hongli Jiang have been numerous and vital. Chris Bretherton, Steve Krueger, Peter Duynkerke and other members of the GCSS boundary layer working group are thanked for their many contributions, particularly their help in formulating the case studies. The Tel-Aviv cloud physics group, as well as the Cotton and Pielke modeling group are thanked for providing the foundation upon which this work is built. This work would not have been possible had it not been for the kind sponsorship over the years from the following agencies: Department of Energy (National Institute for Global and Environmental Change through contract number TUL-021-94/95), NSF (contract number ATM-9420045), and NASA (Graduate Fellowship on Global Change Grant NGT-30231).

Thanks to: my office mate Dave Alexander—working with and getting to know him has been a joy; the Cotton group as a whole, (not to mention many members of the Randall, Kreidenweis, Johnson and Schubert groups) interactions with whom have benefitted me in many indescribable ways; Erik, Ligia, Jim, Sheila, Tak, my family, and everyone in Ames Iowa for their ongoing support and camaraderie. Finally I thank Andrea Brose for her many intellectual, physical, and emotional contributions to this work and the Zeitgeist of the period surrounding it.

TABLE OF CONTENTS

1 Introduction	1
1.1 Early studies of stratocumulus	2
1.2 Contemporary studies of stratocumulus	6
1.3 Some outstanding questions	9
2 Approach	11
2.1 The Model	13
2.2 Numerical methods	16
2.3 Previous Results and Critique of Method	17
3 A Case Study	20
3.1 ERM control integrations	21
3.1.1 <i>ERM-BM integration</i>	21
3.1.2 <i>ERM-NM integration</i>	25
3.2 ERM “steady-state” integrations	26
3.3 Large Eddy Simulation	32
3.4 Conceptual Cartoon	39
4 Sensitivity Studies	41
4.1 Preliminary sensitivity studies	43
4.1.1 <i>Sensitivity to grid spacing</i>	45
4.1.2 <i>Sensitivity to domain size</i>	48
4.1.3 <i>Sensitivity to turbulence closure model</i>	49
4.1.4 <i>Sensitivity to kernel</i>	50
4.1.5 <i>Sensitivity to ventilation effects</i>	51
4.1.6 <i>Sensitivity to sounding</i>	51
4.2 Sensitivity to CCN concentrations	51
4.2.1 <i>Time-sequences and snap-shots</i>	52
4.2.2 <i>Mean profiles, fluxes, and budgets</i>	57
4.2.3 <i>Scalar statistics</i>	61
4.3 Subsequent sensitivity studies	64
4.3.1 <i>Sensitivity to domain size</i>	65
4.3.2 <i>Sensitivity to thermodynamic jumps</i>	65
4.4 Attracting states of ERM integrations	68
4.5 Large Eddy Simulation	69
4.5.1 <i>Small mean wind</i>	70
4.5.2 <i>Large mean wind</i>	75
4.6 Summary	76

5	Simple models	79
5.1	Mixed-layer models (MLMs)	79
5.1.1	<i>Basic formulation</i>	80
5.1.2	<i>Entrainment closures</i>	82
5.1.3	<i>Numerical methods and integration specifics</i>	85
5.1.4	<i>Sensitivity of models to specified drizzle</i>	87
5.1.5	<i>Approach to equilibrium</i>	89
5.1.6	<i>Sensitivity of models to parameterized drizzle</i>	91
5.1.7	<i>Comparison to ERM simulations</i>	93
5.2	Two layer models	95
5.2.1	<i>The Turton and Nicholls model</i>	96
5.2.2	<i>A new, simple, two-layer model</i>	98
5.2.3	<i>Integrations of the new, simple, two layer model</i>	104
5.3	Summary	108
6	Conclusions	110
6.1	Previous studies	110
6.1.1	<i>Paluch and Lenschow PL</i>	110
6.1.2	<i>Pincus and Baker</i>	111
6.1.3	<i>Chen and Cotton</i>	113
6.1.4	<i>Albrecht</i>	113
6.1.5	<i>Feingold et al.</i>	114
6.1.6	<i>Austin et al.</i>	114
6.1.7	<i>Wang and Wang</i>	114
6.2	Summary	115
6.3	Limitations, speculation, and future work	118
A	Model Particulars	120
A.1	Continuity Equation	120
A.2	Scalar Budgets & Quasi-Steady states	121
A.3	TKE Budgets	123
A.3.1	<i>Continuous Equations</i>	123
A.3.2	<i>Discrete approximations</i>	125
B	Miscellaneous Derivations	127
B.1	Saturation pressure level	127
B.2	Ventilative enhancement of droplet evaporation	128

LIST OF FIGURES

3.1	Time series of collected statistics from 42 hour Lagrangian I ERM-BM integration.	23
3.2	Time height contour of mean liquid-water contents. (a) ERM-BM integration, (b) Observations. Contours every 0.1 gkg^{-1}	24
3.3	As in Fig. 3.1 but for the integration of the ERM-NM.	25
3.4	As in Fig. 3.1 but for the integration with no time-dependent forcing.	27
3.5	Time evolution of domain averaged q_l as a function of height for integrations with no time-dependent forcing: (a) ERM-BM; (b) ERM-NM. Contours every 0.1 gkg^{-1}	28
3.6	Profiles of various space and time averaged quantities from the fifth hour of the ERM-BM (solid lines) and ERM-NM (dashed) integrations: (a) $\overline{w'w'}$, vertical velocity variance; (b) $\overline{\theta_l}$ (thick lines) and $\overline{\theta_v}$ (thin lines); (c) $\overline{q_T}$ (thick lines), $10 \times \overline{q_l}$ (thin lines).	29
3.7	Time series of various statistics ERM-BM (solid lines) and ERM-NM (dashed) integrations: (a) Sub-cloud $\overline{\theta_l}$ gradient (note if the ordinate is replaced by one with units of gkg^{-1} these lines also well describe the sub-cloud gradient in $\overline{q_T}$). (b) Drizzle flux convergence in sub-cloud layer; (c) Ratio of negative to positive area in buoyancy flux profile.	30
3.8	Profiles of various space and time averaged quantities from the LES-BM (solid lines) and LES-NM (dashed) integrations: (a) vertical velocity variance; (b) θ_l (thick lines) and θ_v (thin lines); (c) q_T (thick lines), $10 \times q_l$ (thin lines).	33
3.9	Profiles of space and time averaged fluxes: (a) Total water flux (turbulent flux of total water in LES-BM denoted by solid line, other fluxes labeled on plot) (b) θ_l fluxes (turbulent fluxes of θ_l given by thick solid line (LES-BM) and thick-dotted line (LES-NM) other fluxes labeled; (c) Radiative fluxes (LES-BM solid, LES-NM dotted).	34
3.10	Vertical velocity of lifting-condensation level, w_{lcl} , in boundary layer due to fluxes of various quantities. (a) Contributions to w_{lcl} from θ_l budget for LES-BM integration. Contributions from: F_Θ (solid); $\overline{w'\theta_l}$ (long-dashed); $-\sum_{k=1}^{25} \overline{(w_t q_l)_k}$ (short dashed); F_{rad} (dotted). (b) Contributions to w_{lcl} from r_T budget in LES-BM integration. Contributions from: F_Q (solid); $\overline{w'q_T}$ (long-dashed); $\sum_{k=1}^{25} \overline{(w_t q_l)_k}$ (short dashed). (c) Total values of w_{lcl} for LES-BM integration (thick line), and LES-NM (thin-line).	37
3.11	Profiles of various terms in TKE budget. Shear production (solid), dissipation (dotted), buoyancy production (long dash), transport (short dash). (a) LES-BM, (b) LES-NM	38
3.12	Conceptual cartoon of the structure of a precipitating stratocumulus topped boundary layer.	40

4.1	Scalar time sequences from experiments CCN20 (solid), CCN150(long dash) and CCN750 (short dash). (a) Cloud top height (km); (b) maximum value of $(\overline{w'w'})^{1/2}$ (ms^{-1}); (c) Domain averaged LWP g m^{-2} ; (d) Surface latent heat flux (Wm^{-2}); Surface sensible heat flux (Wm^{-2}); (e) Surface drizzle flux (Wm^{-2}).	53
4.2	Snapshots of flow structure from experiment CCN20 at 14 hours. Upper panel: liquid water mixing ratio (gkg^{-1}) shaded and from 0.02 to 1.02 in 0.1 gkg^{-1} increments. w contoured from -1 to 1 ms^{-1} in ten increments, thick line is zero contour. Lower panel: θ_l shaded from 287-292 K in 0.5 K increments and total-water mixing ratio contoured from 7-11 (gkg^{-1}) in ten increments with thick line denoting the 9 gkg^{-1} contour. Spatial dimensions normalized by inversion height: $Z_I = 615$ m.	55
4.3	As in previous figure but for experiment CCN750; $Z_I = 894$ m.	56
4.4	Comparison of various mean quantities for experiments CCN20 (solid line), CCN150 (long dash) and CCN750 (short dash): (a) $\overline{w'w'}$; (b) θ_l (thick lines) and θ_v (thin lines); (c) $q_l \times 10$ (thick lines) and q_t (thin lines).	57
4.5	Comparison of various fluxes for experiments CCN20 (solid line), CCN150 (long dash) and CCN750 (short dash): (a) F_Q (thick lines), drizzle flux (thin lines); (b) F_Θ (thick lines) and $\overline{w'\theta'_l}$ (thin lines); (c) Radiative flux minus radiative flux at ground.	58
4.6	Comparison of various TKE budgets for experiments CCN20 (a); CCN150 (b); and CCN750 (c). Shear production term (solid line), Buoyancy production (long dash), transport (short dash), dissipation (dotted), accumulation (dash-dot), residual (dash-dot-dot). Units are $\text{cm}^2 \text{s}^{-3}$	60
4.7	Liquid-water mixing-ratio [gkg^{-1}] (shaded and from 0.02 to 1.02 in 0.1 gkg^{-1}) from experiment CCN20-Big Domain at two times. Upper panel: Snapshot at 2 hours. Lower panel: Snapshot at 15 hours.	66
4.8	Time-sequence data (a)-(f) and layer means averaged over third hour (g)-(i). LES-NM (dotted), LES-BM (solid). Dashed line shows an LES-NM integration for which the radiative cooling was allowed to happen over a deeper layer. (a) z_i (m); (b) z_b (m); (c) LWP (gm^{-2}); (d) $(\int \overline{w'w'})^{1/2}$ ms^{-1} ; (e) Drizzle flux (Wm^{-2});(f) Sensible heat flux (Wm^{-2}); (g) $\overline{w'w'}$; (h) θ_l (thick), θ_v (thin); (i) q_t (thick), $10q_l$ (thin).	71
4.9	Heat and moisture fluxes averaged over third hour (a) LES-NM, F_Q (long-dash), $(\overline{w'q'_t})_{total}$ (solid), $(\overline{w'q'_t})_{sgrid}$ (dotted); (b) LES-NM, F_Θ (dash-dot-dot), $(\overline{w'\theta'_l})_{total}$ (solid), $(\overline{w'\theta'_l})_{sgrid}$ (dotted). (c) Same as (a) but for LES-BM, also plotted is drizzle flux (dash-dot-dot); (d) same as (b) but for LES-BM. (e) Vertical velocity skewness for LES-NM (solid), LES-BM (dashed).	72
4.10	TKE budgets LES-NM (a); LES-BM (b). Shear term (solid), buoyancy (long-dash), transport (short-dash), dissipation (dotted).	74
4.11	Time-sequence data as in Fig. 4.8 except for simulations with strong mean wind and here the dashed line shows an LES-NM integration spawned from the 90 minute mark of the LES-BM.	75
5.1	Diagram of mixed layer model.	81

5.2	Steady states of mixed-layer model with GCSS-3 sounding (upper panels) and Oakland sounding (lower panels). Results plotted for $F_{rad} = 75 \text{ Wm}^{-2}$ as a function of specified value of \mathcal{F}_{drz} . Note that 24 Wm^{-2} of drizzle is approximately 0.8 mm day^{-1} . First column is for $(\mathcal{F}_{sv})_{min}$ closure with $k = 0.2$, second is for the Δ_m closure, third column uses e_2 closure with $\Lambda = 0.5$. Plotted are cloud top (solid lines), cloud base (dotted lines), and LWP in gm^{-2} (dashed lines).	88
5.3	Drizzle production and LWP from steady state solutions of mixed layer models with different closures: (a) $(\mathcal{F}_{sv})_{min}$ closure; (b) Δ_m closure; (c) e_2 closure. Oakland sounding with $n = 3$ (thick solid line); GCSS-3 sounding with $n = 0$ (solid line); GCSS-3 sounding with $n = 1$ (long-dashed line); GCSS-3 sounding with $n = 2$ (short-dashed line); GCSS-3 sounding with $n = 3$ (dotted line); GCSS-3 sounding with $n = 3$ and sub-cloud evaporation (dash-dot line).	92
5.4	Time-sequence of cloud properties and surface fluxes for MLMs and ERM integrations. Four panels are plotted. Each panel contains four plots from left to right these are: MLM with $(\mathcal{F}_{sv})_{min}$ closure; MLM with Δ_m closure, MLM with e_2 closure; ERM integration. No drizzle (upper), drizzle (lower) panel. Left panels plot cloud top (solid line), cloud base (dotted line), LWP (dash dot line). For ERM integrations the second (lower) dotted line refers to the cloud base associated with the mean boundary layer properties. Right panels: Latent heat flux (solid line), sensible heat flux (dotted line), drizzle flux (dash-dot line).	94
5.5	Diagram of two layer model.	99
5.6	72 hour two layer model integration. GCSS sounding, columns (a)-(c) no drizzle, columns (d)-(f) with drizzle. (a) and (d) are one-layer model. For the two layer mode columns (b) and (e) have $e_* = 0.2$, while columns (c) and (f) have $e_* = 0.5$. First row: $\Delta\theta_v(z_3)$ solid line; A_n/A_p dotted line; e_2 dash-dot line. Second row, fluxes in Wm^{-2} : $\mathcal{F}_\theta(0^+)$ solid; $\mathcal{F}_{qt}(0^+)$ dotted; $-\mathcal{D}(z_3)$ dash-dot; $-\mathcal{D}(0^+)$ dash-dot-dot. Third row: z_i solid; z_c dotted; z_3 dash-dot. In decoupled layers the equivalent mixed layer cloud depth is also plotted with dash-dot-dot lines	105
5.7	Same as previous figure except $C_m = 0.5C_t$	106

LIST OF TABLES

3.1	Model configuration for ERM integrations.	22
4.1	Sensitivity of selected statistics to different initial random perturbations	43
4.2	Sensitivity of selected statistics to different initial random perturbations in non-drizzling ERM-NM model at two resolutions (regular and half resolution). Given are the mean values and standard deviations from three realizations of the flow.	44
4.3	Normalized statistics from sensitivity runs	45
4.4	Sensitivity of selected statistics to different initial random perturbations, and choice of kernel. Mean values over last ten hours of a fifteen hour integration. Symbols as in previous tables except for dZ_i/dt which is the rate at which the 292 K θ_l surface moves in mms^{-1}	52
4.5	Sensitivity of selected statistics to different CCN concentrations. Tabulated data is the time average of the instantaneous domain averages collected every 30 seconds over last ten hours of a fifteen hour integration. Included are: vertically integrated liquid water \mathcal{L} in gm^{-2} ; \mathcal{P}_{smi} pressure (in hPa) for which parcels containing the mean mixed-layer thermodynamic properties become saturated; the height of the $\theta_l = 292$ K surface; dZ_i/dt , rate of change in inversion height in mms^{-1} ; w_2 , square-root of mean variance; $\Delta\theta_l$ difference in θ_l between cloud layer and value at 37.5 m; \mathcal{D}_{srf} , drizzle flux at surface in Wm^{-2} ; \mathcal{D}_{max} , maximum drizzle flux at any level; LHF the surface latent heat flux in Wm^{-2} ; SHF the surface sensible heat flux in Wm^{-2} . * indicates use of 4329 random seed, † indicates use of 11111 random seed, all other experiments use random seed of unity. CCN = ∞ implies the use of the ERM-NM	62
4.6	Sensitivity of selected statistics to a larger domain size and different free atmospheric properties. Tabulated data is of the same type as in previous table. Experiment “Big Domain” is the same as the 20 per mg experiment of the previous section, but with the horizontal domain size increased from 64 (3km) points to 194 (9.7km) points. Experiments D50 and WD50 are both experiments with the 50 CCN per mg, the former differs from experiment CCN50 in that the free troposphere is dried 2 gkg^{-1} , the latter also has the free troposphere warmed 2K.	65
5.1	Basic state configuration used in mixed-layer model integrations. Units are as follows h [kJ kg^{-1}], z [km], q_t [gkg^{-1}], T [K], p_{00} [hPa], D [10^{-6} s^{-1}], v_2 [ms^{-1}]	87

Chapter 1

INTRODUCTION

In one way or another our lack of understanding of stratocumulus has manifested itself as a forecasting problem—namely how to forecast when they will form and when they will dissipate. Through the middle part of this century study of the forecast problem was motivated by a burgeoning aircraft industry. More recent motivations include the recognition that stratocumulus play an important role in determining the nature of the earth's energy balance. Notwithstanding the changing motivations for good stratocumulus forecasts, the need to accurately predict their evolution in terms of a minimum set of variables remains with us.

Many introductions to stratocumulus begin with Lilly's (1968) paper on cloud-topped mixed layers. This seminal paper is an appropriate beginning for many reasons. Nonetheless, more was known about stratocumulus prior to Lilly's paper than most people realize. For instance, Dean Blake (an early pioneer in stratocumulus research), recognized Alexander McAdie's 1903 climatology of California as an early attempt to provide a rational explanation for the formation of California stratus (American Meteorological Society, 1952). Given the current interest in processes that regulate global albedo it is fitting that one of the earliest measurements made of stratocumulus was of its albedo (Aldrich, 1919). In the 1920s and 1930s a flurry of stratocumulus studies, many with in-situ observations, was brought on by the growth of aviation. In §1 below I sketch an outline through some of these studies, focusing on their discussion of the role of many physical processes whose details today's atmospheric scientists are still attempting to unravel.

If Lilly's paper didn't mark the beginning of stratocumulus research, it at least marked the beginning of a new era. While the early era documented many features of stratocumulus clouds and raised many questions, observational and theoretical techniques proved

incapable of providing satisfactory answers. Lilly's mixed layer model was the first, and perhaps simplest, of a hierarchy of models that continue to be used in an attempt to understand the physics of marine stratocumulus. Use of such models as well as the significant sophistication in observational techniques has allowed us to gradually begin to understand the role of different processes in boundary layer evolution. In §2 below we review a subset of the studies that have been conducted over the years. No attempt is made to be exhaustive in our review; rather, we intend only to illustrate the direction of the progression of our understanding, and how it has led to the questions to be addressed in this dissertation. In addition to outlining the remainder of this study §3 raises the questions which we address in subsequent chapters.

1.1 Early studies of stratocumulus

Although stratocumulus clouds exist in a variety of conditions, for the purposes of this study, we concern ourselves primarily with those that favor eastern edges of subtropical highs. These regions are characterized by the contrast between large-scale oceanic and atmospheric divergence. The former generates cold up-welling while the latter results in large scale subsidence; thus warm dry air is brought down to meet the cool moist surface. The "marked inversion" that forms, and separates air with surface-like properties from air with free-atmospheric properties, is an essential ingredient in stratocumulus formation (Blake, 1928). Early observations of stratocumulus revealed pronounced anti-diurnal cycles in inversion height and cloudiness, both of which were negatively correlated with solar insolation; the distinct dryness of the free tropospheric air was also recognized (Blake, 1933; Blake, 1934). The source of this above inversion air remained controversial for some time, although Reeds¹ idea that it was associated with the subsident air in the downward branch of the Hadley cell is now widely accepted. Anderson (1931) suggested that stratocumulus form under the influence of surface fluxes from an ocean that progressively cools as the shoreline is approached. His observations also invalidated the idea that stratocumulus

¹T.R. Reed was credited with scribbling this idea in a margin note while reviewing Blake's (1934) manuscript.

are a purely coastal phenomena. Using more sophisticated data sets and comprehensive global analyses Klein and Hartmann (1993) have put the basic idea that stratocumulus are a cloud type that lives off the thermodynamic contrast between cold ocean up-welling and warm atmospheric down-welling on a firm quantitative footing.

Neiburger (1944) proposed a theory for the formation and dissipation of coastal stratocumulus that incorporated the observed correlation between cloudiness and inversion height and the anti-correlation between the inversion height and solar insolation. He postulated that the latter was caused by the alternate compression and expansion of boundary layer columns through sea-breeze circulations, and that by predicting the evolution of the inversion, stratocumulus forecasts could be improved. In the same study the importance of cloud-top radiational cooling for driving turbulent circulations from pre-existent stratocumulus decks was recognized. Neiburger also argued that an earlier idea, whereby the observed top-down building of stratus decks was attributed to radiative cooling of the moist (but unsaturated) stratum (Bowie, 1933; Blake, 1934), was wrong because its justification for neglecting the contribution to the down-welling radiative flux from the very warm and very dry air above the strong temperature inversion was not justified. In other words, the added emission from the warmth of the air was sufficient to offset the expected lack of emission given the dryness of air.

Searching for an empirical method of forecasting North-Sea stratocumulus James (1955) compiled and studied aircraft data in an attempt to correlate the breakup of stratocumulus with the lapse rates in temperature and moisture above and below the cloud layers. His conclusion that "turbulent mixing of the cloud with the dry air above seemed to be significant in the subsequent behavior of the cloud," foreshadowed a great deal of research over the past 15 years on the role of turbulent entrainment and the jumps in thermodynamic variables across cloud top. James (1959) also noted the common occurrence of cumulus within and underlying stratus. Such a situation was noted by Mason (1952) in addition to others (Anderson, 1931; Jones, 1951), and has come to represent a critical component of current conceptual models describing the transition from the stratocumulus-topped to the cumulus-topped trade-

wind boundary layer (Bretherton, 1992; Krueger et al., 1995a; Krueger et al., 1995b; Wyant et al., 1996).

The idea that Lilly exploited, whereby stratocumulus are thought to cap mixed-layers coupled directly to the surface, was called into question by aircraft observations (Nicholls et al., 1983; Nicholls, 1984). Nicholl's observations (1984) showed daytime stratus to be separated from the surface by a distinct stable layer. The idea that the evolution in boundary-layer vertical structure is important to stratocumulus cloud fraction is, however, well illustrated much earlier. Apart from the above mentioned interaction between cumulus and stratus, Vernon (1936) showed that the diurnal evolution of ceiling height per degree dew-point depression (a measure of how well mixed the boundary layer is) undergoes a marked diurnal cycle that leads the diurnal cycle in cloudiness. The boundary layer tends to be least well mixed around local noon, several hours before the minimum in cloud coverage. This observation is consistent with James' (1955) conclusion that the sub-cloud hydro-lapse is a statistically significant indicator of subsequent stratocumulus breakup.

Neiburger (1949) used a blimp to make solar radiation measurements above and below cloud for comparison with theoretical calculations. His study indicated that (i) cloud albedo varies significantly with cloud depth [thus confirming Luckiesh's (1919) observations], and (ii) variations of albedo measured at a given depth tend to be greater for thinner clouds. The first point suggests that stratus albedos are susceptible to processes that deepen the cloud, an idea exploited in a recent hypothesis (Pincus and Baker, 1994) whereby enhanced drizzle production reduces cloud liquid water thus diminishing cloud albedo. Neiburger attributes the second point to the greater sensitivity of thin clouds to details of the distribution of liquid water; as he recognized the process whereby increased drop number concentrations leads to increased short-wave albedos in thin clouds. Twomey's (1974, 1977) subsequent studies of this process illustrated that significant climatic effects could result from systematic changes in cloud albedo due to forced changes in condensation nuclei climatology. This effect has motivated much interest in stratocumulus clouds over the past two decades.

The liquid-water content and droplet-spectral characteristics of stratocumulus were first investigated by Diem in the early 1940s, and subsequently by Frith (1951). Neiburger (1949) also measured the microphysical properties of warm-weather stratocumulus; as he documented a near adiabatic rise in cloud-liquid-water content, and the strong modality in the drop-diameter spectrum near 15 μm . His measurements also suggested that drop concentrations increased with height in the cloud, although such a result is now seen as the exception to the rule whereby most drop activation is at cloud base and droplet concentrations remain constant with height (Noonkester, 1984; Nicholls, 1984; Stevens et al., 1996).

Drizzle production is intimately connected to the microphysical structure of stratocumulus. Its effect on the evolution of boundary layer structure, and the processes that regulate it constitute a primary focus of this study. A discussion of drizzle is largely absent in the early works on stratocumulus. A systematic evaluation of drizzle production doesn't appear to exist prior to Mason and Howarth's (1952) study which found that drizzle formation was more likely as stratocumulus depth increased. Bowen's (1952) study of warm rain formation yields similar conclusions. Subsequent studies (Mason, 1952; Mason, 1960; Feingold et al., 1996a) suggest that in addition to cloud depth, turbulence is important for drizzle production in stratocumulus. In addition Kraus and Lee² (1963) identified a distinct diurnal cycle in stratocumulus precipitation that is related to the reduction in cloud-liquid-water contents due to the in-cloud absorption of solar radiation.

In summary we note that prior to 1968 most of the physical processes currently thought to play a role in the evolution of stratocumulus had been identified and studied. These processes being (1) the role of the cold underlying ocean and surface fluxes of moisture and temperature therefrom; (2) the role of subsidence and a strong capping inversion; (3) short and long-wave radiative interactions with the cloud layer; (4) the role of vertical structure and the deepening of the boundary layer; (5) drizzle formation within

²Actually Kraus is listed as the sole author, but since he acknowledges Ms. Lee for doing most of the calculations and typing the manuscript I took the liberty of elevating her to second author status!

stratocumulus; (6) interactions with the overlying air; (7) turbulence and its interaction with microphysics. Below we briefly review how a hierarchy of models has been subsequently used to develop our understanding of, and raise additional questions about, these processes.

1.2 Contemporary studies of stratocumulus

Mixed-layer models such as Lilly's forgo a consideration of the detailed boundary layer structure and assume that turbulence is at all times sufficient to maintain a well-mixed state, one for which the potential energy of the boundary layer is maximized. The simplicity that results from this assumption allows one to clearly understand the relationships between a variety of processes and bulk boundary-layer quantities such as cloud depth and boundary layer height. From a study of the steady states produced by these models a great deal can be learned (or conjectured) about how different processes affect the equilibrium boundary layer structure. For instance, by studying the relationship between large-scale forcing (e.g., sea-surface temperatures and large-scale divergence) it has been argued that equilibrium boundary layers deepen strongly, with little change in cloud base height, as divergence decreases; in other words, they appear to seek a particular rate of subsidence for a given radiative forcing (Schubert, 1976; Schubert et al., 1979). A more realistic treatment of radiation within the cloudy layer suggests that in regions of weak divergence the boundary layer has two stable equilibria, one cloud and one clear, and one unstable equilibrium; moreover, there may exist a pronounced hysteresis as the boundary layer is forced from one attracting basin to the next (Randall and Suarez, 1984). More recently, Bretherton and Wyant (1996) compared mixed-layer-model computations to two-dimensional eddy-resolving simulations and noted that for a reasonable entrainment closure in the former, the ratio of the negative sub-cloud buoyancy flux to the positive in-cloud flux can serve as an indicator of decoupling. Unfortunately in mixed-layer models one's choice of entrainment closure determines the form of the buoyancy flux (Kraus and Schaller, 1978). Consequently, apart from the fact that well-mixed layers are an idealization infrequently realized by nature, the documented sensitivity of mixed-layer

models to the details of the entrainment closure leaves many questions open to further investigation.

In an attempt to represent more degrees of freedom of the physical system, more complicated models of the stratocumulus topped boundary layer have also been formulated. Two-layer models relax the mixed layer assumption (Albrecht et al., 1979; Nicholls, 1987; Wang, 1993), although (like mixed-layer models) they remain sensitive to poorly justified closure assumptions (Bretherton, 1993). Higher-order turbulent-closure models attempt to represent moments of the turbulence budget over a one- or two-dimensional mesh. Using third-order closure on a one-dimensional mesh Bougeault (1985) investigated the influence of the diurnal cycle and large scale forcing on stratocumulus dynamics. His model found well-mixed steady-states associated with both phases of the diurnal cycle, although the transition between attracting basins was characterized by a period of decoupling and intermittent cumulus convection. Chen and Cotton (1987) used a second-order-closure model to study the sensitivity of the observations of Brost et al., (1982a, 1982b) to shear, solar radiation, large-scale divergence and drizzle production. Moeng and Arakawa (1980) and Krueger (1985) used third-order closure on a two dimensional grid with the idea of resolving the energetic elements of the boundary layer circulation and parameterizing others. On the basis of such an approach it has been hypothesized that the observed transition between sub-tropical stratocumulus and trade-wind cumulus is due to the progressive rise in sea-surface temperatures (Krueger et al., 1995a; Krueger et al., 1995b).

Moeng (1986) began systematically using the Large Eddy Simulation (LES) technique developed by Deardorff (1970, 1980b) to understand the nature of the turbulence budgets in nocturnal stratocumulus. Indeed, the previous studies using higher-order-closure models raised many questions about the nature of various closure assumptions, questions well suited to investigation by LES. The LES technique has gained wide favor for practical as well as theoretical reasons (Mason, 1994). In the case of the former it has been shown to be relatively insensitive to its closure assumptions. In the case of the latter its appeal derives from the fact that as one takes the limit of the equation set as the grid spacing goes to zero

one arrives at the Navier-Stokes equations. Thus this technique straddles the void between direct numerical integrations of the governing equations and low-dimensional models of the boundary layer dynamics. Its chief limitation is that it is computationally intensive and thus is limited to short time-scale and small spatial-scale studies. Furthermore, in simulations with strong capping inversions current computational resources may prove to be insufficient to provide enough degrees of freedom to properly represent the processes near the entraining interface.

In some respects observations of stratocumulus have progressed substantially since the seminal studies of 15 years ago (Roach et al., 1982; Caughey et al., 1982; Slingo et al., 1982; Brost et al., 1982a; Brost et al., 1982b) as an evaluation of turbulent budgets is now almost routine. It remains challenging however to accurately measure large-scale divergence or the thermodynamic and microphysical quantities in clouds, thus making it difficult for present observations to adequately constrain the models. Nevertheless observations such as those made during FIRE [First ISCCP (International Satellite Cloud Climatology Project) Regional Experiment] or ASTEX (the Atlantic Stratocumulus Transition Experiment) have made a number of points clear [see (Randall et al., 1996) for a review]: (1) considerable boundary layer structure is a ubiquitous feature of the observations, although, it remains unclear to what extent such structure is important for the boundary layers dynamical evolution. (2) Significant drizzle is common, although again its role in regulating boundary layer structure is unclear. (3) Diurnal cycles in boundary layer cloudiness are marked. (4) Cloud-top entrainment instability (Kraus, 1963; Lilly, 1968; Randall, 1980; Deardorff, 1980a) is not a ubiquitous regulator of marine boundary layer clouds.

The suggestion that drizzle may impact boundary layer dynamics (Brost et al., 1982b) has helped motivate a number of studies of drizzle in stratocumulus topped boundary layer. Nicholls (1984) measured drizzle fluxes of order 1 mm day^{-1} 200 m below the base of stratocumulus that were 450 m deep with near adiabatic liquid water mixing ratios and with droplet concentrations approaching 200 cm^{-3} . In attempting to model these observations Nicholls (1987) found that drizzle production exhibited a significant sensitivity to cloud

liquid-water path³ and suggested “that this process may be an important constraint on the liquid water content of thick cloud layers.” In contrast, observations of clouds during FIRE (Austin et al., 1995) showed little correlation between drizzle rates and cloud depth; thus suggesting that other factors (e.g., entrainment, condensation nuclei characteristics, turbulence levels) are important in regulating drizzle production from stratocumulus. Paluch and Lenschow (1991) went so far as to incorporate drizzle as an integral part of their conceptual model of boundary layer cloud evolution, as they argued that its conditioning of the sub-cloud layer promoted the development of a conditionally unstable layer that favored cumulus convection. Suggesting a role for drizzle of commensurate importance Pincus and Baker (1994) hypothesize that the equilibria of stratocumulus have a marked sensitivity to drizzle efficiency⁴. A point I shall address in more detail below.

1.3 Some outstanding questions

As suggested by the above overview there are a large number of outstanding questions regarding the evolution and equilibria of stratocumulus boundary layers. Here we concern ourselves with only two. First, how does the structure of stratocumulus topped boundary layers depend on drizzle? Second, what processes regulate drizzle production in stratocumulus layers? In addition to the suggestion that drizzle may limit cloud liquid water (Nicholls, 1987), and the conceptual model of Paluch and Lenschow (1991), an appropriate starting point for considering these questions is the hypothesis of Pincus and Baker (1994).

Pincus and Baker present steady-state solutions from a mixed-layer model in support of their hypothesis, which more or less states that drizzling stratocumulus entrain less yet dry the boundary layer more so that the lifting-condensation level is marginally higher

³The term liquid-water path (LWP) is used to describe the vertically integrated liquid water, it has units of mass per area.

⁴Actually Wang and Albrecht (1986) included drizzle in a mixed-layer model and discussed this effect extensively although they did not specifically frame the question (of how drizzle impacts boundary layer properties) in terms of climate.

and the cloud top is significantly lower for increased drizzle efficiency. This result depends on the drying from the drizzle flux being greater than the drying from the additional entrainment flux in the absence of drizzle, and (at first glance) would appear to depend on the thermodynamic characteristics of the overlying air. In their formulation the details of drizzle formation and its interaction with the turbulence was neglected through the assumption that the boundary layer is at all times well mixed. The constraints this assumption places on the evolution of the layer needs to be evaluated.

In order to address the questions we have posed we analyze a number of simulations from a numerical model designed to represent the detailed interactions between turbulence, radiation and microphysics in the stratocumulus topped boundary layer. A description of the model and a further discussion of our approach is given in Chapter 2. In Chapter 3 we focus on how drizzle impacted a specific case study, namely the first Lagrangian of the Atlantic Stratocumulus Experiment (ASTEX). Through a number of numerical simulations we evaluate both the ability of the model to accurately simulate an observed case and the role of drizzle in producing the observed boundary layer evolution. In Chapter 4 we step back and conduct a number of sensitivity studies designed to elucidate mechanisms for drizzle formation and the impact of drizzle on boundary layer structure. This chapter most specifically addresses the Pincus and Baker (1994) hypothesis, as well as the questions posed above. In Chapter 5 we evaluate the ability of a number of theoretical models to capture important elements of the dynamics of precipitating stratocumulus topped boundary layers. We summarize our work in Chapter 6.

Chapter 2

APPROACH

Actually being able to write down a mathematical description of a physical system represents a considerable achievement in understanding. Nevertheless, being able to describe the system in terms of a set of partial differential equations is not necessarily an appealing place to stop one's investigation; the character of the solutions to the governing equations under a variety of different situations is often of great interest. It is commonly observed that a system with a large number of degrees of freedom organizes itself in a way that suggests a reasonable description in terms of only a few degrees of freedom. One goal of the atmospheric scientist may thus be construed as attempting to uncover the lowest order representation of a physical system that reasonably captures its behavior. One may think of this as an attempt to mathematically characterize an assumed low-dimensional manifold of the high-dimensional system. Sometimes, this simplification constitutes what we call understanding. How can we achieve this? While there is no best answer, a number of strategies have been, and continue to be employed.

For instance, if the system of interest is observable (which is true in principle—although difficult in practice—for the atmosphere) one could simply sit down and watch it for a long time. Eventually a data base could be built which illustrates the behavior of the system over a reasonable range of parameter space. With some effort a theory could be derived that attempts to describe important elements of the system in terms of a minimal set of observable parameters. Good examples of this strategy abound. A particularly appealing one is Woodcock's observations of seagulls from which he deduced the parameter regime for which boundary-layer rolls are favored (Riehl, 1954). Unfortunately, direct observations are limited by the fact that the system is often difficult to interrogate and

control, thus making it challenging to isolate the impact and behavior of specific physical processes.

As a complementary approach, consider that given a system of partial differential equations, one can transform these into an infinite system of ordinary differential equations. Because the physically relevant degrees of freedom are thought to be finite this system may, in principle, be integrated numerically. These integrations, or simulations, can then be explored for low-dimensional structure. Often however, the degrees of freedom in the physical system are so numerous that they can not all be accounted for—even if one uses the most powerful computers. For instance, by equating the number of grid points necessary to perform a direct numerical simulation of the dry convective boundary layer (CBL) with the degrees of freedom of the system we find that CBL simulations require $O(10^{18})$ degrees of freedom. In contrast, state of the art computers are only able to represent $O(10^9)$, so even by monopolizing the resources of the most powerful computers one remains well short of a true simulation of even a relatively simple meteorological flow. Consequently, while numerical experiments have the advantage of being easy to control and interrogate, the integrations are invariably of prematurely truncated systems of equations, where the premature truncation [at say $O(10^9)$ compared to $O(10^{18})$ degrees of freedom] invariably compromises the physics. So *even if* we were able, with perfect confidence, to exactly characterize a system through a set of mathematical relations, limited computational power necessitates the continued use of complementary observations.

In order to address the questions identified in the introduction we use the second approach. Specifically we analyze data generated by a collection of Eddy Resolving Model (ERM) integrations and Large Eddy Simulations (LES) for low-dimensional structure. The ERM is just the LES code integrated over two spatial dimensions under the assumption of slab symmetry. The reason for using the two-dimensional version of the code is purely practical. LES is extremely expensive, particularly when fifty plus scalars are added to the set of prognostic variables in order to accurately predict the evolution of the liquid water. The use of the ERM to represent an inherently three-dimensional process (i.e., boundary layer turbulence) is questionable, especially because many of the prior results

upon which the credibility of LES is built cannot necessarily be extended to the ERM. It has, however, been our observation that for buoyancy-driven flows the ERM produces results which at least qualitatively agree with LES (Moeng et al., 1996). Nevertheless, we recognize the limitation of the ERM (Cotton et al., 1995) and attempt to correct for this by using LES to evaluate (when computationally feasible) every hypothesis formed on the basis of ERM results.

The remainder of the chapter is organized as follows. In §1 the model is described. In §2 details of the discretization are discussed. Section 3 reviews results from past experiments with the model.

2.1 The Model

The model is derived from a coupling of the Regional Atmospheric Modeling System (Pielke et al., 1992) with the bin-resolving microphysical framework described by the Tel-Aviv University group (Tvivion et al., 1987; Tvivion et al., 1989). Because a detailed description of the coupled code (including new additions and resultant modifications) is provided elsewhere (Stevens et al., 1996), it is only briefly summarized here. A few options/changes have been added since our previous study and these are emphasized in our subsequent description.

The model attempts to integrate the pseudo-compressible equations of motion (Durran, 1989). In so doing it solves predictive equations for velocity, u_i , liquid-water potential temperature, θ_l total-water mixing ratio, q_t , and an arbitrary number of scalars. For practical reasons a prognostic equation for the perturbation Exner function is also solved, although the nature of this equation is that it rapidly forces the velocity field to satisfy the continuity relation for the pseudo-compressible system (see Appendix A). Resolved variables are defined by a filtering operation which is implicitly given by the sub-grid scheme, for which we use Lilly's (1962) modification to Smagorinsky's model. In earlier studies we used a lengthscale in the sub-grid scheme given by

$$l = c_s \Delta x$$

where c_s is a constant of order $\frac{1}{5}$ derived from inertial range theory. This has been modified to obtain a better match with similarity theory in the surface layer by using the modified form:

$$l^2 = \frac{(c_s \Delta x)^2}{1 + \left(\frac{\varepsilon_s \Delta x}{kz}\right)^2}$$

where k is von Karman's constant, and z is the height above the surface. As z becomes large relative to Δx (i.e., we move away from the surface) the two definitions give commensurate values.

Large-scale pressure gradients are assumed to be geostrophic, where a constant in time but possibly height-varying pressure gradient is specified. In the horizontal, boundary conditions are doubly periodic. The model top is a rigid lid—with a Rayleigh friction layer to prevent gravity-wave reflection from the upper boundary. The lower surface is a material surface across which fluxes of heat moisture and momentum are solved following Louis (1979). The roughness length of the sea surface is allowed to vary with wind speed (Charnock, 1955).

The model is formulated in a manner that allows it to use a variety of microphysical representations. The simplest is that used by most previous LES of stratocumulus (Deardorff, 1980b; Moeng, 1986). Here the effect of microphysical processes is considered implicitly by assuming that the phase relaxation time for water condensation vanishes; all the water in excess of the saturation mixing ratio is assumed to exist in the liquid phase with zero settling velocity. This approach allows one to diagnose the amount of liquid water by iteratively solving for the value of θ and q_l consistent with the predicted values of π , θ_l and q_t . The use of this specific representation of the microphysics in conjunction with a dynamical model will be indicated through the appendage NM to the model acronym, i.e., ERM-NM indicates the use of the eddy resolving model with no explicit microphysics.

A more detailed representation of the microphysics is also allowed. The use of this representation of the microphysics in conjunction with a dynamical model will be indicated through the appendage BM to the model acronym, i.e., ERM-BM indicates the use of the eddy resolving model with bin microphysics. For this microphysical model the evolution of the drop spectra is resolved by discretizing the size distribution of liquid water over a

fixed grid in mass space. The discretization is defined by the sequence of 25 mass intervals $\{(x_k, x_{k+1})\}_{k=1}^{25}$ (where $x_1 = 16^{-12}g$, and $x_{k+1} = 2x_k$) that spans the diameter interval $D[\mu m] = (3.125, 1008)$. This formulation requires the prediction of a set of 50 additional variables, $\{N_k, M_k\}_{k=1}^{25}$ describing the mass and number-mixing ratio of cloud drops within the k th grid interval.

This detailed or bin-microphysical representation requires that equations for droplet activation, condensational/evaporational growth, collision-coalescence and sedimentation all be explicitly solved. Because stratocumulus are not expected to produce drops of sizes for which breakup is important, this process is neglected. The evolution of the supersaturation over the course of a time-step, and the prediction of the number of newly activated drops is described in Stevens et al. (1996). Activation is based on the assumption of a time-invariant distribution of aerosol characterized by a log-normal distribution whose parameters correspond to the accumulation mode measured by Shettle and Fenn (1979). Condensation and evaporation are also solved according to methods developed in Stevens et al. (1996). Droplet sedimentation is solved using upstream advection with the terminal velocities of Gunn and Kinzer (1949). Collision-Coalescence is calculated using solutions to the quasi-stochastic equations as described in Tsvivion et al., (1987).

Radiation is treated a number of different ways. Three dimensional simulations presented in Chapter 3 use a long-wave parameterization based on the bulk emissivity method described in Chen and Cotton (1987). ERM simulations in Chapter 3 use a two-stream method recently developed by Harrington (personal communication), this method is slower but much more accurate—particularly in the short-wave where the other scheme is unacceptably inaccurate. When the two-stream scheme is used heating rates are calculated along every other column and interpolated to intervening columns. Such an approach is consistent with the fact that heating rates are rarely recalculated at every time-step. For the simulations in Chapter 4 a very simple parameterization is used. This parameterization accounts only for the radiative effects of liquid water and is discussed in more detail in Chapter 4.

2.2 Numerical methods

Various time-marching schemes are used in the model, however all explicit time-marching schemes—apart from the one used to solve for acoustic terms in the Exner function equation—use the same time discretization. Radiation calculations are generally done less frequently, although heating/cooling rates are applied at each time-step. In the momentum equations leap-frog time differencing is used for the advective terms, while sound-wave terms along with the pressure equation are time-split and integrated on a short time-step using a semi-implicit scheme in the vertical. Alternately, a diagnostic pressure solver routine has been written for the model, in which case pressure is solved by inverting the Poisson equation using Fourier transforms (consistent with the finite difference operators) in the horizontal and a line inversion in the vertical. Solutions using this more precise method, agree well with solutions for which pressure is prognosticated. So unless otherwise noted, pressure is prognosticated throughout. Diffusion terms are integrated implicitly in the vertical and explicitly in the horizontal. Forward time-differencing is used for the scalar transport equations, which facilitates the use of non-linear flux correctors in the representation of scalar advection.

Variables are defined on the Arakawa C grid for which grid stretching and interactive nesting are available options. Finite differences are used to approximate all derivatives. In a departure from previous studies the eddy diffusivities are now calculated at w points, although the integrations appear insensitive to this change. The nonlinear advection of momentum is computed using 4th order centered-in-space differences. Scalars are advected using 6th order differences (Tremback et al., 1987) coupled with the flux limiters designed to preserve monotonicity under advection. The flux limiters are built according to the FCT methodology of Boris and Book (Smolarkiewicz and Grabowski, 1990; Zalesak, 1979). In our implementation limiters are constructed as described in Smolarkiewicz and Grabowski with modifications as in Zalesak. All advection schemes are formally one-dimensional and are successively (through the course of a time step) applied to each spatial direction in turn. Because of the geometry of our flows, significant departures from monotonicity occur primarily in vertical advection. Realizing this we experimented with the use of limiters

only in the vertical advection equation. We found that although the statistics were largely similar, the failure to use limiters in the horizontal direction lead to the generation of unacceptable amounts of small-scale noise. This added small-scale noise led to an overly active sub-grid scheme, particularly near the surface. Unfortunately this wasn't recognized until near the end of the study (since the decision to not use the limiters in the first place was based on an analysis of the statistics from simulations with no mean horizontal wind). Nonetheless, all of the affected three dimensional simulations were re-run with the limiters in the horizontal. ERM simulations were not re-integrated as the along domain component of the wind in these simulations was always weak.

2.3 Previous Results and Critique of Method

The internal consistency of the numerical code has been demonstrated in a number of studies. The first and second moments derived from ERM integrations and LES have been evaluated and found to be broadly consistent with one another and with other models (Moeng et al., 1996). An interesting result from this study was that the ERM produced similar turbulent kinetic energy budgets, although the partitioning of the transport between the pressure and turbulence terms was significantly different. ERM results also favored more roll-like circulations with vertical velocity variances peaked in the center of the boundary layer, compared to the LES for which w variances had a maximum shifted closer toward the midpoint of cloud where the buoyancy production term tends to be largest.

The ability of the model to represent the entrainment process has also been considered on the basis of radiatively-active-smoke cloud simulations. Here again the code produced results consistent with other models (as revealed in comparisons at the second GEWEX Cloud Systems Studies workshop held at KMNI in the The Netherlands), although entrainment rates derived from integrations of different codes differed by nearly a factor of two and none of the models showed evidence of resolving the dynamics of the interfacial layer at the entraining interface. A comparison of LES and ERM results indicated that the ERM integrations again tended to have more symmetric circulations and entrained

more rapidly than their LES counterparts. These results support our earlier suggestion that LES are most limited in regions where significant portions of the energy remain unresolved; that is near boundaries or in stably-stratified layers. Because the simulations described herein are of turbulent flow capped by a poorly resolved layer of strong stratification, errors in the entrainment zone tend to be of greater concern than errors in the surface layer. In other words one of the largest areas of uncertainty is in the ability of the simulations to reasonably represent the entrainment process.

The ability of the BM model to capture the condensation-nucleation process has also been considered in detail (Stevens et al., 1996). In this study LES-BM results were compared to those produced by a Lagrangian parcel model (with Lagrangian microphysics) over an ensemble of trajectories derived from LES. It was found that the LES-BM captures the quality of the microphysical interactions although limited resolution in the vertical tends to smear out the cloud-base supersaturation peak resulting in a slight underestimation of the number of newly activated drops. A comparison of LES with ERM results also shows that the mean time of in-cloud circulations tends to be about equal, although the more organized circulations in the ERM tend to generate less variance (Stevens et al., 1996). Such a result is consistent with less energy in small scales in the ERM, an expected byproduct of the simulation of turbulence in two-dimensions. A companion study (Stevens et al., 1996) illustrates that one severe limitation of the present framework is that the failure to represent fractional (sub-grid) cloudiness results in microphysical errors at cloud edges. These errors manifest themselves as anomalous cloud-top supersaturations and undermine the ability of the model to capture the effects on the droplet spectrum of mixing across cloud interfacial boundaries.

In summary we have built a model that endeavors to represent the physical system at a high level of detail. In so doing it is able to reasonably capture the evolution of the large-eddies that dominate the boundary layer dynamics. As a result the model appears to well represent the bulk of the energetic interactions within the convective boundary layer. Nevertheless, a host of limitations should provide ample reminder that regardless of the level of sophistication of the model, *it is still a model*; and though the LES-BM

may represent several million degrees of freedom, compared to the physical system this is still a small number. Specific, previously identified, limitations of our approach can be enumerated as follows: (i) interfacial dynamics are not well resolved in simulations with large interfacial stability; (ii) ERM results are often analogous to LES results, but the structure of the circulations, and hence time-scales, tends to differ; (iii) Mixing across cloud interfacial boundaries is not properly represented and causes errors in the supersaturation field at cloud edges other than cloud base; (iv) the effects of cloud processing on the aerosol distribution are not considered, thereby preventing us from considering how this important feedback pathway may affect cloud dynamical evolution. Although recently an attempt has been made to quantify the importance of this pathway (Feingold et al., 1996b).

These constitute formidable limitations. Nonetheless, external constraints (such as time, social pressure, money and computational resources) prevent us from making a more realistic model at this time. Moreover, because we believe that the realism of the model is sufficient to capture the basic elements of the low-dimensional behavior of the stratocumulus-topped boundary layer it behooves us to investigate the behavior of the model before building yet more sophisticated ones. Nonetheless, good sense must continually be employed to challenge this belief, or assumption, that the model is a reasonable analog to reality. It will be left to further investigations to determine whether our good sense was effectively employed. Given this assumption the identification of the above limitations can at least be used to inform our interpretations of the simulations, as well as remind us that we are dealing with a model, which despite (or perhaps because of) its complexity, is still a rather crude, sometimes ugly, representation of that which we hope to understand.

Chapter 3

A CASE STUDY

In this chapter we use LES and ERM integrations to investigate how drizzle may have affected the evolution of the boundary layer as observed during the first ASTEX Lagrangian experiment. The ASTEX Lagrangian experiments were designed to illustrate the evolution in the internal structure of a boundary-layer air mass as it advects over warmer water (Bretherton and Pincus, 1995a). The approach is based on the assumption that columns of boundary-layer air, $O(50\text{km})$ in diameter, remain reasonably intact during the course of boundary layer evolution—a good assumption when there is little vertical shear in the horizontal winds and small gradients in air-mass properties on scales of order 50 km. There were two Lagrangian experiments, here we only consider the first (L1), which began on the late afternoon of June 12, 1992. Both experiments are well described in the literature (Bretherton and Pincus, 1995a; Bretherton et al., 1995b), but a brief review of L1 shall prove useful to our subsequent discussions.

The trajectory and structure of the air-mass during L1 remains in doubt for two reasons. First, the constant-volume balloons designed to track the airmass did not work; they spent less than four hours in the airmass they were designed to track. Second, a period of critical boundary layer evolution was not directly observed because poor visibility grounded aircraft for 14 hours. Nevertheless, using observed winds, ships and European Centre for Medium-Range Weather Forecasts (ECMWF) analyses the trajectory of the air mass was estimated. Subsequent, although limited, observations provide the following first-order characterization of the evolution in boundary layer structure. Initially the boundary layer was well-mixed with negative surface sensible-heat fluxes. Low-lying stratocumulus capped the layer. Droplet concentrations were approximately constant at

about 100 cm^{-3} and drizzle rates of order 1 mm day^{-1} were measured near the surface. Around the time of the first morning, sea-surface temperatures (SSTs) began increasing dramatically. Cumulus began forming below and feeding into an overlying stratocumulus deck. Eventually this stratocumulus deck thinned and dissipated, leaving behind scattered cumulus under a trade inversion. Over the course of the experiment the boundary layer (defined by cloud top heights) deepened by a factor of two.

Myriad processes are evident in the above overview; drizzle is significant early, solar radiation is becoming a factor as cloud begins to break, and SSTs are changing dramatically. Numerical experiments provide an ideal framework for understanding how various processes contribute to the evolution of a simulated boundary layer, and can be helpful in elucidating cause and effect for the physical system. With this in mind, we have done a variety of simulations designed to understand the role of processes like solar insolation, and SST variations. However, because our focus is on how drizzle impacts the evolution of the simulated boundary layer, these simulations will only be discussed to the extent they relate to the topic at hand. In §3.1 below we discuss the ability of an ERM-BM integration to match the observed evolution of the boundary layer during L1. We also discuss an identical integration using the ERM-NM, which doesn't allow drizzle formation, and examine how this impacts the simulated boundary layer evolution. It turns out that if large-scale features of the flow are maintained at their initial conditions the boundary-layer is well approximated by a steady state with significant drizzle. Consequently, in §3.2 we consider the structure of this "steady-state" drizzling boundary layer. We then prohibit the formation of drizzle and examine how this impacts the solutions. Section 3.3 refines the analysis of the previous sections using LES while §3.4 summarizes with a conceptual model.

3.1 ERM control integrations

3.1.1 *ERM-BM integration*

We initialized the model using the sounding taken from the first hour of L1. The configuration of the model is given in Table 3.1. Sensitivity tests show that the evolution

of the boundary layer is not strongly dependent on an accurate prediction of the large-scale winds—which are beyond the local control of the boundary layer. Consequently simulations were initialized with winds at their geostrophic values of $(u, v) = (u_g, v_g) = (2, -8) \text{ ms}^{-1}$ and large-scale pressure gradients were prescribed to force the winds toward their initial values on a time-scale defined by the local value of the Coriolis parameter. Other variables beyond local control are the free-tropospheric temperatures and water mixing-ratios; both were nudged on a three hour time-scale toward their observed mean values. For the purposes of the nudging the free-troposphere is defined as the set of all points with $z > Z_I + 2\Delta z$, where Z_I is the height of the simulated inversion, and Δz is the grid spacing. Because the simulated boundary layer tends to grow more rapidly than observed we do not have to worry about nudging the simulated free-troposphere toward states observed within the boundary layer. Large-scale divergence and SST were also prescribed to evolve in accord with the observations.

Table 3.1: Model configuration for ERM integrations.

Parameter	Setting
Δx	100 m
Δz	50 m with 10% grid stretching above 2000 m
Domain Height	3100 m
Domain Width	6400 m
Time-step	4 s, Radiation tendencies compute every 30 s

Selective model statistics were collected every minute and either written directly to a file or accumulated into hourly averages. A subset of the statistics are plotted as time sequences in Fig. 3.1. The most striking feature of the data is the qualitative change in the characteristics of the time sequence at about hour 18. In the first period the boundary layer grows modestly, produces significant drizzle, maintains solid cloud coverage and is characterized by less variability in w_{max} and q_{max} . As was observed during L1 a number of things are happening around the time of the break. Solar insolation and SSTs are increasing and drizzle is diminishing. In the second period the stratocumulus begins breaking up, the boundary layer grows more rapidly and by the 27th hour cumulus

convection becomes prominent. The change in the convective circulation from stratus-like to cumulus-like results in the large time variability in quantities like LWP, w_{max} , and $q_{l,max}$. The more spike-like features of these fields over the latter period are the signature of cumulus in a domain too small to instantaneously represent an ensemble of cloud activity. During the period of diminishing cloud fraction cloud base also rises and what drizzle that is produced generally evaporates before reaching the ground.

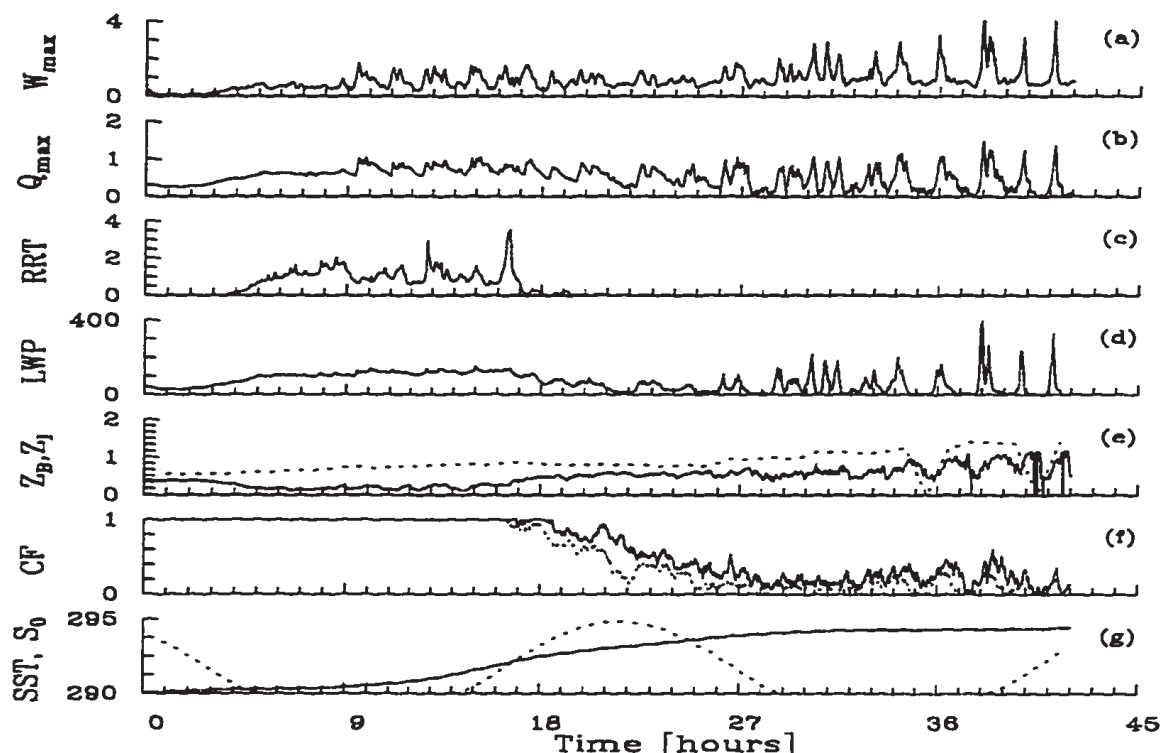


Figure 3.1: Time series of collected statistics from 42 hour Lagrangian I ERM-BM integration. (a) Maximum vertical velocity [m/s]; (b) Maximum liquid water [g/kg]; (c) Rain rate [mm/day]; (d) LWP [g/m²]; (e) Cloud base (solid) and Cloud top (dashed) heights [km]; (f) Two measures of cloud fraction (solid line uses presence of liquid water to indicate cloud in a column, dashed line requires column integrated liquid water to be greater than 13 g/m²); (g) SSTs [K] (solid) and relative solar insolation (dashed).

With respect to mean fields, *the difference* between the observations and the ERM-BM¹ integration is best illustrated by the time-height cross sections of mean liquid-water

¹Recall our notation of chapter 2, ERM-BM refers to the two-dimensional eddy-resolving model with a binned representation of the microphysics. ERM-NM is the same dynamical host model, but uses a saturation adjustment (i.e., no microphysical prognostic equations).

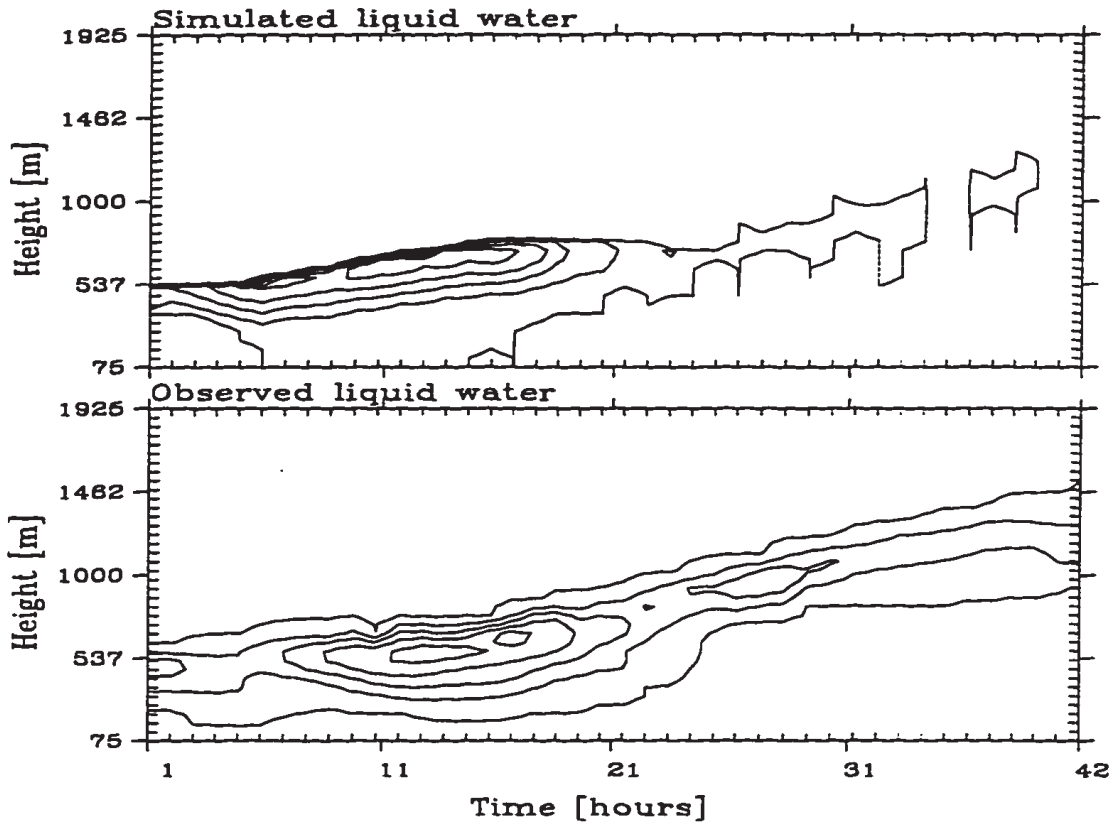


Figure 3.2: Time height contour of mean liquid-water contents. (a) ERM-BM integration, (b) Observations. Contours every 0.1 gkg^{-1}

mixing-ratio, \bar{q}_l , given in Fig. 3.2. The discrepancy in boundary layer growth is immediately apparent, where in contrast to the observations, the growth in the simulated boundary layer is well correlated with solar insolation (evidenced by the reduced amount of entrainment between the 16th and 24 hours). During the first 18 hours the ERM-BM grows the boundary layer more rapidly than observed² but it grows less rapidly at other times resulting in net growth rates being within a few percent of those observed. An encouraging aspect of the coarse-resolution ERM integration is that the qualitative evolution in boundary-layer structure appears to be well represented. For instance, the ERM-BM produces values of \bar{q}_l which reach a maximum of $\approx 0.5 \text{ gkg}^{-1}$, near the 11th hour (Fig. 3.2) before falling off sharply after the 20th hour. A similar evolution is evident

²One might be tempted to say that the ERM entrains more rapidly, but this need not be the case. Given that boundary layer growth results from both subsidence and entrainment it is plausible that the discrepancy is due to “observed” divergence rates (which are prescribed as forcing in the ERM) being significantly in error.

in the observations. The cumulus convection which was observed at later times (but does not show up in the contoured sounding data) is also evident in simulated \bar{q}_l after the 25th hour.

3.1.2 ERM-NM integration

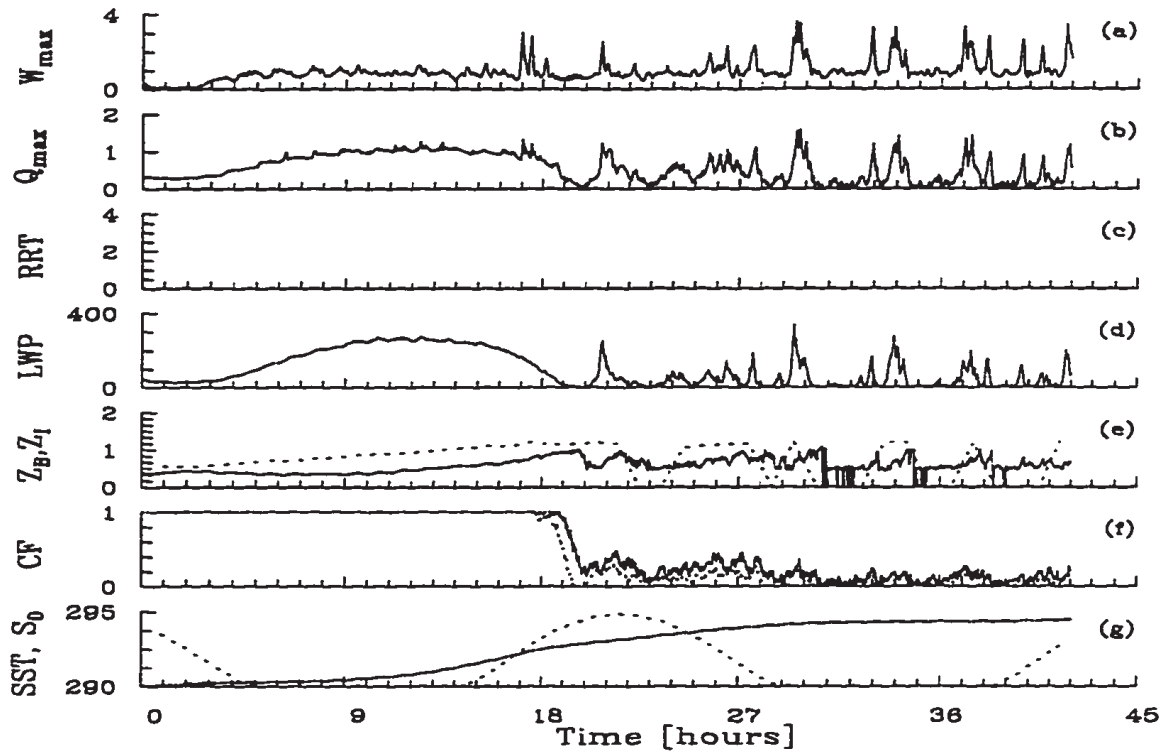


Figure 3.3: As in Fig. 3.1 but for the integration of the ERM-NM.

The correspondence between observations and the ERM-BM simulation is not perfect; nonetheless, it is sufficiently reasonable to warrant further sensitivity tests worthwhile. In order to understand the role of drizzle in the observed boundary layer evolution we repeated the integration using the ERM-NM. Nothing else was changed; the model initialization procedure, forcing and configuration are identical to those in the ERM-BM integration. In Fig 3.3 the time-series data from the ERM-NM integration is plotted. In many ways the simulations look similar as the marked transition in the quality of the time sequence around the 18th hour is evident in both Figs. 3.1 and 3.3. There are, however, important differences. For instance, during the first period entrainment rates and LWP differ significantly between the simulations; after 15 hours the ERM-NM integration yields

a boundary layer 200 m deeper than that produced by the ERM-BM, with LWPs about twice as large. We expect such a response, which is similar to what is hypothesized by Pincus and Baker (1994), to be dependent on the jump in moisture across the inversion. This issue is addressed further in Chapter 4. Cloud fraction decreases more strongly in the absence of drizzle during the second (or more trade-wind like) period of the simulation. This result does not agree with the hypothesis that drizzle leads to smaller cloud fractions (Albrecht, 1989)—although one should keep in mind that we limited drizzle by the extreme assumption of zero phase relaxation time, for which clouds in a subsaturated environment evaporate immediately.

3.2 ERM “steady-state” integrations

In the above integrations drizzle is not a necessary condition for the cloudiness transition. Indeed, for this case study, the presence of the transition, and the quality of the transition appear to be little influenced by drizzle. Drizzle does significantly influence the evolution of the boundary layer prior to the transition; it also raises the following questions. How does drizzle affect the development of a steady-state boundary layer? Can drizzling steady states be achieved, and if so what do they look like? How do equilibrium drizzling boundary layers behave when drizzle is suppressed?

To answer these questions we conducted a family of ERM-BM integrations systematically modified to remove (one by one) the time variation in external forcing. The diurnal cycle only affects the results of the integration in that it forces the solutions toward different equilibrium states. The nocturnal solution discussed below is characterized by a deeper precipitating cloud layer. The daytime solution has a thinner, more broken, cloud with less or no precipitation reaching the ground. Such a result is consistent with observations (Kraus, 1963) and previous modeling studies (Bougeault, 1985; Krueger et al., 1995a; Wyant et al., 1996). Changes in the character of the system are largely forced by changes in the boundary conditions, i.e., changes in the thermodynamic properties of the free-troposphere or changes in the SSTs. In our simulations the latter effect dominates, a finding consistent with earlier investigations (Krueger et al., 1995a; Krueger et al., 1995b; Bretherton and Wyant, 1996; Wyant et al., 1996).

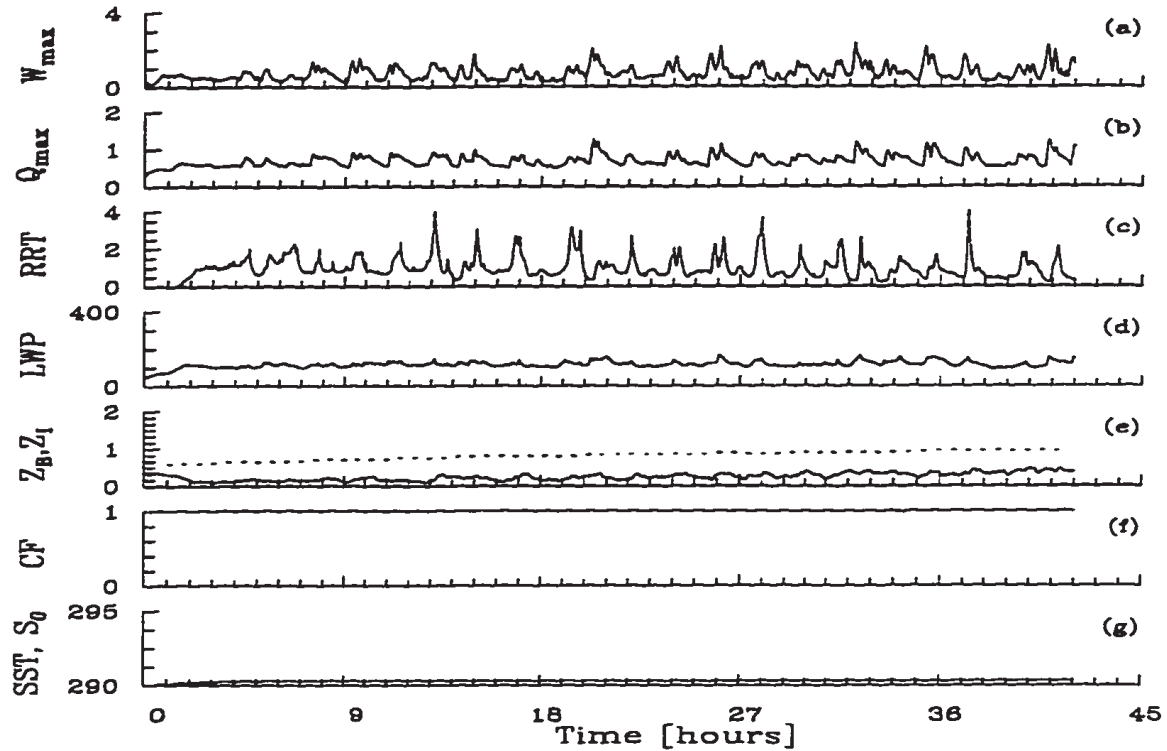


Figure 3.4: As in Fig. 3.1 but for the integration with no time-dependent forcing.

For the nocturnal boundary layer, with SSTs constant at their initial values and free-atmospheric variables forced toward their initial state, the ERM-BM integrations generated solutions which were very nearly steady in time. The character of the solution is well illustrated by the time-sequence data (Fig. 3.4). Cloud fraction remains at unity as w_{max} , q_{max} , LWP and drizzle rates stay approximately constant over a nearly two day integration.³ The integrations do not yield a perfect steady state as there is a short time oscillation (order two hours) particularly evident in the drizzle production, and a steady trend in the inversion height on the time-scale of the integration. The oscillation is of order two-hours and is well correlated with the evolution of convective elements which fill the ERM domain. The long-time trend is more evident in the time-height plot of the mean liquid-water mixing ratio (Fig. 3.5) which shows the steady rise of cloud-base and cloud-top. As cloud base moves further off the surface, the baseline drizzle rates decrease

³Recall that our assumption of fixed CCN concentrations helps to make such a response possible.

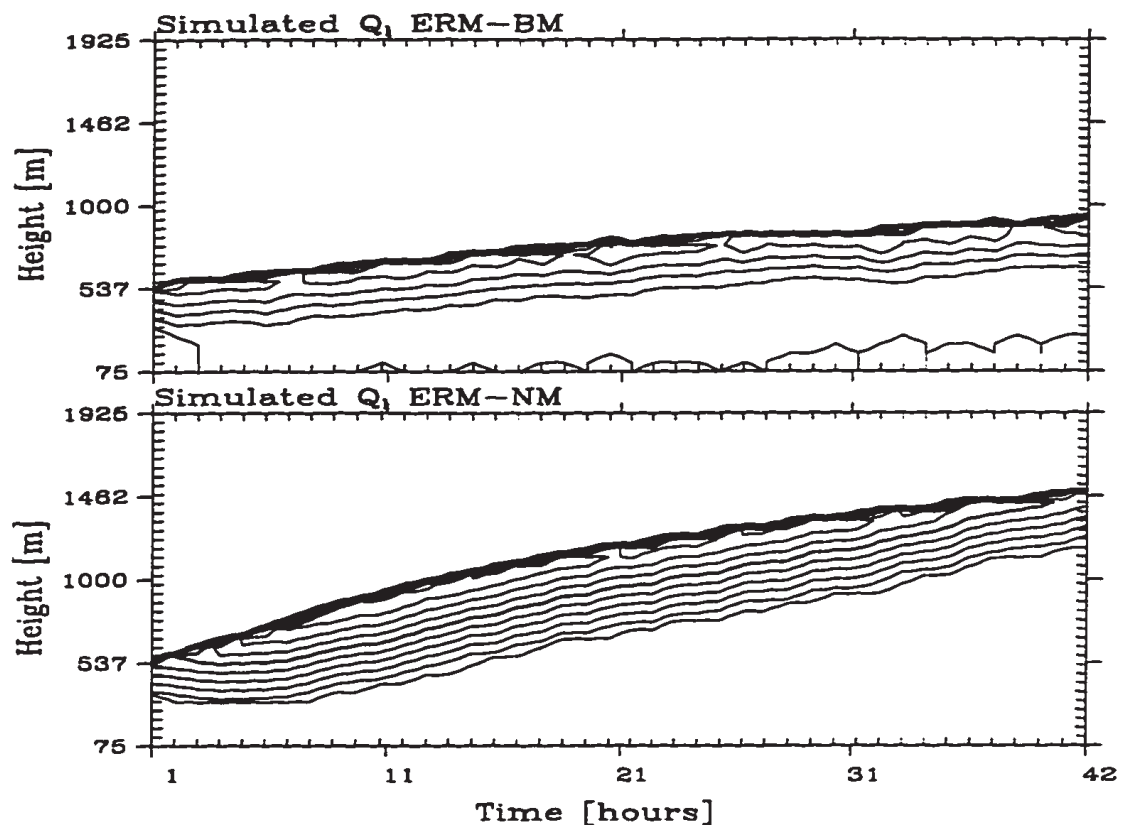


Figure 3.5: Time evolution of domain averaged q_l as a function of height for integrations with no time-dependent forcing: (a) ERM-BM; (b) ERM-NM. Contours every 0.1 gkg^{-1}

slightly and the short-time variation of drizzle becomes more pronounced. Nevertheless when compared to the earlier integrations the evolution in boundary layer structure is small.

Integrating the ERM-NM with the same forcing results in a very different solution, largely because of significantly different entrainment rates. Again, the particulars of the sounding allow the entraining cloud to deepen so that \bar{q}_l gets much larger in the ERM-NM integration (compare Figs. 3.5a and b). One could imagine that a cloud with more liquid water may result in more radiative forcing, or more buoyancy production, thus resulting in more entrainment. Later we will show that a reduction in drizzle results in more entrainment even for cases where cloud does not deepen, hence this supports our conjecture that the added entrainment leads to the deeper cloud, rather than the other way around (i.e., less drizzle leads to deeper clouds which generate more buoyancy and more entrainment). Differences in the solutions are well illustrated by the profiles of $\overline{w'^2}$, $\overline{\theta_l}$, $\overline{\theta_v}$, $\overline{q_T}$ and $\overline{q_l}$ plotted in Fig. 3.6. In addition to spatial averaging we have averaged

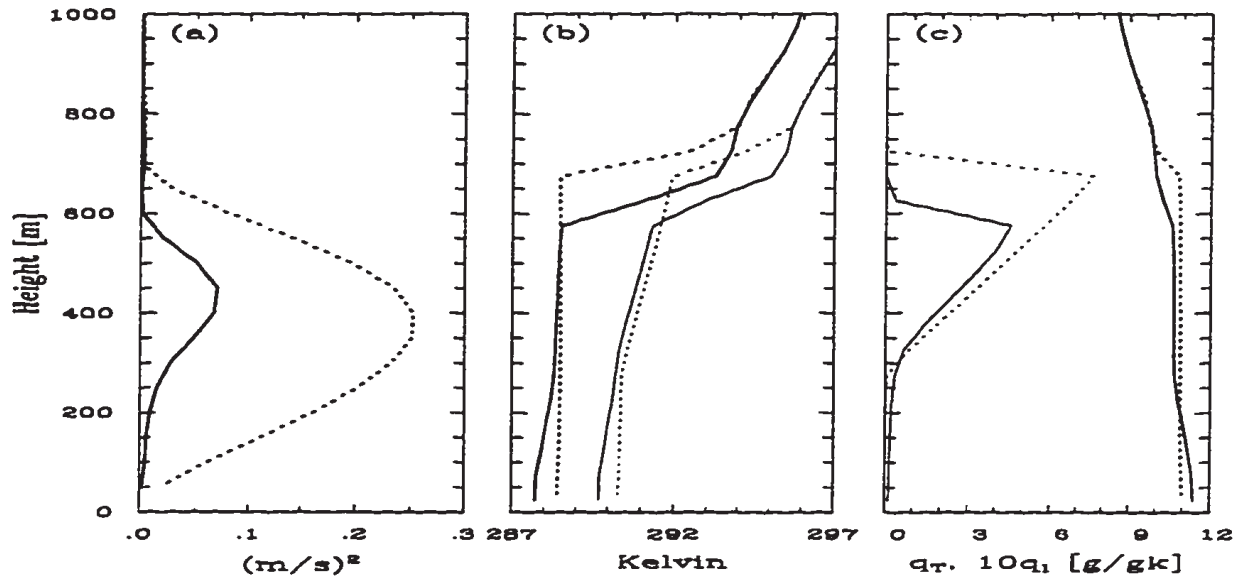


Figure 3.6: Profiles of various space and time averaged quantities from the fifth hour of the ERM-BM (solid lines) and ERM-NM (dashed) integrations: (a) $\overline{w'w'}$, vertical velocity variance; (b) $\overline{\theta_l}$ (thick lines) and $\overline{\theta_v}$ (thin lines); (c) $\overline{q_T}$ (thick lines), $10 \times \overline{q_l}$ (thin lines).

over time-levels during the fifth hour—at later times the different evolution of the two simulations begins to obscure comparisons. The ERM-BM shows ≈ 1 K of stabilization in the sub-cloud layer, inhibiting mixing between it and the cloud layer. In contrast to the non-drizzling solution, convective circulations in the ERM-BM integration are confined to the cloud layer; $\overline{w'^2}$ is small in the sub-cloud layer where gradients in thermodynamic variables are significant. Both integrations put the cloud base at about the same level, although the drizzling solution has a liquid water tail extending down to the surface. An analysis of the turbulence budgets and layer mean profiles suggests that by stabilizing the sub-cloud layer relative to the cloud layer, drizzle directly suppresses the buoyant production of turbulent kinetic energy (TKE) near cloud base.

Fig. 3.7 gives yet another view of the time-evolution of the two simulations. In response to the drizzle the ERM-BM integration rapidly develops a stable sub-cloud layer with gradient in θ_l of $O(2\text{K km}^{-1})$. It takes about 1000 Jkg^{-1} to cool BL air by 1 K, so that the 1 K stabilization of the 200 m deep cloud layer requires $c_p \rho_0 (\Delta\theta_l) (\Delta z) \approx 250000 \text{ J m}^{-2}$. This corresponds to a consumption of about 15 Wm^{-2} for a period of five hours. Interactions with the surface extract on average $3\text{-}4 \text{ Wm}^{-2}$ consequently a convergence

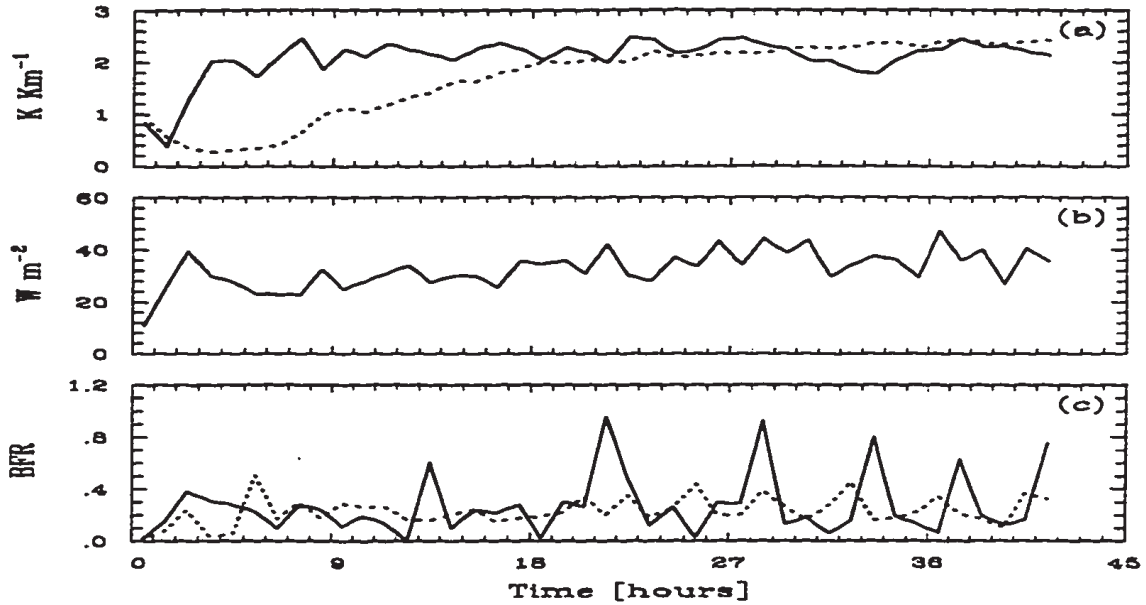


Figure 3.7: Time series of various statistics ERM-BM (solid lines) and ERM-NM (dashed) integrations: (a) Sub-cloud $\bar{\theta}'_l$ gradient (note if the ordinate is replaced by one with units of gkg^{-1} these lines also well describe the sub-cloud gradient in \bar{q}_T). (b) Drizzle flux convergence in sub-cloud layer; (c) Ratio of negative to positive area in buoyancy flux profile.

in the drizzle flux must cool the layer at a rate of about 11 Wm^{-2} . The sub-cloud drizzle flux convergence is on the order of 30 Wm^{-2} indicating that most of the cooling due to drizzle is mixed out by turbulent mixing between the cloud and sub-cloud layers. Over time the ERM-NM integration also develops a stable sub-cloud layer with similar gradients (albeit over a much deeper layer), but by a different process. As the boundary layer deepens it warms so that through the duration of the simulation surface-sensible heat fluxes are negative, in contrast to the ERM-BM integration where after the fourth hour drizzle has cooled the sub-cloud layer to temperatures below that of the lower surface. For the non-precipitating integration, turbulence generated as a result of cloud-top cooling at an increasingly distant interface becomes increasingly unable to do the work against buoyancy necessary to mix-out the cool sub-cloud and surface air.

It has recently been suggested (Bretherton and Wyant, 1996) that the ratio of negative to positive area in the graph of $\overline{\theta'_v w'}(z)$ could serve as a measure of decoupling. This ratio (which Bretherton and Wyant call the buoyancy-flux ratio BFR) is defined as

follows,

$$BFR \equiv -\frac{\int_0^{Z_I} \min(0, \overline{\theta'_v w'}) dz}{\int_0^{Z_I} \max(0, \overline{\theta'_v w'}) dz}. \quad (3.1)$$

On the basis of ERM integrations Bretherton and Wyant suggest $BFR > 0.2$ as a threshold for decoupled states. With this in mind we plotted the hourly averaged values of BFR in Fig. 3.7c. Comparing θ_l gradients with the BFR for the ERM-NM integration provides little evidence of a correlation between the two. More remarkable than the relation—or lack thereof—between the BFR and sub-cloud gradients is the fact that for both integrations the mean value of the BFR over the 42 hour experiment was 0.23. This result suggests that, in our simulations, the turbulence is unwilling to allow much more than a fifth of the energy created by buoyancy in the cloud layer to be used to do work against buoyancy in the sub-cloud layer. Other investigators have found a similar result for the dry-convective boundary layer (Stull, 1976). While the two-dimensional simulations also appear to be unwilling to allow $BFR > 0.2$, this result might well be an artifact of two-dimensional dynamics, as for cloud free boundary layers, with weak convective forcing and moderate shear, high resolution three-dimensional simulations suggest that shear production of TKE allows more negative area in the buoyancy flux to develop and the BFR may approach 0.5 (Moeng and Sullivan, 1994). The ASTEX case study does have significant shear production, although based on a comparison of ERM and LES integrations (Moeng et al., 1996) for a similar case it is doubtful that it is well represented by the ERM. Consequently, we hesitate to draw conclusions (based on these or other ERM integrations) regarding the ability of the BFR to serve as a measure of decoupling.

In summary, our results indicate that at least in some cases boundary layer structure is a strong function of drizzle production. The similarity between the slowly-evolving solutions of the ERM-BM and the observed and simulated structure of L1 10 hours after the start of the experiment suggests that the slowly-evolving solutions may be relevant to the physical system. Moderate amounts of drizzle appear to slow the evolution in boundary layer structure. As previously suggested drizzle does lead to the formation of a thermodynamically distinct sub-cloud layer, but this need not result in the generation of convective instability which eventually will break up the stratocumulus. Consequently,

the suggestion (Paluch and Lenschow, 1991) that precipitation portends stratocumulus breakup is not supported for our simulations with moderate drizzle. The use of LES will also facilitate a more meaningful analysis of how drizzle affects the budgets of energy and other conservative quantities.

3.3 Large Eddy Simulation

The LES was initialized using a sounding taken from the 12th hour of L1. Because we only planned to do relatively short integrations a refined mesh was used: $\Delta x = \Delta y = 55$ m, $\Delta z = 25$ m, and $\Delta t = 2$ s. Short time integrations also allowed us to forgo any nudging of the free-atmosphere thermodynamic variables in addition to considering a domain of smaller vertical extent—the grid was stretched by 10% above 850 m and the model top was at 1600m. The simulations discussed here were initialized using the observed winds above the boundary layer $[(u, v) \approx (-2, -9) \text{ ms}^{-1}]$, and the mean boundary-layer winds for all levels within the boundary layer $[(u, v) \approx (0.4, -10) \text{ ms}^{-1}]$, the geostrophic forcing was toward the initial state, changes in the mean-state temperature implied by the small jump in the geostrophic winds across the inversion were neglected. SSTs were increased during the course of the simulation in accord with the observations. Although the LES does not correspond exactly to any of the ERM integrations discussed above, the sounding is characteristic of the slowly varying drizzling states observed and simulated during the first night. The refined mesh and full three-dimensional representation of the turbulence gives us more confidence in our solutions. In retrospect it would have been better to do the simulation without a time varying lower boundary; but these simulations were initially carried out for a GCSS (GEWEX Cloud Systems Studies) inter-comparison and we felt that the added complexity of a warming lower boundary was not sufficiently onerous to warrant re-simulating the case.

Two LES will be discussed here. The first uses the NM model and the second uses the BM model with CCN concentrations fixed at 100 cm^{-3} . Each simulation was integrated for 12600s (210 minutes) and mean profiles averaged over the last 2400s (40 minutes) are given in Fig. 3.8. The LES-BM produces significant drizzle, the drizzle tail is evident in the

profile of $\overline{q_l}$ and precipitation rates at the ground (not shown) averaged about 1 mm day^{-1} (commensurate with the ERM-BM). The solutions from the LES-NM have no drizzle. A comparison of the features of the two integrations illustrates that, at least qualitatively speaking, a number of the sensitivities seen in the ERM simulations are reproduced by the LES. For instance, the strongly drizzling solution is characterized by substantially reduced incloud values of $\overline{w'w'}$, less entrainment, and a more pronounced stable sub-cloud layer. Relative to the LES, the ERM exaggerates the differences between the drizzling and non-drizzling solutions. Nonetheless, these results support our arguments of Chapter 2 which stated that ERM integrations often serve as a good indicator of the behavior of LES.

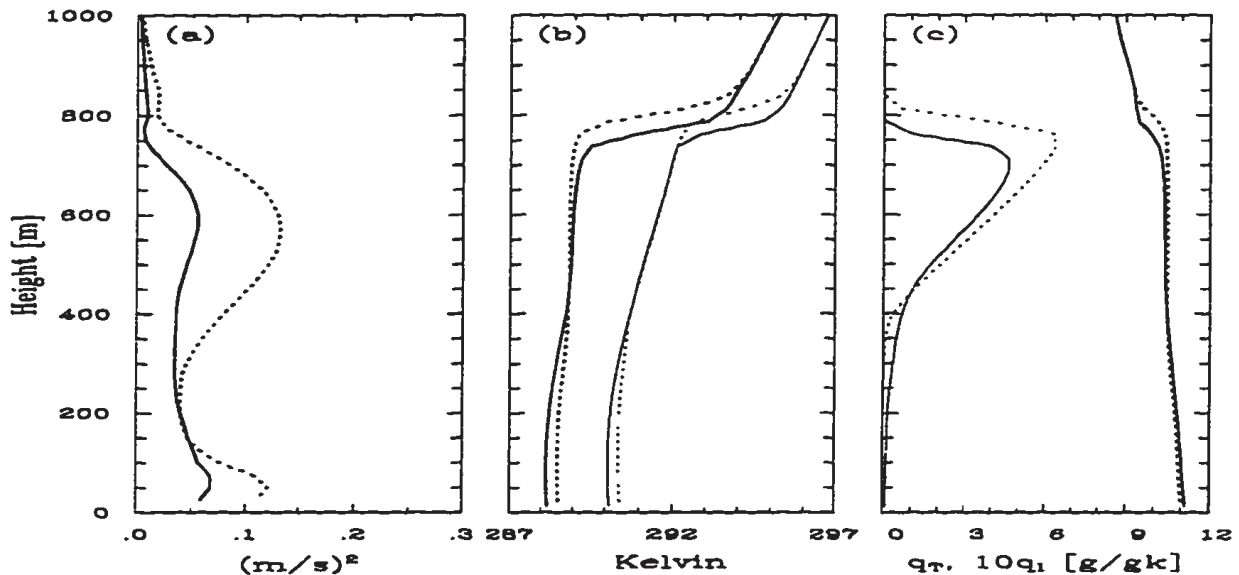


Figure 3.8: Profiles of various space and time averaged quantities from the LES-BM (solid lines) and LES-NM (dashed) integrations: (a) vertical velocity variance; (b) θ_l (thick lines) and θ_v (thin lines); (c) q_T (thick lines), $10 \times q_l$ (thin lines).

Some of the differences between the LES and the ERM solutions (such as the low-level maximum in $\overline{w'w'}$) can be reconciled by the fact that the LES has a surface boundary condition that changes with time, such that a strong surface buoyancy flux is maintained through out all the LES simulations. Other differences are more formulaic. A characteristic difference between non-precipitating LES and ERM integrations is that in the absence of surface forcing LES predicts a $\overline{w'w'}$ profile peaked near cloud-top and decreasing nearly

linearly toward zero at the ground, in contrast to the tendency of the ERM to predict symmetric Gaussian-like profiles centered near the middle of a well mixed boundary layer. Our purpose here is not, however, to definitively compare the dynamics of the LES and ERM. Suffice to say that the qualitative nature of the sensitivity of the LES and ERM to drizzle appears similar but the differences are sufficiently strong to motivate the additional computational cost of selected LES. Because of its more representative treatment of the dynamics, subsequent discussion in this chapter focuses on the difference between the LES-BM and LES-NM.

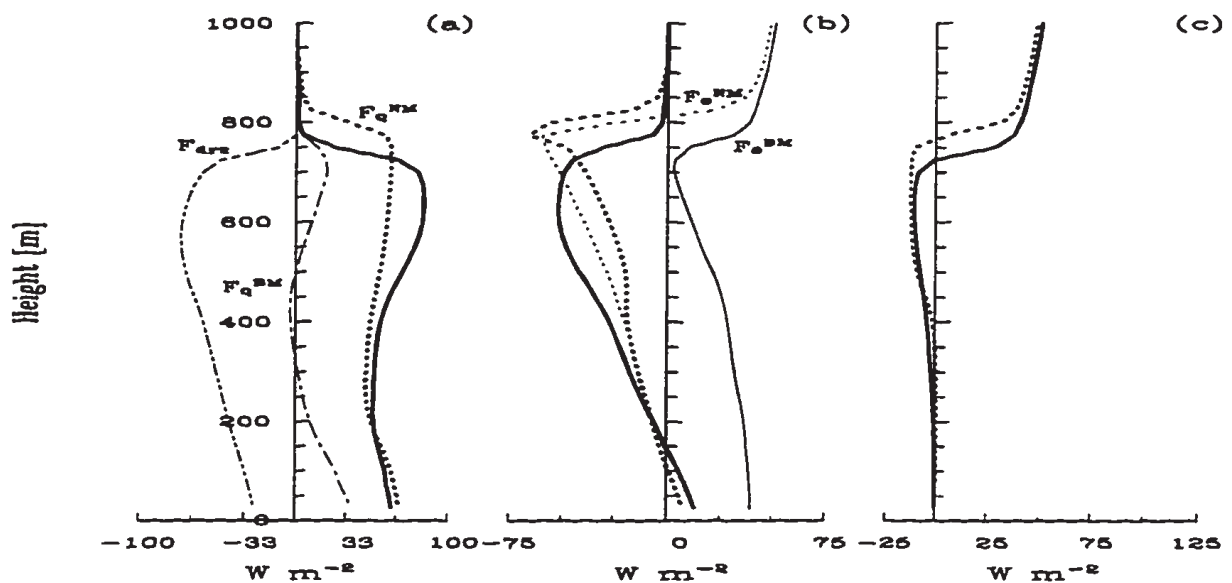


Figure 3.9: Profiles of space and time averaged fluxes: (a) Total water flux (turbulent flux of total water in LES-BM denoted by solid line, other fluxes labeled on plot) (b) θ_l fluxes (turbulent fluxes of θ_l given by thick solid line (LES-BM) and thick-dotted line (LES-NM) other fluxes labeled; (c) Radiative fluxes (LES-BM solid, LES-NM dotted).

Thermodynamic profiles for both LES suggest a two layer structure, with local minima in $\overline{w'w'}$ below cloud base. The relationship between the two layers does however appear to differ significantly for each simulation. The minimum in $\overline{w'w'}$ is much nearer cloud base and less pronounced for the LES-BM although the contrast between the thermodynamic properties of the two layers (i.e., θ_l) is more pronounced. If the LES-BM and LES-NM are equally efficient at mixing out gradients in θ_l or q_t one would expect the LES-BM to have larger gradients due to the continual forcing of the precipitation flux. Ultimately,

the degree of stratification in the mean profiles is not a good indicator of decoupling; for this we must examine the fluxes.

When examining fluxes it is worthwhile to consider the sum of all fluxes that contribute to the evolution of a particular variable. Hence, in addition to physically intuitive fluxes, the superposition of certain fluxes are also interesting to look at. In particular, we can define two fluxes

$$F_Q = \rho_0 L \overline{w'q'_T} + F_{drz}, \quad \text{where} \quad F_{drz} = \rho_0 L \sum_{k=1}^{25} \overline{w_t(\bar{q}_{l,k})q_{l,k}}, \quad (3.2)$$

$$F_\Theta = \rho_0 c_p \overline{w'\theta'_l} - F_{drz} + F_{rad}, \quad (3.3)$$

whose divergence represents the sole contribution to the evolution of \bar{q}_l and $\bar{\theta}_l$ respectively (see Appendix A.2 for a derivation of the above equations and a discussion of how the fluxes are calculated in the model). The drizzle flux, F_{drz} is the product of the total mass in a drop bin and the terminal velocity of the averaged sized drop in that size bin, hence the $\bar{q}_{l,k}$ dependence in w_t . By definition, specification of F_Q or F_Θ is all that is needed to diagnose how the mean state is changing. When they are linear in height *the shape* of the mean state is time invariant, if they are constant in height *the mean state itself* is time-invariant. The latter is a true steady state; the former is often referred to as a quasi-steady state (see Appendix A.2).

Fig. 3.9 illustrates the structure of a variety of fluxes, including F_Q and F_Θ . These flux profiles do suggest that precipitation and the increase in sub-cloud stratification profoundly affect stratocumulus dynamics. The LES-NM predicts F_Θ approximately linear with height, indicative of the fact that this initially well-mixed field field is remaining so. There is more evidence of a developing two-layer structure in F_Q , with moistening below and weak drying above 200 m. Over the analysis period the fluxes generated by the LES-BM are consistent with an enhancement in the cloud base stratification of q_l and θ_l . Above/below cloud base ($\approx 400\text{m}$) F_Q is well approximated as linearly increasing/decreasing with height; indicating the drying/moistening in the cloud/sub-cloud layer. These two effects largely compensate each other so that the net drying of the entire boundary layer is minimal. F_Θ is nearly constant below and linearly decreasing with height above

400 m. A closer look indicates that $\overline{\theta}_l$ is not changing in the sub-cloud layer as warming through mixing (see the profile of $\overline{w'\theta'_l}$) is approximately offset by precipitation. Within the cloud layer $\overline{\theta}_l$ is increasing; note however, that between 600 and 700m (in the upper portion of the cloud) most of this increase is associated with the sedimentation flux as $\overline{w'\theta'_l}$ is approximately constant. The fact that drizzle has a significant impact on the structure of the boundary layer is underscored by the fact that the transport of total water by turbulent motions at 600 m is completely offset by the sedimentation of liquid water; and drizzle fluxes are of the same order as turbulent fluxes of total water through the depth of the boundary layer. However, to the extent that decoupling is identified with the vanishing of the fluxes over a finite depth, neither of the integrations is decoupled. In fact, the turbulent flux of water above 200 m is actually larger for the LES-BM than it is for the LES-NM, although due to precipitation the net flux, F_Q is less. This underlines an important point: *the sub-cloud and cloud layer may be very effectively coupled, despite the presence of substantial stratification near cloud base, and the tendency of the respective layers to be evolving in different directions.*

How do these fluxes affect the evolution of cloud base? The rate of change of the saturation point (or lifting condensation level), w_{lcl} , can be related to changes in conserved variables as follows:

$$w_{lcl} \approx -C_\Theta \frac{\partial F_\Theta}{\partial z} + C_Q \frac{\partial F_Q}{\partial z}. \quad (3.4)$$

Here C_Θ and C_Q are positive definite thermodynamic constants moderately dependent on the mean state (see Appendix B for a derivation). For values of q_T and θ_l characteristic of our mean state, their values are 0.105 and 0.0628 respectively. Using the above relationship the fluxes from the LES-BM are translated into equivalent values of w_{lcl} and analyzed. For instance from Fig. 3.9 we recall that F_Θ for the LES-BM becomes increasingly negative with height below 700m (i.e. $F_\Theta(z) < F_\Theta(z + \varepsilon)$ where $\varepsilon > 0$). This implies that $\frac{dF_\Theta}{dz} < 0$ and $w_{lcl} > 0$ by Eq. 3.4. Thus the contribution to w_{lcl} from F_Θ is positive (see solid line in Fig. 3.10a which represents w_{lcl} due solely to the $\frac{dF_\Theta}{dz}$ contribution), indicating that F_Θ leads to a progressive rise in cloud base.

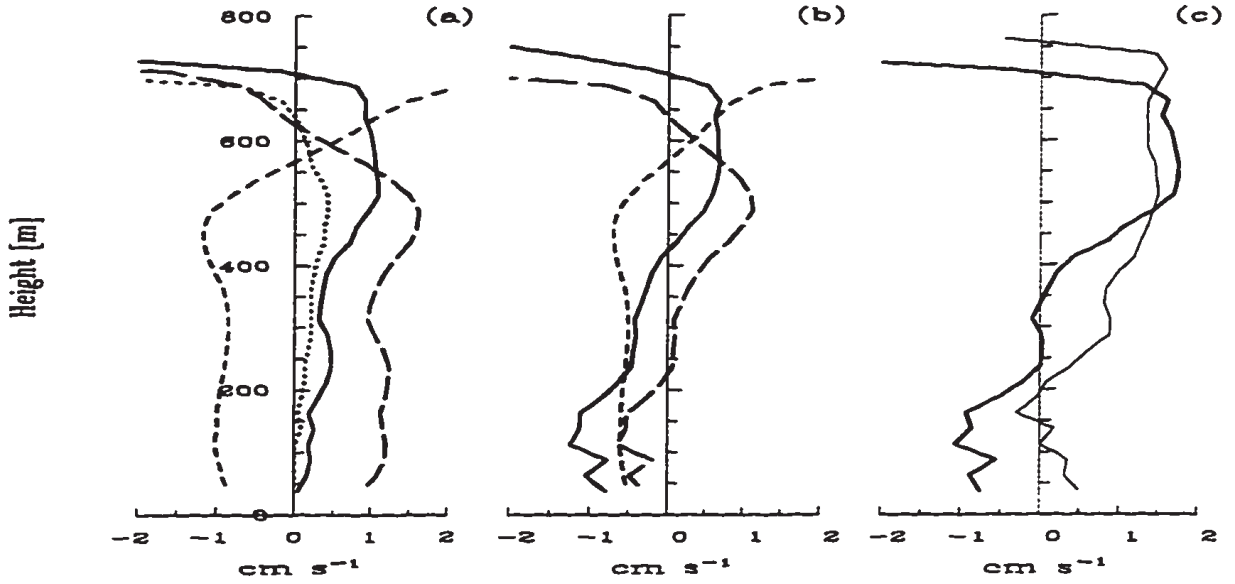


Figure 3.10: Vertical velocity of lifting-condensation level, w_{lcl} , in boundary layer due to fluxes of various quantities. (a) Contributions to w_{lcl} from θ_l budget for LES-BM integration. Contributions from: F_Θ (solid); $\overline{w'\theta'_l}$ (long-dashed); $-\sum_{k=1}^{25} \overline{(w_t q_l)_k}$ (short dashed); F_{rad} (dotted). (b) Contributions to w_{lcl} from r_T budget in LES-BM integration. Contributions from: F_Q (solid); $\overline{w'q'_T}$ (long-dashed); $\sum_{k=1}^{25} \overline{(w_t q_l)_k}$ (short dashed). (c) Total values of w_{lcl} for LES-BM integration (thick line), and LES-NM (thin-line).

The tendency of heat fluxes to raise cloud base is due to turbulent circulations, although such circulations are significantly mitigated by the drizzle flux convergence which, from the perspective of the sensible heat budget, attempts to lower cloud base at all levels below 550m. The upper part of the cloud layer (above 600m) is most strongly impacted by drizzle flux divergence, and radiation has a minor effect within the boundary layer. From the perspective of the water budget, drizzle flux convergence and low-level turbulent moisture fluxes (dominated by surface fluxes) moisten the surface layer (see Fig. 3.10), contributing to a reduction in the saturation level. In the cloud layer the drying influence of entrainment dominates so that changes in q_T would, in the absence of other effects, lead to $w_{lcl} > 0$. Overall the convergence of F_Θ and F_Q contribute about equally to the evolution of the saturation point in the cloud layer, although the evolution in the saturation point is dominated by F_Q in the sub-cloud layer. The net value of w_{lcl} changes sign near 300m (Fig. 3.10c), under-scoring our previous conclusion that a two layer structure is characteristic of the drizzling boundary layer. Such a structure is not as evident in values of w_{lcl} computed from the fluxes in the LES-NM integration (thin line in panel c).

The time-evolving lower boundary in the LES simulations (in contrast to the ERM which had a fixed temperature lower boundary for the nearly steady-state integrations) prevents these integrations from approaching a steady state. Moreover, the w_{lcl} field in the LES-BM integration suggests that the boundary layer is evolving in a manner that favors the development of cumulus clouds emerging from a moistening sub-cloud layer. Because the LES-BM generates values of w_{lcl} 2-3 times larger than dz_I/dt , the cloud is thinning. In contrast the entrainment rate in the LES-NM integration is about 4 times as rapid—leading to a deeper cloud. These results are consistent with what was found in the ERM integrations in that less drizzle favors a deeper cloud. The tendency toward cumulus cloud formation out of a sub-cloud layer separated from a stratified cloud layer is in line with the suggestions of Paluch and Lenschow (1991), although keep in mind the lower boundary is warming with time.

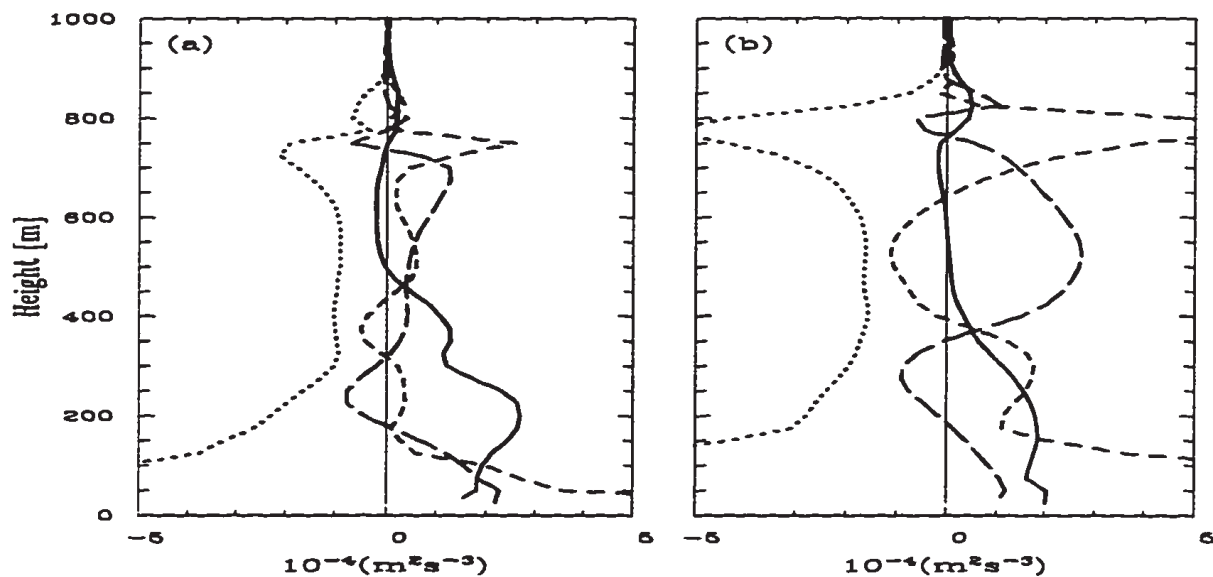


Figure 3.11: Profiles of various terms in TKE budget. Shear production (solid), dissipation (dotted), buoyancy production (long dash), transport (short dash). (a) LES-BM, (b) LES-NM

Why does the LES-BM entrain less than the LES-NM? Or if one assumes that $\overline{w'w'}$ is correlated with entrainment, then why does the LES-BM generate significantly smaller

values of cloud top $\overline{w'w'}$? To address these questions we consider the TKE budgets⁴ from the simulations whose various terms are plotted in Fig 3.11. The most dramatic difference is in the buoyancy production and to a lesser extent the transport terms. The LES-NM has a much larger buoyant production of TKE in the cloud layer. This allows significant amounts of TKE to be transported into the interfacial zone to do the work against buoyancy necessary for entrainment to proceed at the observed rate. Although there is considerable time variability in $\overline{w'\theta'_v}$ (the buoyancy flux, which is a production term in the TKE budget), values produced by the LES-BM are consistently less than what is seen in the LES-NM; the greatest differences are in the cloud layer (between 300 and 500 m) as the vertical distribution of buoyancy production and destruction of TKE differs little between the simulations. Reasons for less buoyancy production of TKE in association with heavy precipitation are explored further toward the end of the next chapter.

Most of the shear production is confined to the sub-cloud layer. The net effect of this term is considerable, but similar, in both simulations. Although because of the reduction in the buoyancy flux, shear production actually dominates the TKE budget in the LES-BM. Because of the significant production of TKE by shear, we suspect that the effect of precipitation fluxes in stabilizing the sub-cloud layer is actually less than what it would be in the absence of shear. As for the shear-free case the reduction in the buoyancy flux more singularly affects the production of TKE

3.4 Conceptual Cartoon

The above analysis can best be summarized using the conceptual cartoon of a slowly evolving precipitating stratocumulus topped boundary layer sketched in Fig. 3.12. Here the boundary layer is divided into two deep layers (a sub-cloud layer, and a cloud layer) separated by a shallow transition layer. Mixing between the sub-cloud layer and surface occurs in a shallow surface layer, while mixing between the cloud layer and the free troposphere occurs in the shallow entrainment layer. Both the transition and entrainment

⁴See Appendix A.3 for a discussion of the different terms in the TKE budgets and how they are diagnosed from the integrations.

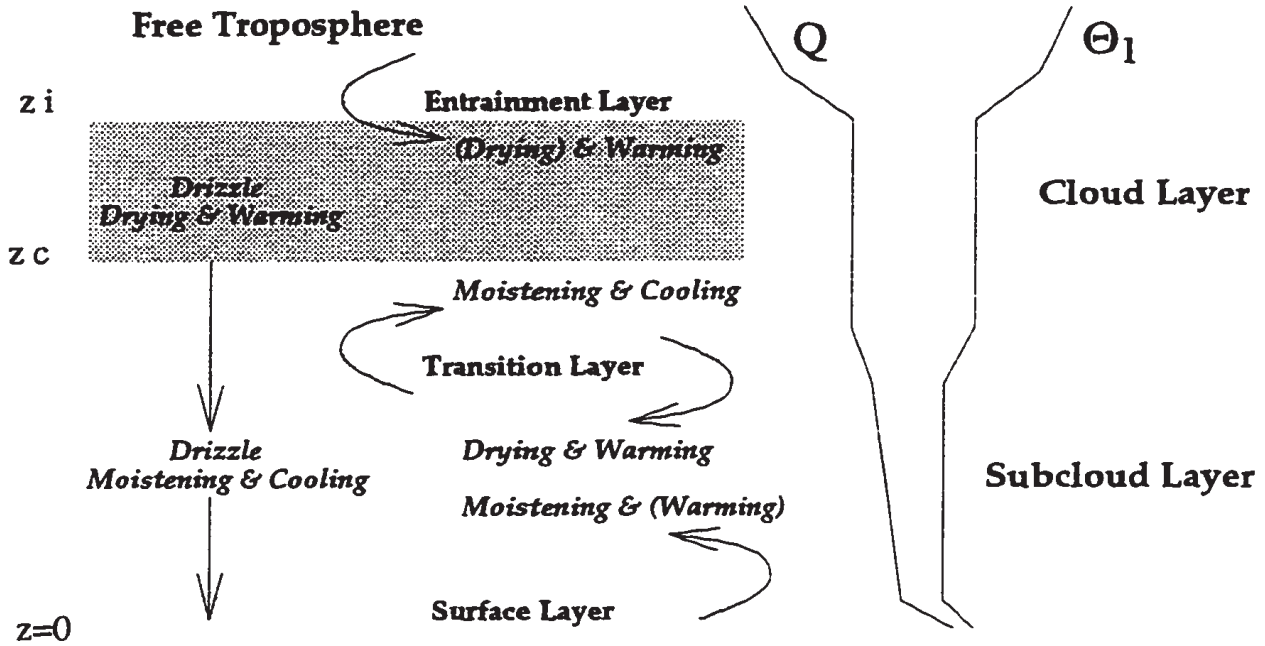


Figure 3.12: Conceptual cartoon of the structure of a precipitating stratocumulus topped boundary layer.

layers are stably stratified, although the surface region is unstable. In our composite most of the turbulence is generated in the cloud layer which is well mixed in all conservative variables. The surface layer is well mixed in potential temperature, but allows moderate moisture gradients. Mixing between the cloud and sub-cloud layers cools and moistens the former, while warming and drying the latter. Surface fluxes warm and moisten the sub-cloud layer while entrainment fluxes warm and dry the cloud layer. The presence of drizzle flux divergence in the upper cloud layer and convergence in the sub-cloud layer (drying and warming the former while cooling and moistening the latter) balances the budgets of heat and moisture, and is critical in the development of the stably stratified transition region. Because of this stabilization the production of TKE through buoyancy is reduced, thereby mitigating the amount of warming and drying of the cloud layer through entrainment.

Chapter 4

SENSITIVITY STUDIES

In the previous chapter, we examined the behavior of the model in the context of a specific case study. From this case study we addressed the relevance of equilibrium solutions to boundary layer circulations, and discussed how drizzle may have impacted the state of an observed boundary layer. In this chapter we generalize our understanding to a wider range of parameter space and return to some questions raised in Chapter 1. For instance, how does drizzle production impact equilibrium solutions for boundary layer structure? Do drizzling boundary layers entrain less and produce shallower clouds than their non drizzling counterparts, as hypothesized by Pincus and Baker (1994), and if so is this result dependent on one's choice of initial sounding? Our approach is to start with a sounding similar to that produced by the "steady-state" ERM-BM integrations of L1 and examine the sensitivity of the model to different CCN concentrations. A subset of sensitivity runs are then re-integrated for soundings which differ in their free-atmospheric properties. Before beginning these sensitivity studies, we first consider the sensitivity of the ERM integrations to a number of other factors which are often arbitrarily specified.

Unless otherwise indicated integrations are initialized using the following piecewise-linear initial conditions (where z is in meters, θ_l is in Kelvin, and q_T is in g kg^{-1}):

$$(\theta_l, q_T) = \begin{cases} (288.0 + \delta\theta_l, 10.2) & z \leq 662.5 \\ (288.0 + \delta\theta_l, 10.2) + (0.110, -0.0220) \cdot (z - 662.5) & 662.5 < z \leq 687.5 \\ (288.0, 10.2) + (0.110, -0.0220) \cdot (z - 662.5) & 687.5 < z \leq 712.5 \\ (293.5, 9.1) + (0.006, -0.0028) \cdot (z - 712.5) & \text{otherwise} \end{cases} \quad (4.1)$$

The pseudo-random perturbation, $\delta\theta_l \in (-0.1, 0.1)$, is applied at each grid-point and forced to satisfy $\int_X(\delta\theta_l)dx = 0$ at every level. Geostrophic winds are set: $(u_g, v_g) = -(2, 10) \text{ ms}^{-1}$.

For the calculations in this chapter a simple long-wave radiative scheme is used. The radiative flux is a function only of liquid-water path, LWP , and solves for the net radiative flux F_{rad} such that

$$F_{rad}(z) = F_0 e^{-\alpha(LWP(z))}, \quad \text{where} \quad LWP(z) = \int_z^{z_{top}} \rho_0 q_l dz. \quad (4.2)$$

Here F_0 is the maximum rate at which energy can be extracted, and α is a parameter which regulates the depth of the cloud layer over which this extraction takes place, ρ_0 is the basic state density, q_l is the liquid water mixing ratio and z_{top} is the top of the model. In accord with the 3rd GCSS case study we initially choose $\alpha = 130 \text{ m}^2 \text{ kg}^{-1}$ and $F_0 = 74 \text{ W m}^{-2}$, which leads to cooling rates of about $7\text{-}9 \text{ K hr}^{-1}$ being confined to the top 25 m of cloud. Real clouds are sensitive to the radiative forcing in a number of ways. For instance clouds in a deeper boundary layer warm more at their base than do clouds which form in a shallower boundary layer. Clouds underlying a moist free-troposphere also cool less than those underlying a dry free-troposphere. Our approach to radiative transfer neglects these effects in that it only considers radiative flux divergence associated with the presence of liquid water. Moreover, the magnitude of α implies that even relatively shallow clouds will lose as much energy as their thicker counterparts. This approach has the advantage of simplicity and it makes interpretation of our results more straightforward as it eliminates most radiative feedbacks. With the above choice of constants the net radiative-flux divergence within the boundary layer is less, although the cooling tends to be more focused than was the case in the previous chapter. Another change in the model is in the specification of the CCN spectra; we now use a narrower spectrum centered at a larger mode radius, $(D_g, \sigma_d) = (0.2\mu\text{m}, 1.5)$. This change tends to make drop and CCN concentrations more commensurate, since the former are more readily accessible given the range of super-saturations typically produced. The large-scale divergence is fixed at $5 \times 10^{-6} \text{ s}^{-1}$, identical to the integrations in the previous chapter.

With respect to numerical details of the integration, most of the studies in this chapter will be carried out using the ERM with a discretization of $(\Delta x, \Delta z, \delta t) = (50\text{m}, 25\text{m}, 2\text{s})$. This resolution is twice as fine as (and hence $2^3 = 8$ times more expensive than) the

ERM studies in Chapter 3; it is computationally affordable (in the case of the BM integrations) only because integrations are not carried out longer than 15 hours. A progressively stretched grid is used above 800 m, with grid-stretch ratio of 10% to the model top at 1500 m. A Rayleigh friction damping layer is applied in the upper 400 m (7 layers) of the domain with a damping time-scale of 60 s.

4.1 Preliminary sensitivity studies

Here we attempt to characterize the sensitivity of the integrations to a variety of factors. Many tests are made with respect to a change in a model parameter whose exact specification is subject to a certain amount of arbitrariness (i.e., the discretization, domain size, turbulence closure for drops, collection kernel) although in one case we add a physical effect (i.e., the ventilative enhancement of evaporation from precipitating drops), and in another we explore the sensitivity of the simulations to slight changes in the sounding.

Table 4.1: Sensitivity of selected statistics to different initial random perturbations

Integration	\mathcal{L}	\mathcal{D}	Z_I	w_2	$\Delta\Theta_I$
CNTRL1	203.0	14.4	855	0.276	0.554
CNTRL2	221.6	12.2	864	0.307	0.395
CNTRL3	201.4	18.3	835	0.302	0.421
\bar{x}	208.7	15.0	851	0.295	0.455
σ_x	11.2	3.1	15	0.016	0.088

To best evaluate the significance of the model response to a change in a specific parameter we conducted three eight hour baseline simulations. The only difference among the integrations was in the choice of the initial random seed (i.e., the sequence of random perturbations to the initial temperature field is changed). The integrations generate a tremendous amount of data, and it is difficult to come up with simple scalar measures which can characterize the behavior of the integrations. We have chosen to look at five parameters, none of which are necessarily independent of one another, but each of which should contribute to a better understanding of the gross properties of each integration. These parameters are: (i) \mathcal{L} the domain averaged value of *LWP*; (ii) \mathcal{D} , the domain

averaged drizzle flux across the lower boundary in units of Wm^{-2} ; (iii) Z_I , the cloud top height which we define to be the uppermost point at which half of the model columns are cloudy; (iv) $w_2 = \langle \overline{w'w'} \rangle^{1/2}$, is the square-root of the boundary layer averaged value of the vertical velocity variance and is thus a measure of the turbulence activity; (v) $\Delta\Theta_l$, a measure of the stability of the sub-cloud layer defined by the difference between $\overline{\theta}_l$ averaged over all completely cloudy layers, and $\overline{\theta}_l$ at the third model level. The statistics of \mathcal{L} and \mathcal{D} are relatively steady after the 4th hour, and are thus averaged over the period from hours 4-8. The other variables are averaged only over the last three hours.

Table 4.2: Sensitivity of selected statistics to different initial random perturbations in non-drizzling ERM-NM model at two resolutions (regular and half resolution). Given are the mean values and standard deviations from three realizations of the flow.

Integration	\mathcal{L}	Z_I	w_2	$\Delta\Theta_l$
CNTRL-NM	213 ± 7	934 ± 4	0.391 ± 0.017	0.410 ± 0.065
HLFRS-NM	216 ± 2	904 ± 4	0.337 ± 0.021	0.360 ± 0.038

Results are given in Table 4.1. Immediately apparent is the significant variability among the integrations. The standard deviations of \mathcal{D} and $\Delta\Theta_l$ are 20% of the mean, and the variation in \mathcal{L} , w_2 and Z_I is also appreciable. The highly intermittent nature of the drizzle production (see for instance the integrations of the previous chapter) contributes to the variability in most fields as the standard deviations of the statistics in the non-precipitating integrations are smaller (cf. Table 4.2), but perhaps not as dramatically as one would expect. As will be shown later much of the variability among realizations is due to the fact that the integrations are not approaching a statistically steady state, so that the ergodic hypothesis (which states that a time average can be substituted for an ensemble average) fails.

Because of the significant variability among the above simulations subsequent comparisons are based on normalized statistics; namely given some parameter x from an integration, we tabulate $x_* = (x - \bar{x})/\sigma_x$ where \bar{x} and σ_x are taken from Table 4.1. Consequently $|x_*|$ large implies that the difference between a simulation and the mean of the control runs is large relative to the standard deviation among the control runs. The results

Table 4.3: Normalized statistics from sensitivity runs

Integration	\mathcal{L}	\mathcal{D}	Z_I	w_2	$\Delta\Theta_l$	comment
CNTRL1	-0.5	-0.2	0.2	-1.1	1.1	
CNTRL2	1.2	-0.9	0.9	0.6	-0.7	
CNTRL3	-0.7	1.1	-1.1	0.5	-0.4	
RES1	-2.5	4.2	-2.5	-4.6	2.7	$2(\Delta x, \Delta z, \delta t)_{cntrl}$
RES2	-3.7	2.5	-1.1	-4.7	3.3	$2(\Delta z, \delta t)_{cntrl}$
RES3	-3.8	1.4	-0.1	-4.3	2.8	$2(\delta t)_{cntrl}$
DMN	1.2	0.7	0.0	0.1	1.0	Doubled domain size
SNDNG	-0.3	1.7	-0.3	-0.3	1.7	Moistened sounding
TURB	-1.4	0.6	-0.4	-0.2	0.6	No diffusion for drops
HALL	1.3	-2.0	0.7	2.0	-0.9	Halls kernel for collection
VENT	-0.5	-1.6	0.8	-0.5	1.7	Added ventilation effects

from all cases (including the control runs from which \bar{x} and σ_x are derived) are placed in Table 4.3, from which it is apparent that $|x_*| > 1.2$ is significant. The simulations are discussed in more detail below.

4.1.1 Sensitivity to grid spacing

The sounding specified in Eq. 4.1 is similar to the soundings produced by the “steady-state” ERM integrations in the previous chapter. Apart from small differences in the sounding and the method of computing radiative transfer the control runs differ from the steady-state ERM integrations of the previous chapter only in the characteristic shape (not concentration) of the CCN spectrum and in the choice of grid-spacing. To explore the effect of resolution we repeated a control simulation with double the grid spacing in both spatial dimensions and in time. This integration, designated as RES1 in Table 4.3, produced more drizzle, which significantly depletes the mean liquid-water path, generates more stability across cloud base and consequently less entrainment. In an attempt to understand what produced this behavior we returned the horizontal resolution back to its original value. An examination of RES2 suggests that this mitigated the differences in \mathcal{D} and Z_i , but aggravated the departures in $\Delta\Theta_l$, w_2 , and \mathcal{L} . RES3 for which only the time-step was doubled, produced results similar to RES2 although the increase in drizzle production was mitigated.

That the ERM-BM integrations are sensitive to resolution may, in retrospect, not be surprising, as the turbulent closure scheme is based on the properties of three-dimensional turbulence, for which there is an active cascade of energy to smaller scales. In dry ERM integrations increasing the resolution tends to increase the strength of the turbulence. This is because of a well known property of two-dimensional turbulence—the up-scale cascade of energy. The greater dynamic range in scales increases the separation between the energy containing scales and the dissipation scales, and thus the energy dissipation balances its production at a higher level of turbulent kinetic energy. To see this consider the dissipation term in the model. It comes about from forming the inner product between the velocity and the divergence of the sub-grid-stress:

$$u_i \frac{\partial \tau_{ij}}{\partial x_j} = \frac{\partial (u_i \tau_{ij})}{\partial x_j} - \epsilon, \quad \text{where} \quad \epsilon = \tau_{ij} \frac{\partial u_i}{\partial x_j} = \frac{1}{2} \tau_{ij} D_{ij}, \quad (4.3)$$

where D_{ij} is the deformation:

$$D_{ij} = \left(\frac{\partial u_i}{\partial x_j} + \frac{\partial u_j}{\partial x_i} \right)$$

and τ_{ij} is the sub-grid stress (proportional to an eddy diffusivity K):

$$\tau_{ij} = K D_{ij} \quad \text{where} \quad K \propto l_0^2 D \quad \text{and} \quad D \equiv |D_{ij}|,$$

and l_0 is a length scale proportional to the grid-scale. This all implies that $\epsilon \propto l_0^2 D^3$ so that for a given flow the dissipation will be constant as l_0 is changed (within an inertial range) so long as $D \propto l_0^{-2/3}$. In the inertial sub-range of three-dimensional turbulence, this scaling relationship is satisfied, e.g., see Lilly (1967). For this reason resolved properties of three-dimensional flow should not change as resolution is increased so long as l_0 is held fixed—hence, l_0 is sometimes called “the filter scale” which with appropriate choice of constants is usually made commensurate with the grid scale (Mason, 1994). In two-dimensional turbulence however, this is not the case as D falls off much more rapidly with inverse length-scale. For instance, if in analogy with three-dimensional turbulence we take $D^2 \propto k^3 E(k)$, where $E(k)$ is the energy density and k is an inverse length-scale (i.e.,

$k \propto l_0^{-1}$), we get $D \propto k^{-1}$ where for simplicity we have assumed¹ that the enstrophy range scaling for two dimensional turbulence is $E(k) \propto k^{-4}$. This leads to less dissipation for a given flow as the resolution is increased, i.e., $\epsilon \propto l_0^{7/2}$. Once the flow assumes a quasi-steady state (i.e., dissipation balances production) $\epsilon \propto l_*^{-1}(\text{TKE})^{3/2}$ where l_* is a length scale that characterizes the flow as a whole (not to be confused with l_0). Because in a *given* 2-D flow there is less dissipation for increased resolution, as resolution is increased a quasi-steady balance between TKE production and dissipation can only be formed for larger values of TKE. In other words, given that all the simulations are forced equally, at steady state (time invariant TKE) they will all have exactly the same amount of dissipation, since time invariant TKE implies a balance between production and dissipation and the former is fixed externally. However, given equal amounts of dissipation, the above arguments indicated that simulations with finer resolution will have more TKE as this is the only way for them to achieve the required rate of dissipation.

As a consequence of the above arguments we expect w_2 to decrease as the grid mesh is made coarser (this is well illustrated by comparing the statistics of the ERM-NM integrations in Table 4.2); however, this in turn leads to less entrainment. The fact that \mathcal{L} is lower and \mathcal{D} is larger (especially for experiments RES2 and RES3) implies coarse vertical resolution leads to the more efficient production of precipitation. This is consistent with the fact that larger vertical discretization in and of itself (as well as in combination with weaker turbulent circulations) results in smaller grid-averaged super-saturations, e.g, Stevens et al., (1996). Consequently fewer drops are activated, a broader spectrum is established, and the initial stages of drizzle production are enhanced. This effect appears to dominate the hypothesized decrease in drizzle production due to the lack of turbulent support for drizzle size drops in a weaker circulation (Feingold et al., 1996a). More drizzle in turn is a

¹Exactly how the energy spectrum scales is still controversial. On dimensional grounds one can argue that $E(k) \propto k^{-3}$, but this leads to a singularity which is removed through the corrected log scaling proposed by Kraichnan. Here $E(k) \propto k^{-3}(\ln(k))^{-1/3}$. Our choice of k^{-4} scaling is motivated by numerical experiments which tend to provide scaling laws with this exponent [see Bowman (1996) for a discussion of the current status of these issues]. Regardless, given energy spectral density scaling $E(k) = k^{-n}$, so long as $n > (5/3)$ the essence of our argument is unchanged.

positive feedback as it enhances the stabilization of the sub-cloud layer and suppresses w_2 . These results suggest that ERM simulations will be more sensitive to resolution changes when drizzle is active, than one would otherwise suspect. The fact that $\Delta\Theta_l$ is larger for RES2 despite it drizzling less than RES1 appears to be related to a warmer cloud layer in the former, commensurate with more entrainment and smaller values of \mathcal{L} . Notwithstanding that comparisons among sensitivity runs are difficult due to the limited sample set and the degree of variability in the integrations for any one particular configuration of the model.

Given these results perhaps a better name for the ERM is a LEM, a large eddy model. As opposed to an LES which (by definition) is a simulation of the large-eddies of boundary layer turbulence, an LEM is a crude model of large eddies, better perhaps than mean-field theories based on moment decompositions of the turbulence, or bulk models, it is still an imperfect attempt at modeling the behavior of high-Reynolds number boundary layer flows. With an appropriate choice of dissipation it is reasonably able to predict the evolution of a narrow range of scales, and to the extent that the evolution of the flow is dependent on this narrow range of scales it should do a reasonable job at predicting the evolution of the flow as a whole. Two-dimensional models are, however, limited by the fact that increasing the resolution does not necessarily improve the representation of the turbulence, although it might be necessary to resolve sharp features in the flow (i.e., the inversion). Despite its limitations, for the case of convectively-forced flow, two-dimensional models often do a good job in predicting, at least qualitatively, what will happen in three dimensions. For this reason, the use of two-dimensional models is appropriate in sketching the contours of the solution space in advance of more computationally intensive LES and DNS (direct numerical simulations).

4.1.2 *Sensitivity to domain size*

DMN represents an integration identical to CNTRL1 except for the fact that the horizontal size of the domain was doubled. The absence of substantial departures in the statistics, when compared to the variability amongst the control runs, suggests that the size of our domain is not impacting the nature of our solutions. We shall later see that

this result does not hold in general as more strongly drizzling cases exhibit a significant sensitivity to domain size, at least with respect to the qualitative structure of the flow.

4.1.3 Sensitivity to turbulence closure model

The turbulence closure model (for scalars and momentum) is based on the assumption that the collective effect of sub-grid scale processes can be represented by diffusion using eddy-diffusivities diagnosed based on the properties of the resolved flow. Such an approach effectively smoothes out quantities on the grid-scale. It is well justified for variables conserved in a Lagrangian sense (i.e., following the motion of a fluid parcel) but is questionable for non-conservative variables (i.e., liquid water and potential temperature are not conserved along a moist-adiabat). By requiring the sub-grid diffusion term to represent the collective effect of all sub-grid processes (i.e, not just mixing by small-scale motions, but condensation as well), and assuming that the phase relaxation time of drops is zero, one can represent the turbulent flux of non-conserved quantities (such as q_l and θ) in terms of the turbulent flux of conserved quantities. Consequently, simple cloud models often partition the liquid water into two bins: a cloud-water category, q_{cw} , assumed to move with the turbulent motions and adjust to the ambient saturation vapor pressure infinitely fast, and a rain-water category, q_{rw} , assumed to have sufficient inertia to be independent of small scale motions (Krueger, 1985). So doing allows one to neglect the effect of sub-grid motions on q_{rw} while representing the sub-grid flux of cloud water as $(\overline{w'q'_{cw}})_{sgrid} = a(\overline{w'\theta'})_{sgrid} + b(\overline{w'q'_t})_{sgrid}$, where a and b are thermodynamic constants depending on the mean state (Deardorff, 1976).

In our model, the liquid water is partitioned into 25 size bins, and no *qualitative* differentiation is made between bins. Liquid water in each bin is assigned a fall velocity based on the average size of the drops in that category, and every attempt is made to accurately predict the finite phase relaxation times of liquid water. While one could imagine developing a rather complex parameterization scheme which would account for phase relaxation times and drop-inertial effects it seems worthwhile to first ask how sensitive are the results to the details of the representation of the sub-grid fluxes of liquid water. In sensitivity test TURB we set the sub-grid fluxes of liquid water to zero for the duration

of the integration; so doing indicates that the results are not obviously sensitive to the manner in which $(\overline{w'q'_{cu}})_{sgrid}$ is specified. Consequently, we shall not (at this time) pursue the matter further.

4.1.4 Sensitivity to kernel

The quasi-stochastic collection equation

$$\frac{\partial n(x, t)}{\partial t} = \frac{1}{2} \int_0^x n(x-y, t)n(y, t)\mathcal{K}(x-y, y)dy - n(x, t) \int_0^\infty n(y, t)\mathcal{K}(x, y)dy \quad (4.4)$$

describes the time rate of change in the droplet spectral distribution function $n(x, t)$ due to binary drop interactions. The kernel $\mathcal{K}(x, y)$, which is a measure of the probability that two drops of respective masses x and y will collide and coalesce, is formulated on the basis of a gravitational collection mechanism:

$$\mathcal{K}(x, y) = \pi [r(x) + r(y)]^2 E_c(x, y)E_s(x, y) |V_T(x) - V_T(y)| \quad (4.5)$$

where $r(x)$ and $V_T(x)$ are respectively the radius and terminal velocity of a drop with mass x . The collision and coalescence efficiencies, $E_c(x, y)$ and $E_s(x, y)$ respectively, are empirically—or theoretically—determined mappings of (x, y) to the interval $[0, 1]$. In solving the above equation we numerically integrate Eq. 4.4 assuming a kernel which is piecewise bilinear over each bin pair. So for interactions involving drops of size $x \in (x_i, x_{i+1})$ and $y \in (y_j, y_{j+1})$ the kernel takes the form $\mathcal{K}(x, y) = (x + y)\mathcal{K}_{ij}$. This relation implicitly defines \mathcal{K}_{ij} as the $(x + y)^{-1}$ weighted kernel averaged over bins (x_i, x_{i+1}) and (y_j, y_{j+1}) . Given E_s and E_c it is straightforward to compute. Generally we calculate \mathcal{K}_{ij} following Long (1974) where E_s is taken to be unity and E_c is varied according to a functional fit to experimental data. In experiment HALL we calculate \mathcal{K}_{ij} differently—a piecewise linear fit to the collection efficiencies tabulated by Hall (1980) is used. Defining $\mathcal{K} = \sum_i \sum_j \mathcal{K}_{ij}$, we find that for summations over all bins containing drops of diameters less than $80\mu\text{m}$, $\mathcal{K}_{Long}/\mathcal{K}_{Hall} \approx 1.08$. Given the limited amount of empirical data, and largely theoretical nature of the kernels, and their lack of consideration of turbulent effects, we take this difference as a conservative measure of the uncertainty involved in formulating any set of values of $\mathcal{K}(x, y)$. Comparing experiment HALL with the control run indicates

that for this particular case, small uncertainties in the specification of the kernel can produce significant changes in the statistics of the integration.

4.1.5 *Sensitivity to ventilation effects*

Prior to this point the ventilative enhancement of the vapor and heat diffusion from falling precipitation drops has been neglected. Due to these effects drops with diameters greater than $80 \mu\text{m}$ begin to see a significant enhancement in their evaporation times, with the largest drops represented by our model (of order $800 \mu\text{m}$) evaporating up to five times as fast as they would if ventilation effects were not accounted for. To examine the effect of enhanced evaporation from precipitating drops we included the effect as per the description in Appendix 3. The integration with ventilative effects included is called VENT. The primary difference between this and the control integration is in accord with ones intuition; more drizzle evaporates in the sub-cloud layer, leading to greater stabilization, and less precipitation at the ground.

4.1.6 *Sensitivity to sounding*

To help put our results in perspective we repeated the control integration with a 1% moister sounding (i.e., the total water mixing ratio was uniformly increased by 0.1 g kg^{-1}). The results from the integration are tabulated under the SNDNG heading in Table 4.3. The increased water in the initialization has a significant effect on the amount of precipitation produced during the integration which in turn results in more stabilization of the sub-cloud layers. Given these systematic effects the lack of significant change in w_2 , Z_I and \mathcal{L} is surprising. Nonetheless, these results suggest that attempting to match simulated and observed surface drizzle fluxes may be difficult to do with any precision.

4.2 *Sensitivity to CCN concentrations*

Herein we systematically address Pincus and Baker's hypothesis: Given a thermodynamic sounding how does the attracting state or time-evolving boundary layer differ as a function of CCN concentrations. In order to force a greater correspondence between temporal and ensemble averages we halved the value of F_0 in Eq 4.2. So doing results

in cooling rates of less than 5.5 K in the top 25 meters of the cloud, but does generate more slowly evolving integrations with less variability among similarly configured simulations; e.g., compare experiments CCN150A and CCN150B in Table 4.4 which differ only in choice of initial random seed.

Table 4.4: Sensitivity of selected statistics to different initial random perturbations, and choice of kernel. Mean values over last ten hours of a fifteen hour integration. Symbols as in previous tables except for dZ_i/dt which is the rate at which the 292 K θ_l surface moves in mms^{-1} .

Integration	\mathcal{L}	\mathcal{D}	dZ_i/dt	w_2	$\Delta\Theta_l$
CCN150A	157.5	8.6	1.4	0.224	0.464
CCN150B	154.2	9.0	1.1	0.223	0.457
CCN150-HALL	172.6	5.8	1.4	0.236	0.410

In total we examine 7 integrations with fixed CCN mixing ratios ($\#$ per mg dry air, which is equivalent to $\#$ per cm^{-3} when the density of air is 1 kgm^{-3}) as given by the following sequence $\{7, 20, 50, 150, 450, 750, 1500\}$. Each experiment is given the name CCNX where “X” is the appropriate CCN mixing ratio. All integrations include the ventilative enhancement of evaporation from precipitation sized drops, as this effect was shown to be physically significant. We use Long’s kernel in the equations for quasi-stochastic collection. Our previous results (corroborated by another sensitivity study, e.g., Table 4.4) indicate that this kernel favors the production of precipitation relative to Hall’s kernel, but does not dramatically alter the qualitative aspects of the simulations. In §4.2.1 we examine some time-sequence data and snap-shots of a representative subset of the experiments. In §4.2.2 we analyze mean profiles and turbulent budgets and thermodynamic fluxes over a range of precipitation efficiencies. In §4.2.3 we discuss results of the full suite of sensitivity runs using a set of tabulated statistics chosen to summarize how properties of the cloud-topped boundary layer depend on precipitation efficiency.

4.2.1 Time-sequences and snap-shots

In Fig. 4.1 we show selected time-sequences from experiments CCN20, CCN150B and CCN750; this figure was constructed to illustrate how certain bulk properties of the

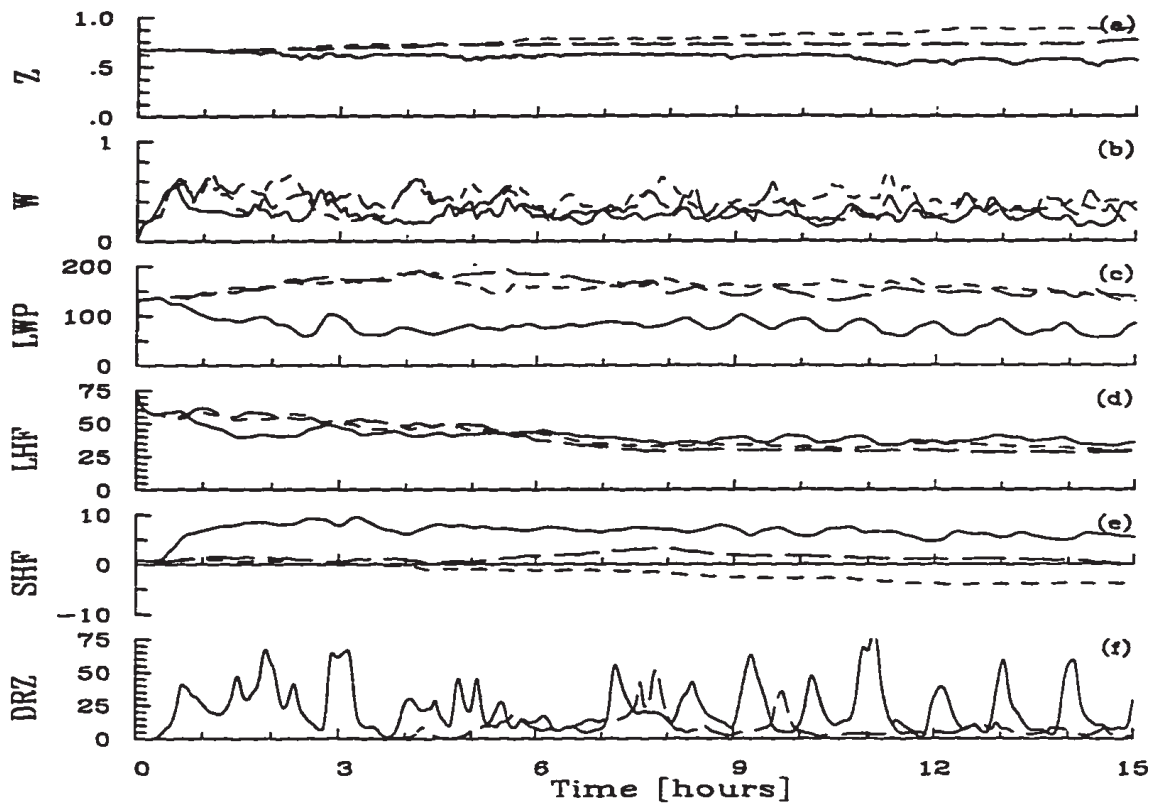


Figure 4.1: Scalar time sequences from experiments CCN20 (solid), CCN150(long dash) and CCN750 (short dash). (a) Cloud top height (km); (b) maximum value of $(\overline{w'w'})^{1/2}$ (ms^{-1}); (c) Domain averaged $LWP \text{ g m}^{-2}$; (d) Surface latent heat flux (Wm^{-2}); Surface sensible heat flux (Wm^{-2}); (e) Surface drizzle flux (Wm^{-2}).

integrations depend on precipitation efficiency. For instance, in accord with the results from the previous chapter [as well as ERM integrations (Feingold et al., 1996a) and third-order closure modeling citeWangS:1994] increased drizzle is associated with reductions in both LWP and w (although the reduction in the latter is not obvious from the plot). Drizzle again increases the stabilization of the sub-cloud layer (with respect to the cloud), but in so doing strongly affects the surface enthalpy fluxes. In the strongly drizzling case (CCN20) drizzle fluxes largely offset surface latent-heat fluxes in the time mean. While among simulations there are quantitative differences in the surface latent and sensible heat fluxes, actually change sign (from negative to positive) as drizzle becomes more prevalent. This indicates that drizzle substantially cools the sub-cloud layer, destabilizing it with respect to the surface while stabilizing it with respect to the cloud layer, while the latter effect has been anticipated (Brost et al., 1982b; Paluch and Lenschow, 1991) the former effect has, to our knowledge, not been discussed. As drizzle is reduced entrainment warms

the boundary layer as a whole and stabilizes both the sub-cloud layer with respect to the surface, as well as the cloud layer with respect to the sub-cloud layer.

Snapshots of experiment CCN20 (Fig. 4.2) reveals more cumulus-like flow structures, where the velocity field is dominated by a single surface-forced updraft compensated by a large region of subsidence. The capping inversion has the characteristics of a low-lying trade inversion that caps the convection and forces the detrainment into a stratus or anvil like layer in the upper portion of the boundary layer. Drizzle (measured here by the 0.02 gkg^{-1} contour) extends to the surface, and is co-located with the updraft. Conservative variables (i.e., θ_l and q_t) are not well mixed; although the manner in which the cumulus attempts to mix the boundary layer is clearly evident. In contrast snapshots of the non-drizzling integration (Fig. 4.3) show a deeper boundary layer with a more stratus-like layer. Eddies are more numerous with up-drafts and down-drafts of commensurate strength centered near cloud base. A deep well-mixed layer is formed, but does not extend to the surface. The lack of activity in the sub-cloud layer is a consequence of the fact that this layer is stable with respect to both the surface and the cloud layer.

Animating such a sequence of snapshots embellishes the qualitative picture developed so far. In strongly drizzling integrations eddies become increasingly surfaced forced and are predominantly confined to the sub-cloud layer. Moist surface-forced eddies which occasionally penetrate into the cloud layer reach their level of condensation well below the local cloud base as defined by the region of detrained stratus. Their rise up into the cloud layer thus causes local enhancements in liquid water and subsequent precipitation. Cumulus eddies have the character of intermittent plumes launched from a sub-cloud layer and compensated for by a broad region of subsidence in the cloud layer—although directly adjacent to the plume anomalously strong down-drafts may be induced. Precipitation tends to originate and remain in shafts co-located with or just downstream of (the geostrophic wind is 2 ms^{-1} from right to left on these plots) side of the cumulus updraft, while entrainment is favored upstream of the convection (although this is not very evident in Fig. 4.2). In non- or weakly-drizzling integrations eddies initially mix through the whole layer, but as the boundary layer deepens mixing becomes increasingly confined to

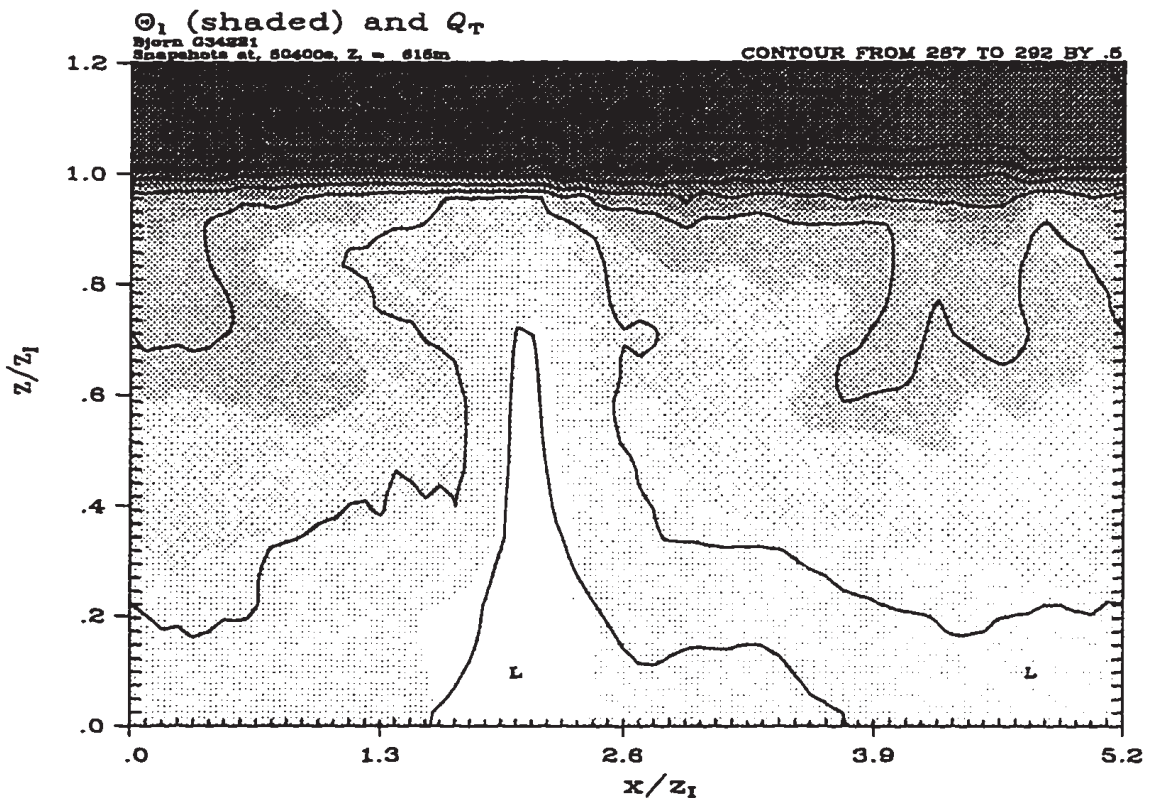
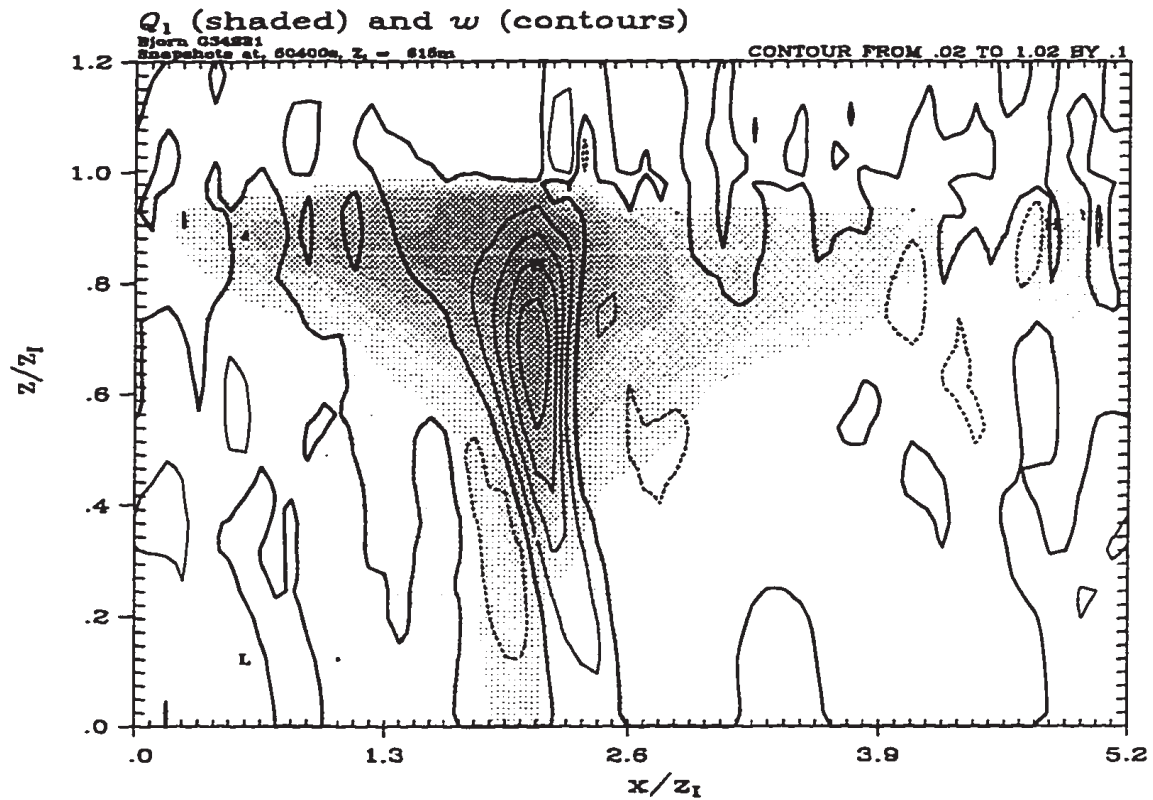


Figure 4.2: Snapshots of flow structure from experiment CCN20 at 14 hours. Upper panel: liquid water mixing ratio (gkg^{-1}) shaded and from 0.02 to 1.02 in 0.1 gkg^{-1} increments. w contoured from -1 to 1 ms^{-1} in ten increments, thick line is zero contour. Lower panel: θ_l shaded from 287-292 K in 0.5 K increments and total-water mixing ratio contoured from 7-11 (gkg^{-1}) in ten increments with thick line denoting the 9 gkg^{-1} contour. Spatial dimensions normalized by inversion height: $Z_I = 615 \text{ m}$.

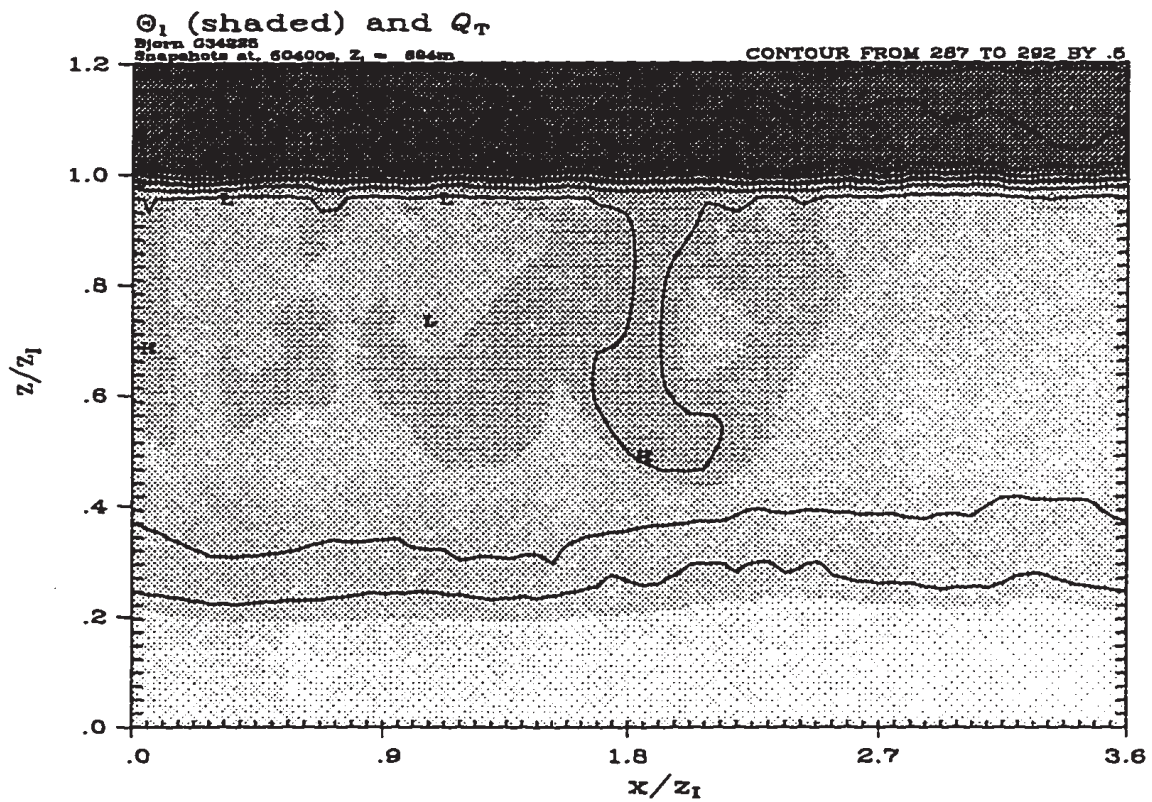
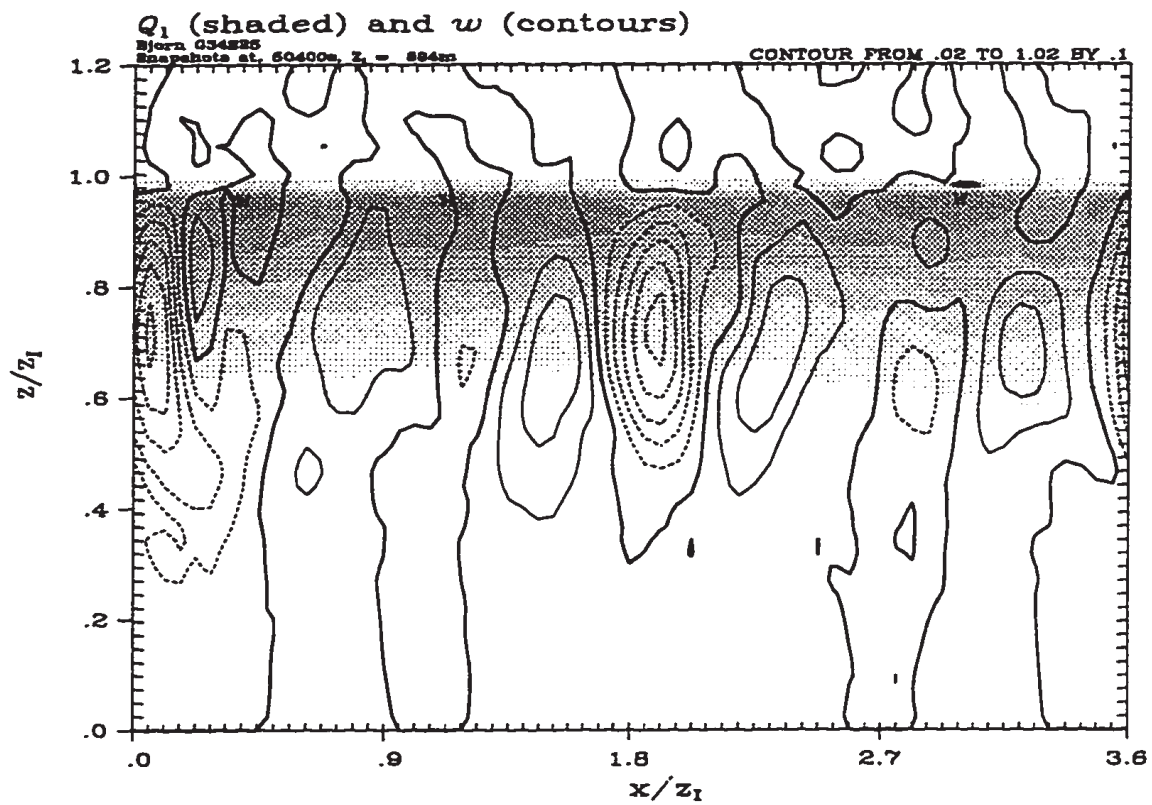


Figure 4.3: As in previous figure but for experiment CCN750; $Z_1 = 894$ m.

an upper mixed layer distinct from the sub-cloud layer. Cloud base is relatively uniform and the cloud maintains a more stratus like character. Consequently if cloud can produce precipitation efficiently, drizzle may be sufficient to maintain a cool-unstable (with respect to the surface) sub-cloud-layer and a warmer cloud-layer, where unlike the strongly entraining boundary layer, we believe that most of the cloud-layer warming is associated with compensating subsidence. Eventually, the upper cloud layer becomes too warm to support stratocumulus and the boundary layer is transformed into a more trade-cumulus like structure.

4.2.2 Mean profiles, fluxes, and budgets

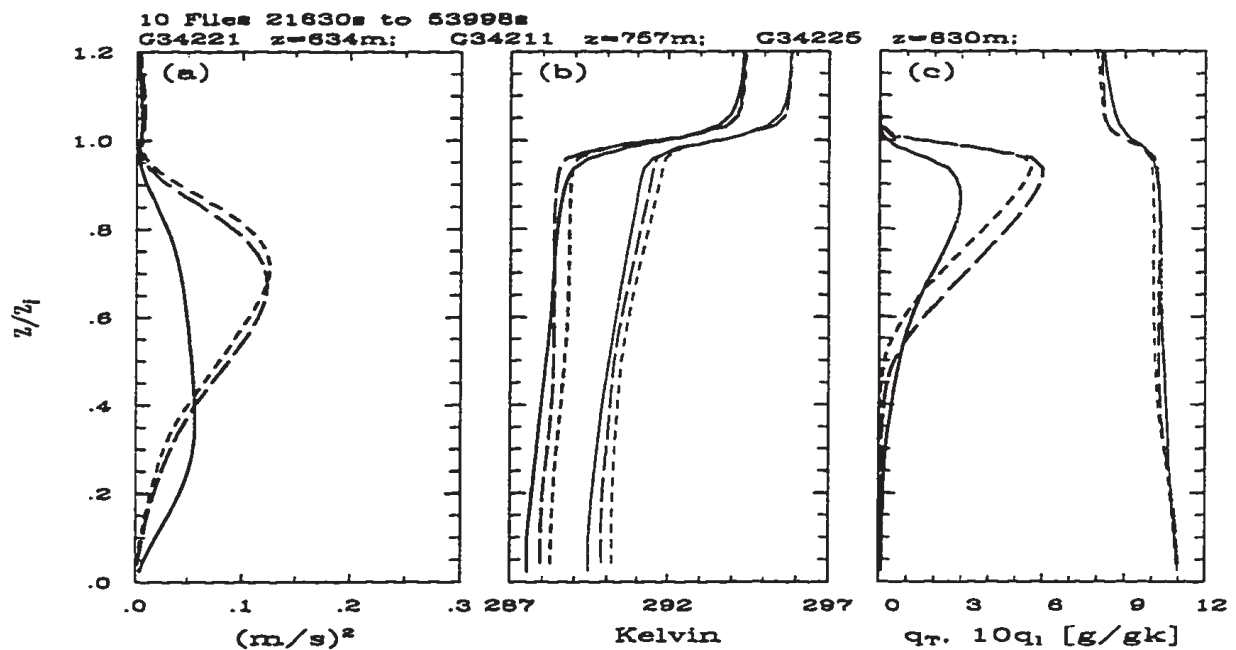


Figure 4.4: Comparison of various mean quantities for experiments CCN20 (solid line), CCN150 (long dash) and CCN750 (short dash): (a) $\overline{w'w'}$; (b) θ_i (thick lines) and θ_v (thin lines); (c) $q_l \times 10$ (thick lines) and q_t (thin lines).

Fig. 4.4-4.6 are compiled from averages taken over the last ten hours of the simulations. Data are collected every 30s and averaged together on one hour intervals. Hourly averaged data are then used to define the height of the inversion (chosen to be the 292 K θ_i surface) and mapped to a normalized grid. Ten hourly-averaged and normalized data sets are averaged together to form the plots given in the figures. Again in these figures we only compare a subset of the experiments (i.e., experiments CCN20, CCN150 and CCN750);

an examination of all the data sets indicates that these well capture the range of simulated behavior.

A progressive reduction in $\overline{w'w'}$ is associated with increasing amounts of drizzle (see Fig. 4.4). Moderate amounts of drizzle don't appear to qualitatively affect the structure of the boundary layer, but sufficiently strong drizzle can affect qualitative changes. In terms of mean profiles this is evidenced by a less-well-mixed cloud layer and a more stabilized (with respect to the cloud layer) sub-cloud layer as well as changes in the *shape* of the $\overline{w'w'}$ and q_l profiles. The drizzle rate is sufficient to affect this change once it is able to maintain a sub-cloud layer destabilized with respect to the surface. Because the local maxima in liquid water in both Figs. 4.2 and 4.3 are similar the reduction in mean cloud water is predominantly a reflection of the reduction in cloud fraction. The idea that increased precipitation efficiency may reduce cloud fraction was first suggested by Albrecht (1989). This idea receives support from this set of simulations, although the integrations of boundary layers more characteristic of the trade-cumulus boundary layers discussed by Albrecht (cf. Chapter 3) do not support it.

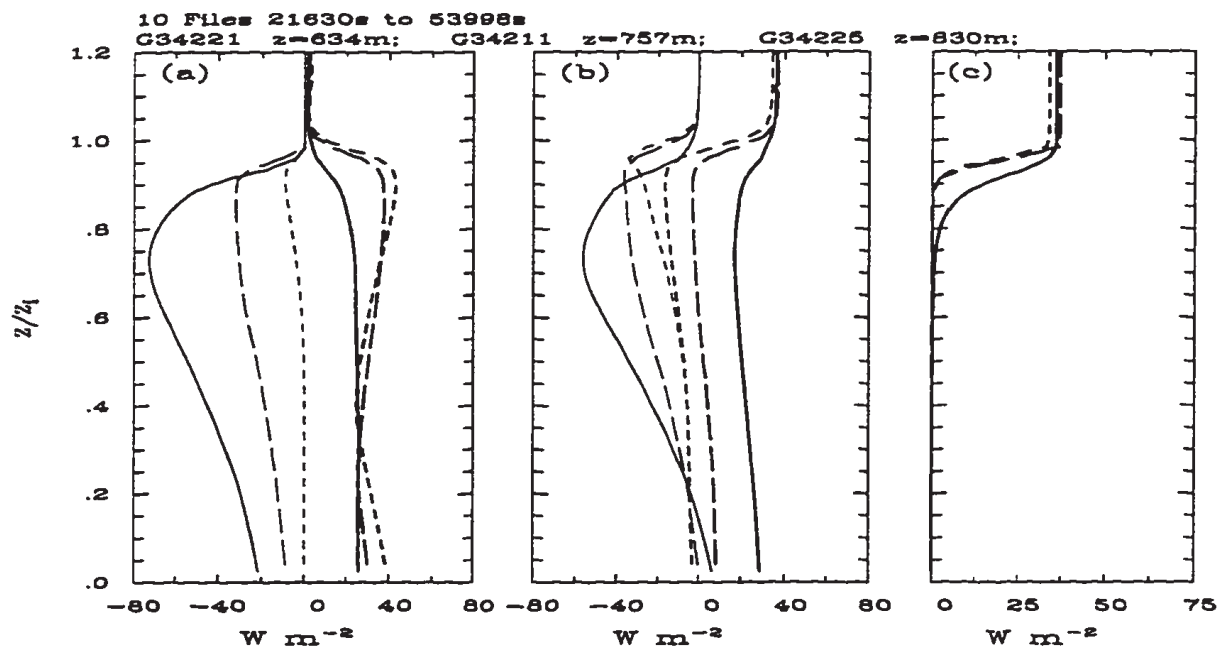


Figure 4.5: Comparison of various fluxes for experiments CCN20 (solid line), CCN150 (long dash) and CCN750 (short dash): (a) F_Q (thick lines), drizzle flux (thin lines); (b) F_Θ (thick lines) and $\overline{w'\theta_l}$ (thin lines); (c) Radiative flux minus radiative flux at ground.

Fluxes affecting the evolution of θ_l and q_l are plotted in Fig. 4.5. In none of the experiments are F_Q and F_Θ constant (or linear) with height, although this characteristic of a steady- (or pseudo-steady) state is most nearly approximated in experiment CCN20. If one measures decoupling by a local flux minimum, increasing drizzle leads to less decoupling, in contrast to the conclusion one would get by correlating decoupling with stabilization (i.e., recall the θ_l profiles in Fig. 4.3). As the boundary layer entrains the mean mixed layer value of θ_l increases, and the surface (held at a fixed temperature) increasingly becomes a stabilizing effect. As the boundary layer deepens the source of turbulence also becomes further removed from the surface, allowing a stable sub-cloud layer to develop. Stabilization of the sub-cloud reduces² surface latent-heat fluxes although total water mixing ratios in the sub-cloud layer are about equal among simulations (Fig. 4.3c). Despite similarities in \bar{q}_l the role of the sub-cloud layer is a strong function of precipitation efficiency: in strongly precipitating boundary layers, turbulence generated in the sub-cloud layer (by enhanced surface buoyancy fluxes) mixes moisture off the surface, through the sub-cloud layer, and into the cloud layer; in weakly precipitating situations dry air is mixed down into a relatively quiescent sub-cloud layer by turbulence generated in the cloud layer.

Drizzle fluxes are ultimately limited by the ability of turbulence to supply water to a stratocumulus layer, or to generate cumulus convection. In the ERM integrations drizzle fluxes increase with increasing precipitation. Near cloud top $\overline{w'w'}$, is considerably reduced as precipitation increases. However, circulations appear to maintain, or increase, their strength at low levels, thereby more efficiently bringing moisture to the cloud layer. Consequently, because enhanced drizzle is associated with more efficient (e.g., larger turbulent fluxes) circulations at mid-levels larger drizzle fluxes are allowed as drizzle forms more efficiently. Were this not the case variations in F_Q would be commensurate with those in F_{drz} . Among simulations F_Θ has a similar shape, albeit different magnitudes reflecting large differences in entrainment rates (i.e., $w_e \Delta\theta_l \approx F_\Theta$ where $\Delta\theta_l$ is the jump in θ_l across

²The flux of liquid water due to turbulent motions can be constructed by subtracting the drizzle flux from F_Q in Fig. 4.5.

the inversion which is nearly constant in all experiments). The fact that all simulations maintain a similar shape (which is nearly linear thereby approaching a quasi-steady state) suggests that within the boundary, *once the characteristics of the sub-cloud layer have been established*, the turbulent flux of θ_l , i.e., $(w'\theta_l)_{turb}$, largely compensates for the warming or cooling associated with a divergence or convergence in the drizzle flux.

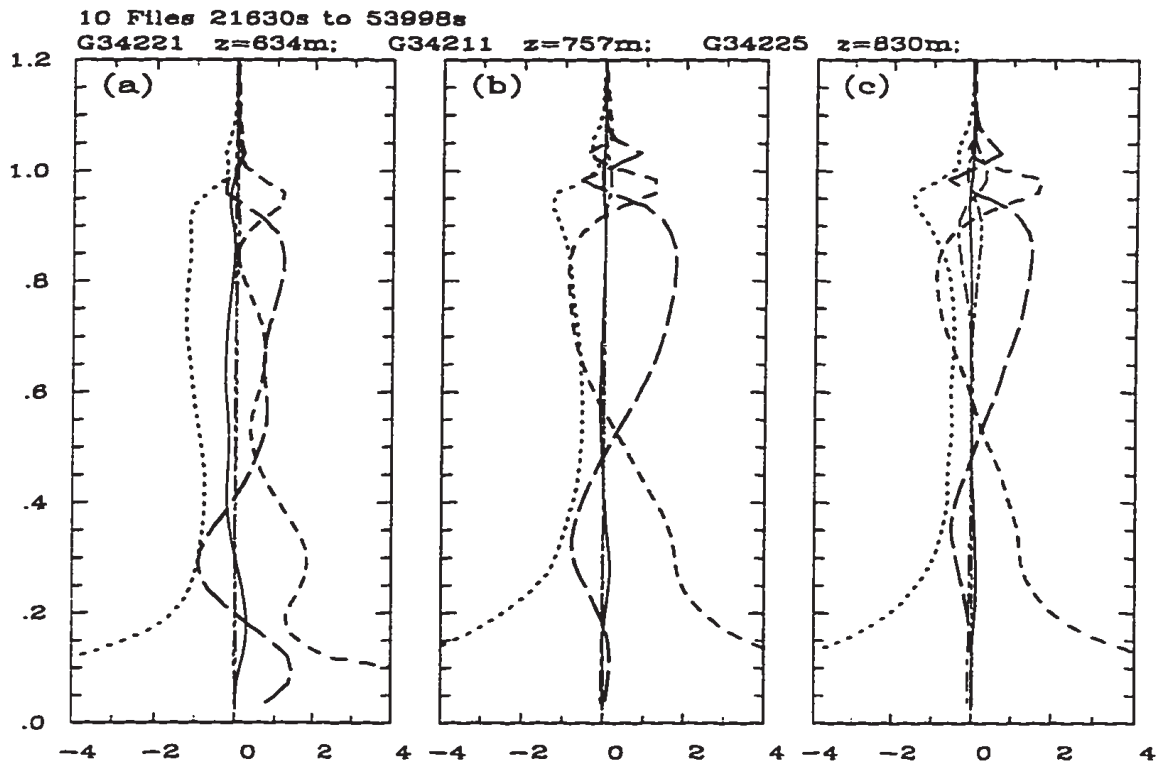


Figure 4.6: Comparison of various TKE budgets for experiments CCN20 (a); CCN150 (b); and CCN750 (c). Shear production term (solid line), Buoyancy production (long dash), transport (short dash), dissipation (dotted), accumulation (dash-dot), residual (dash-dot-dot). Units are $\text{cm}^2 \text{s}^{-3}$.

TKE budgets also show that drizzle is associated with (and probably causes) a reduction in buoyancy generation of TKE within the cloud layer, and when sufficient (e.g., compare Fig. 4.6a and 4.6b) can lead to a significant (even dominant) source of TKE within a convective sub-cloud-layer maintained unstable by the low-level convergence in the drizzle flux. As drizzle increases, instantaneous values of the maximum domain-integrated buoyancy flux diminish in the cloud layer and increases in the sub-cloud layer. These changes reflect changes in the basic state thermodynamic profiles, and explain the

changed shape of the $\overline{w'w'}$ profile. The depth of the stable sub-cloud layer also modulates the depth of the shear zone, as surface forced convection doesn't allow shear to develop over as deep a layer. In simulations with little or moderate drizzle, the region of negative buoyancy flux begins below cloud base and absorbs up to a third of the energy created in regions of positive buoyancy flux. Moreover the time-averaged BFR (buoyancy flux ratio) is more variable among simulations than is the case for the integrations of Chapter 3. In all the experiments shear contributes negligibly to the TKE budgets. This is because the mean winds are strong only in the cross-domain direction. This allows strong surface winds to contribute to an increase ventilation of the surface but not influence the TKE budget directly. Such an unrealistic result illustrates an important limitation of the ERM integrations.

During the course of the integrations we sample the domain to find the maximum magnitude of w at each time. These values are commensurate among simulations indicating that w_{max} is not a strong function of drizzle in the ERM. The fact that the maxima of w and q_l are relatively insensitive to the processes that lead to significant reductions in $\overline{q_l}$, $\overline{w'w'}$, and $\overline{\theta'_v w'}$ suggests that reductions in the latter may be due primarily to the changing nature of the circulations as opposed to their strength. This idea is posed more appropriately as a question: is the reduction in buoyancy flux is merely a reflection of the diminishment of eddy activity as multiple circulations within the stratocumulus layer are replaced by single cumulus cells over a limited area?

4.2.3 *Scalar statistics*

Data from all the CCN sensitivity experiments are collected in Table 4.5. The tabulated experiments suggest a clear mechanism through which drizzle modifies the boundary layer on moderate time-scales; although the integrations do not generate true steady-states (a point we address further in the next section) they do bear directly on the Pincus and Baker hypothesis.

For the moment we will exclude the limiting experiments (i.e, experiments CCN20 and CCN ∞) from the discussion. Among the remaining experiments the one with 450 CCN per mg of dry air is particularly interesting. For this particular sounding, the drizzle

Table 4.5: Sensitivity of selected statistics to different CCN concentrations. Tabulated data is the time average of the instantaneous domain averages collected every 30 seconds over last ten hours of a fifteen hour integration. Included are: vertically integrated liquid water \mathcal{L} in gm^{-2} ; \mathcal{P}_{sml} pressure (in hPa) for which parcels containing the mean mixed-layer thermodynamic properties become saturated; the height of the $\theta_l = 292$ K surface; dZ_i/dt , rate of change in inversion height in mms^{-1} ; w_2 , square-root of mean variance; $\Delta\theta_l$ difference in θ_l between cloud layer and value at 37.5 m; \mathcal{D}_{srf} , drizzle flux at surface in Wm^{-2} ; \mathcal{D}_{max} , maximum drizzle flux at any level; LHF the surface latent heat flux in Wm^{-2} ; SHF the surface sensible heat flux in Wm^{-2} . * indicates use of 4329 random seed, † indicates use of 11111 random seed, all other experiments use random seed of unity. CCN = ∞ implies the use of the ERM-NM

CCN	\mathcal{L}	Z_i	\mathcal{P}_{sml}	dZ_i/dt	w_2	$\Delta\theta_l$	\mathcal{D}_{srf}	\mathcal{D}_{max}	LHF	SHF
7	27.6	608	992	-2.35	0.15	1.28	16.6	45.4	34.3	4.8
20	77.3	636	994	-1.49	0.20	0.82	20.7	76.4	38.0	6.5
50	105.9	662	992	-1.04	0.19	0.57	18.6	60.9	33.8	5.5
150	157.5	750	992	1.35	0.22	0.49	8.6	36.1	31.7	1.5
150*	154.3	755	992	1.62	0.22	0.46	9.0	36.3	31.3	1.5
450	165.3	829	984	3.69	0.24	0.43	0.1	15.2	33.5	-2.4
750	156.7	839	982	4.12	0.25	0.48	.0	11.0	34.4	-2.7
1500	147.7	840	982	4.02	0.23	0.49	.0	7.1	32.9	-2.7
∞	121.1	853	980	4.40	0.20	0.66	.0	0.0	30.2	-2.7
∞^*	124.1	852	980	4.06	0.20	0.61	.0	0.0	29.8	-2.7
∞^\dagger	110.3	850	980	3.81	0.19	0.67	.0	0.0	28.1	-2.3

rates that develop maximize³ \mathcal{L} and w_2 while minimizing $\Delta\theta_l$. What is happening? Our hypothesis is that drizzle formation stabilizes the sub-cloud layer, reduces the buoyancy flux and diminishes entrainment through a reduction of $\overline{w'w'}$ particularly near cloud top. Given the nature of the sounding, the cloud deepens under enhanced entrainment until the boundary layer reaches a certain depth, after which further entrainment leads to a thinning of the cloud. This is evident in time-sequences of LWP (see the plot for experiment CCN750 in Fig. 4.1); LWP peaks after several hours and slowly declines thereafter. If drizzle is insufficient the boundary layer continues deepening until cloud begins to thin.

What about the more heavily drizzling boundary layers? Is the reduction in LWP due to a change in the mean properties of the mixed layer, or is it due to the redistribution of

³Our earlier sensitivity analysis suggests that differences between w_2 in experiments CCN450 and CCN750 is probably not significant.

the moist-enthalpy by drizzle so that cool-moist air underlies warmer and dryer air? It is clear that drizzle leads to a relative lowering of Z_i , but this effect is partially compensated for by the fact that less entrainment leads to a moister and cooler boundary layer, thereby allowing cloud base to lower. By comparing Z_i and \mathcal{P}_{sml} (the saturation pressure for a parcel with the boundary-layer *mean* thermodynamic properties) we find that cloud base in experiment CCN20 is approximately 100 m lower (i.e., \mathcal{P}_{sml} is 10 hPa larger) than in experiment CCN450, a difference more than offset by the 200 m change Z_i . The ratio of LWPs of the mixed layer equivalents⁴ of experiments CCN20 and CCN450 is 0.64, compared to an actual ratio of 0.47. This means that nearly a third of the 50% reduction in simulated LWP is due to an increased separation between the properties of the cloud layer and sub-cloud layers. Consequently, drizzle reduces cloud LWP not only by a lowering of cloud top (something that a less rapid lowering of cloud base partially mitigates) , but also through a redistribution of heat and moisture within the boundary layer. The latter effect is significant and completely unaccounted for by mixed layer models.

While the above arguments suggest how drizzle impacts \mathcal{L} . what about its effect on w_2 and $\Delta\Theta_l$? It turns out that with respect to the former, increased drizzle relative to experiment CCN450 leads to a reduction in w_2 in the cloud layer directly through a reduction in the buoyancy flux. The reduction in w_2 for experiments with less drizzle than CCN450 is interesting, and again is related to the effects of internal stabilization. The more rapidly entraining solutions tend to develop more sub-cloud stabilization (cf. increased values of $\Delta\Theta_l$ with decreasing drizzle after experiment CCN450); in addition, small amounts of drizzle deposited in the transition layer, or any convexity in the drizzle flux profile, will destabilize this layer with respect to layers below it, thus allowing a deeper region of buoyancy production for small amounts of drizzle. So while $\overline{w'w'}$ may be larger within the cloud layer (for less drizzle), the increasing stabilization of the sub-cloud layer (both with respect to the surface and the cloud layer) with decreasing drizzle leads to a smaller value of w_2 when $\overline{w'w'}$ is averaged over the boundary layer as a whole.

⁴This is the LWP that would result if the boundary layer was to become instantaneously well mixed.

This trend, whereby after a certain point less drizzle leads to reductions in w_2 , \mathcal{L} and an increase in Z_i is even evident when comparing three CCN ∞ experiments with experiment CCN1500, suggesting that at least in two-dimensional integrations very small amounts of precipitation can have a noticeable effect on the evolution of the cloud layer.

What about the extreme experiments? Why does a comparison of experiment CCN20 and CCN7 not yield similar conclusions to those produced by a comparison of experiment CCN50 and CCN20? If drizzle forms too efficiently, clouds will not be able to develop beyond a certain point. In a sense they will collapse under the weight of their own liquid water (the liquid-water-path ratio between experiments CCN7 and CCN20 is about 0.36 compared to a value of 0.50 between experiment CCN20 and CCN150). Johnson (1982) used a parcel model to show that the precipitation produced by ultra-giant CCN begins to decrease due to the fact that the amount of time drops spend in cloud (and hence the amount of precipitation they collect) depends on how rapidly they grow. Drops that grow too large too rapidly will never attain heights sufficiently distant from cloud base to generate maximal precipitation—an effect which could be deduced from E.G. Bowen’s (1952) pioneering study of warm rain processes. While this effect mitigates the generation of large values of \mathcal{L} and \mathcal{D} , it does not allow for the generation of more buoyancy as cloud development is curtailed. Moreover, the rapid generation of precipitation reduces the amount of evaporation that takes place in the cloud layer, leading to more net heating there. Although $\Delta\Theta_l$ is larger in experiment CCN7 (relative to experiment CCN20) sensible heat fluxes are less. Consequently the amount of stabilization between the cloud and sub-cloud layers is more strongly influenced by heating in the cloud layer than it is by cooling in the sub-cloud layer.

4.3 Subsequent sensitivity studies

Our results from the previous section suggest a number of other sensitivity studies. Here we pursue two: The first re-examines the issue of domain size sensitivity, this time for a strongly drizzling case. The second looks at how our results are affected by a change in the thermodynamic properties of the free troposphere. Results are tabulated in a form identical to the previous section (see Table 4.6)

Table 4.6: Sensitivity of selected statistics to a larger domain size and different free atmospheric properties. Tabulated data is of the same type as in previous table. Experiment “Big Domain” is the same as the 20 per mg experiment of the previous section, but with the horizontal domain size increased from 64 (3km) points to 194 (9.7km) points. Experiments D50 and WD50 are both experiments with the 50 CCN per mg, the former differs from experiment CCN50 in that the free troposphere is dried 2 gkg^{-1} , the latter also has the free troposphere warmed 2K.

Name	\mathcal{L}	Z_i	\mathcal{P}_{sml}	dZ_i/dt	w_2	$\Delta\Theta_l$	\mathcal{D}_{srf}	\mathcal{D}_{max}	LHF	SHF
Big Domain	66.3	627	992	-1.78	0.18	0.85	24.8	62.6	36.3	6.0
D50	66.7	773	978	1.95	0.23	0.48	1.4	31.7	40.1	-0.0
WD50	72.9	729	982	1.64	0.23	0.37	1.2	33.3	42.6	0.0

4.3.1 Sensitivity to domain size

Experiment “Big Domain” should be compared with experiment CCN20 in the previous section. Apparently the size of the domain does not qualitatively affect the nature of our statistics, although the changes are larger than we might expect to exist among simulations with different random seeds but otherwise identical. A source of some of the difference is that the more cumulus-like dynamics of the strongly drizzling boundary layer appears to induce up-scale growth in the disturbance, leading (at least in two dimensions) to organization on the largest scale available—the domain size. This is illustrated by the two panels of liquid water mixing ratio plotted in Fig. 4.7. The upper panel is a snapshot taken after the second hour and shows many convective cells with drizzle nodes extending to the surface. The lower panel is a snapshot taken at the 15th hour. Here the convective cells are grouped in one convective complex which essentially fills the horizontal extent of the domain. It is unclear how large this complex might grow given an infinitely large domain, and how much the organization is a feature of two-dimensional dynamics.

4.3.2 Sensitivity to thermodynamic jumps

The other experiments tabulated above are best compared to experiment CCN50 of the previous section. Immediately apparent is the reduction in cloud liquid water and the reduction in \mathcal{D}_{srf} . The reduction in the drizzle flux results from a greater contribution to the water budget from entrainment drying—indicating that drizzle production is favored

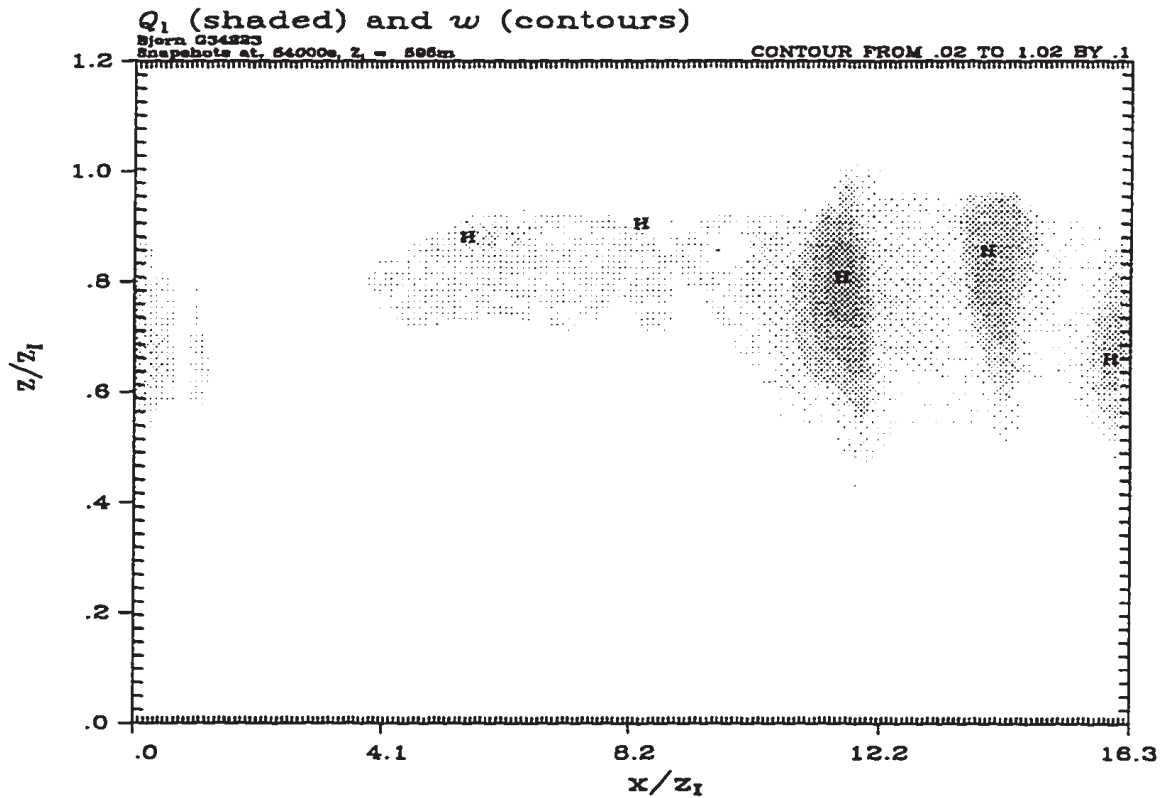
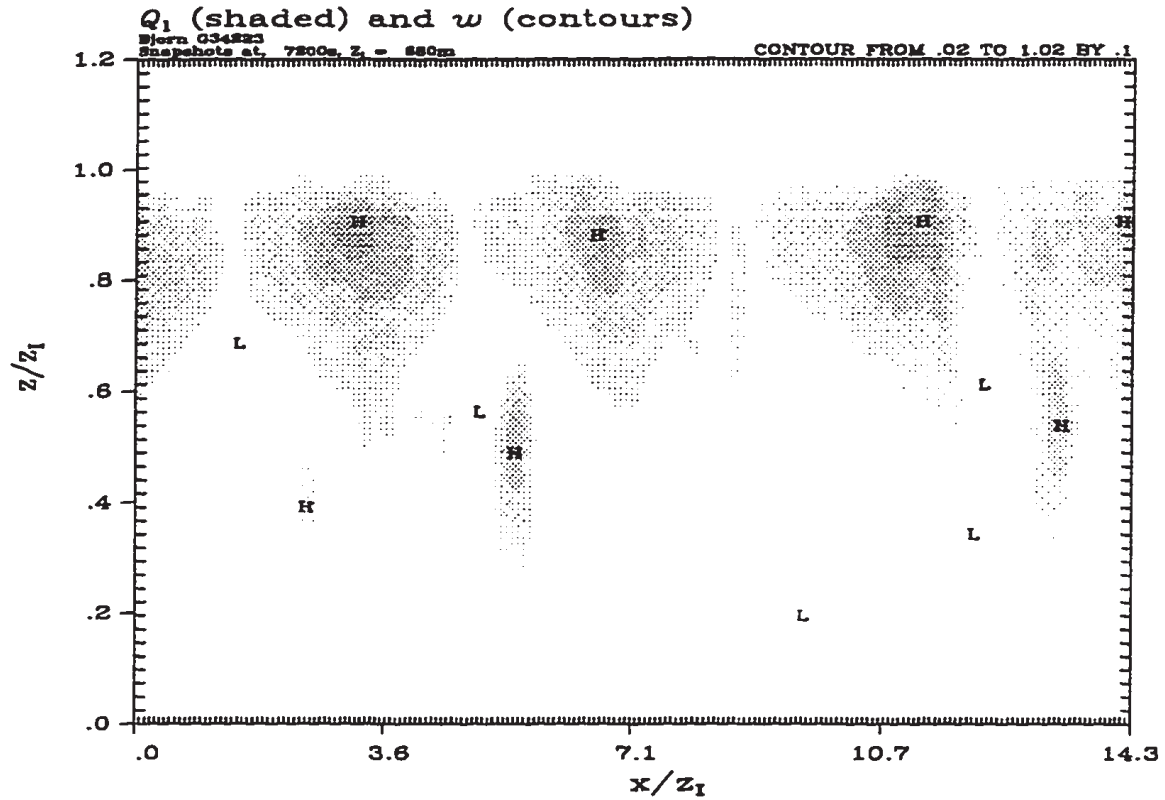


Figure 4.7: Liquid-water mixing-ratio [gkg^{-1}] (shaded and from 0.02 to 1.02 in 0.1 gkg^{-1}) from experiment CCN20-Big Domain at two times. Upper panel: Snapshot at 2 hours. Lower panel: Snapshot at 15 hours.

in clouds with smaller jumps in q_i across the inversion. Consequently, since the radiative forcing at cloud top is often correlated with above cloud moisture content, clouds which are more favored to drizzle may also be, on average, less strongly forced. The reduction in drizzle also is associated with a less stabilization of the sub-cloud layer relative to the cloud layer, more entrainment and more vigorous circulations. The latter two effects are secondary or indirect effects; the drying of the free-troposphere reduces drizzle, which then allows for larger values of $\overline{w'w'}$ and more entrainment. In a sense, most of the statistics map onto what one would expect from an experiment with the original sounding but with $\approx 200 \text{ CCN cm}^{-3}$. This indicates that drizzle production is regulated by both entrainment and CCN concentrations, the former largely due to its effect on maximum cloud liquid water contents. A larger jump in θ_l across the inversion increases the stability of interfacial layer, leading to less entrainment. Although entrainment is less it may have a larger consequence on boundary layer thermodynamic properties as the entrainment sensible heat flux is also proportional to the magnitude of the jump. This is not true for the moisture flux due to entrainment, which is reduced from that in experiment D, leading to larger values of \mathcal{L} .

Although drizzle is small in experiments WD50 and D50, it does still have important dynamical consequences. In identical integrations without drizzle we find that cloud fraction dips below 0.75 after 260 and 300 minutes in experiments WD and D respectively, and eventually goes to zero, with intermittent cumulus activity. As the cloud begins to dissipate the entrainment begins to diminish and eventually dZ_i/dt becomes commensurate with w_{sub} the imposed subsident velocity. For this reason (i.e., the mid-integration switch from a cloudy-turbulent boundary layer to a clear subsidence-dominated boundary layer) the statistics of the WD and D experiments produced by integration of the ERM-NM model are not tabulated. Suffice to say that for certain soundings the reduction in w_e through drizzle production allows the cloud layer to persist much longer than it would otherwise. This effect is at odds with the Pincus and Baker hypothesis. Moreover, it clearly illustrates that while the effect of drizzle on cloud depth is ambiguous it consistently leads to less entrainment.

4.4 Attracting states of ERM integrations

Results discussed in previous sections raise questions about our analysis method. Because hypotheses formed on the basis of simple models generally involve an analysis of the steady states we attempted to study the influence of drizzle on marine boundary layers by searching for and analyzing the steady states or apparent attracting states of ERM integrations. By adjusting elements of both the sounding and forcing we can slow down the evolution of the integration by making $\frac{dZ_I}{dt}$ arbitrarily small. Indeed this is what was done by reducing our forcing F_0 in the radiation equation by a factor of 2. Doing so reduced the rate of evolution of the experiments with CCN mixing ratios greater than 150 it did not do so for experiments with smaller mixing ratios. It appears from our tabulation that all experiments with CCN less than ≈ 90 are unable to generate entrainment rates larger than the mean subsidence rate at 700m, thus $w_{sub} < \frac{dZ_I}{dt} < 0$, where at 600 m the large-scale divergence rate of $5 \times 10^{-6} \text{ s}^{-1}$ implies a subsidence rate of $3 \times 10^{-3} \text{ ms}^{-1}$.

Why is this? Why don't the simulated boundary layers grow until they reach a level at which the entrainment rate is exactly balanced by the subsidence velocities (recall that through continuity a fixed large-scale divergence implies w_{sub} linear in height), as predicted by simple mixed layer models? For this to work, consider the case of $\frac{dZ_I}{dt} > 0$, initially. Here the boundary layer grows so that for fixed w_e we expect $\frac{dZ_I}{dt} = w_e - w_{sub}$ to be a decreasing function of time, as w_{sub} is an increasing function of height. Generally we expect that for a cloud layer thinning with increasing Z_i , w_e should decrease due to the reduction of the region of positive buoyancy production of TKE, as w_{sub} increases under the assumption that it is proportional to Z_i one would expect an accelerated approach to equilibrium. But this need not be the case. Since there is no particular reason why $w_{sub} = -w_e$ need imply cloud base latent and sensible heat fluxes exactly balance entrainment fluxes across cloud top. If they are insufficient to do so the cloud may thin, w_e will weaken, and cloud top will descend through cloud base, resulting in the dissipation of the cloud. The above arguments are also based on the assumption that the buoyancy production and entrainment rate are constant in time. Clouds that break up have a more cellular structure as they evolve through a phase of cumulus-like activity for which entrainment

is intermittent. Consequently, the drying out of the boundary layer is accomplished in intermittent bursts not accounted for in the mixed layer analysis. Eventually however, cloud may reform at lower levels continually moistened and cooled by the surface and the process may begin anew. Such dynamics imply that the nature of the attractor for stratocumulus topped boundary layers may be less of a fixed point and more of a limit cycle. We have attempted a cursory examination of this point by integrating the ERM-NM model for 150 hours, at the end of this time, cloud is beginning to reform in a very shallow boundary layer after having dissipated around the 10th hour. Nonetheless these are for the most part heuristic arguments meant to demonstrate the plausibility of the lack of a steady state in ERM integrations and the possibility of fundamentally different dynamics.

4.5 Large Eddy Simulation

The above discussion raises many questions, and suggests that drizzle, even in small amounts, may affect the dynamics of stratocumulus in myriad ways. However, because of the limitations of two-dimensional dynamics, much of the suggested behavior should be seen as just that; suggested behavior, some of which is accessible to LES integrations, some of which is not. Some of the hypotheses which we will not be able to explore with LES, and the reason why, are listed below:

- *Hypothesis: Strongly precipitating solutions prompt up-scale growth in the turbulent circulations.* To test this we need a domain size at least 3-4 times as large and an integration period spanning at least 10 hours, which requires 9-16 times as much computer memory, and takes 30-50 times as long to integrate. This is beyond the resources available us.
- *Hypothesis: There is a precipitation rate which maximizes boundary layer integrated $\overline{w'w'}$, as more/less precipitation reduces $\overline{w'w'}$ in the cloud/sub-cloud layer.* To test this requires doing many more LES. Given that each three hour LES-BM takes about three weeks to integrate, it is not practical to do more than a few experiments, widely separated in parameter space. Moreover, some of the effects may require the

development of an entrainment induced stabilization of the sub-cloud layer. The time-scales for this effect are relatively long, and may require a 5-6 hour integration.

- *Hypothesis: Precipitating boundary layers are sensitive to small changes in initial conditions and ones choice of collection kernel, but are relatively insensitive to how sub-grid scale water fluxes are modeled; moreover, changes in grid-spacing, which strongly impact the two-dimensional results are not thought to strongly influence the three-dimensional dynamics.* These hypotheses can only be tested with more experiments than available resources allow us to perform.
- *Hypothesis: In non-precipitating boundary layers for which clouds thin due to increased entrainment, moderate increases in precipitation efficiency leads to shallower boundary layers with deeper clouds.* In principle this hypothesis is readily testable by LES, but resource limitations prompt us to leave this for subsequent consideration.

There are, however, some issues which we can explore further. These are: (1) Is the stabilization of the sub-cloud layer relative to the cloud layer (and its de-stabilization relative to the surface) evident in LES in which shear generates significant turbulence at low levels and SST's are not increasing with time? (ii) Are the vertical profiles of $\overline{w'w'}$ affected in the same way in three-dimensions as they are in two-dimensions? (iii) Does drizzle primarily affect the turbulent budget through a reduction in the buoyancy flux? (iv) Do turbulent circulations become more efficient as drizzle increases? To answer these questions we have conducted two LES. The sounding used is identical to that specified at the beginning of this chapter. Cloud top radiative forcing is set at 74 Wm^{-2} . This is greater than what was used in the experiments of §4.3 and §4.4, but it facilitates a faster spin-up.

4.5.1 *Small mean wind*

In many ways these experiments are similar to the LES discussed in the previous chapter, one significant difference is that we now hold SST's fixed at their initial value, another is in the reduction of the meridional wind from 10 ms^{-1} to 2 ms^{-1} . This latter

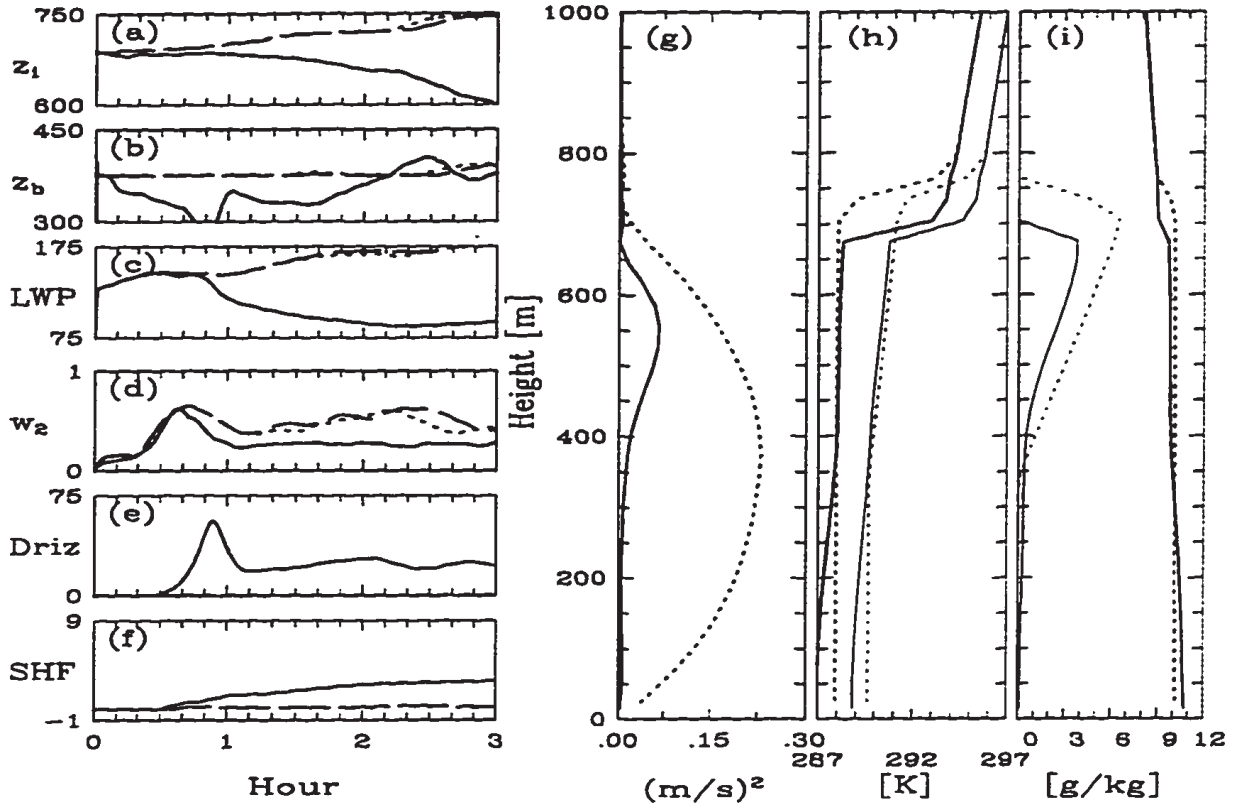


Figure 4.8: Time-sequence data (a)-(f) and layer means averaged over third hour (g)-(i). LES-NM (dotted), LES-BM (solid). Dashed line shows an LES-NM integration for which the radiative cooling was allowed to happen over a deeper layer. (a) z_i (m); (b) z_b (m); (c) LWP (gm^{-2}); (d) $(\overline{w'w'})^{1/2}$ ms^{-1} ; (e) Drizzle flux (Wm^{-2}); (f) Sensible heat flux (Wm^{-2}); (g) $\overline{w'w'}$; (h) θ_l (thick), θ_v (thin); (i) q_t (thick), $10q_l$ (thin).

change effectively eliminates shear as a source of turbulent kinetic energy. The domain is 3.06 km by 3.06 km in the horizontal and 1.823 km in the vertical. Grid spacing is 30 m in the vertical and 60 m in the horizontal (with grid stretching of 10% above 900m). The time-step used was 2s. Statistics are compiled every 30s, and radiative forcing is applied at every time-step. One LES is done using the NM microphysical model (and takes approximately 30 hours of CPU time for each hour of integration on a dedicated machine). The other uses the BM model with CCN concentrations of 25 cm^{-3} , guaranteed to produce significant precipitation.

In Fig. 4.8 we plot selected time-sequences taken over the duration of the experiment, mean profiles averaged over the third hour are also plotted. Both integrations spin-up on approximately equal time-scales and the w_2 statistic varies little with time after the 90 minute mark. The statistics of the integrations begin to diverge significantly, only after

drizzle begins to reach the ground at around the 40 minute mark. After drizzle begins to form, entrainment is significantly reduced, positive surface sensible heat fluxes respond to the cooling of the sub-cloud layer (and the fact that we maintain the lower boundary at a fixed temperature), $\overline{w'w'}$ is reduced throughout the entire boundary layer (although more dramatically in the subcloud layer), and LWP is also reduced (primarily due to a thinning of the cloud). This general behavior is exactly what we had come to expect on the basis of the ERM integrations, although there are some quantitative differences. The most significant being in the shape of the $\overline{w'w'}$ profile. In the LES this profile is more dramatically impacted by precipitation., $\overline{w'w'}$ is nearly zero below cloud base, and very little affected by the de-stabilization of the surface layer with respect to the ground due to the presence of drizzle.

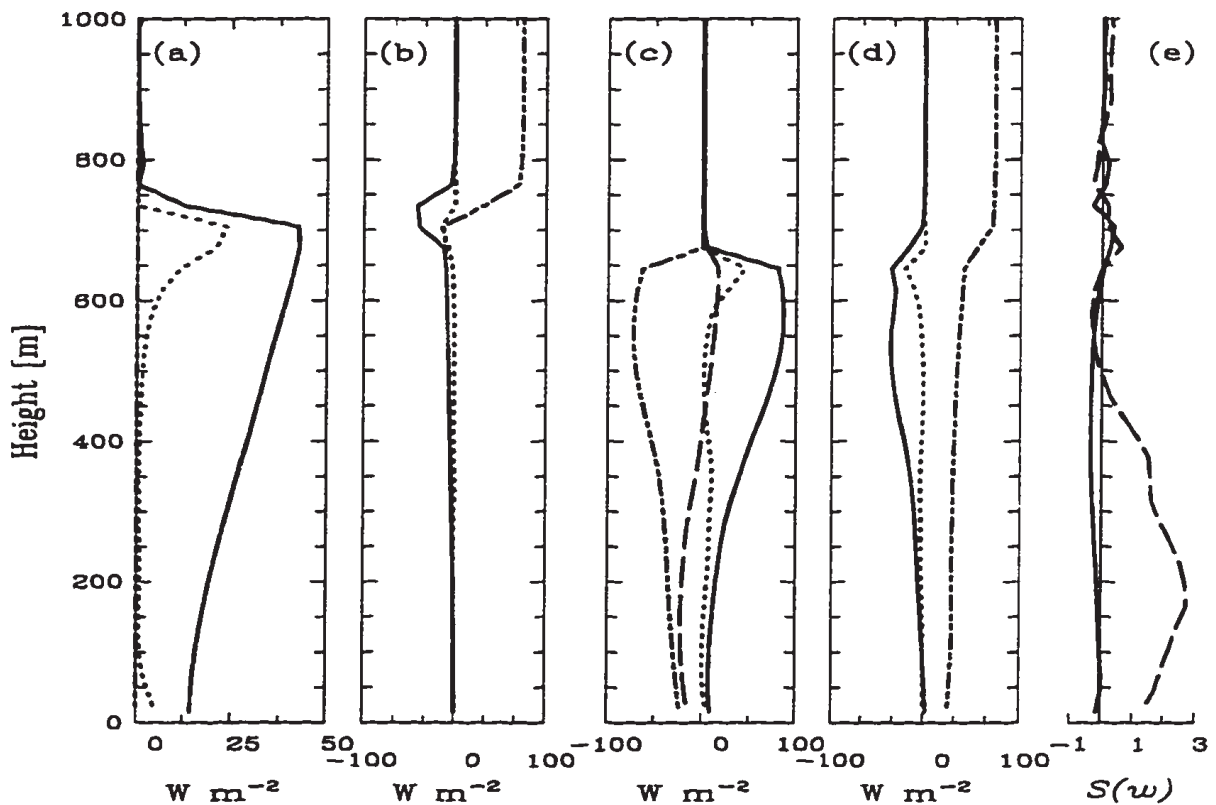


Figure 4.9: Heat and moisture fluxes averaged over third hour (a) LES-NM, F_Q (long-dash), $\overline{(w'q'_t)_{total}}$ (solid), $\overline{(w'q'_t)_{sgrid}}$ (dotted); (b) LES-NM, F_Θ (dash-dot-dot), $\overline{(w'\theta'_t)_{total}}$ (solid), $\overline{(w'\theta'_t)_{sgrid}}$ (dotted). (c) Same as (a) but for LES-BM, also plotted is drizzle flux (dash-dot-dot); (d) same as (b) but for LES-BM. (e) Vertical velocity skewness for LES-NM (solid), LES-BM (dashed).

One idea, which we discounted earlier, is that in a cloud thinned by drizzle the radiative cooling takes place in a deeper layer and that this might generate the observed dynamical and thermodynamical response. To further test this idea (and our supposition that it is not the dominant effect) we integrated the ERM but with the factor α in Eq. 4.2 decreased by a factor of two. This would mimic a twofold reduction in the LWP, commensurate with what is observed in Fig. 4.8 in the presence of drizzle. The time sequence data are plotted along with the other time sequence data in Fig. 4.8 and substantiate our argument that modest changes in the depth of the radiatively active layer cannot explain the differences seen between the precipitating and non-precipitating integrations.

Despite a significant reduction in $\overline{w'w'}$ and the generation of significant stratification in the transition layer turbulent fluxes show little evidence of decoupling (i.e, there is no evidence of a local minimum within the transition layer). In fact, above 250 m total water fluxes are actually larger in the precipitating integration. Below this level, the relatively smaller fluxes of total water reflect the reduction in surface latent heat fluxes associated with the moistening of the sub-cloud layer. Nonetheless, the fact that latent heat fluxes at 250 m in the LES-BM are comparable to those in the LES-NM despite the huge differences in the vertical velocity variance at this level suggests that the circulations become more efficient at transporting water in the precipitating solutions. The reason for this is suggested by the vertical velocity skewness plotted in Fig. 4.9. In the precipitating solutions the skewness becomes much larger near the middle of the sub-cloud layer. For a field whose mean is zero (such as the vertical velocity) a positive skewness implies that up-drafts are narrower and stronger. The very strong positive skewness at mid-levels in the LES-BM integrations suggests that the more efficient circulations are associated with more cumulus like dynamics, rather than the more regular-like overturning characteristic of stratocumulus.

Overall, the turbulent fluxes of water do not achieve a quasi-steady state as an examination of $F_Q =$ (plotted in Fig. 4.9) indicates that even during the third hour the subcloud layer is continuing to moisten gradually while the cloud layer is drying. θ_l on the other hand tends to be more quasi-steady with approximately uniform (although modest)

cooling through out the boundary layer. Thus for this case, where shear production of TKE is negligible, further stratification of the sub-cloud layer by precipitation is inhibited by turbulent mixing.

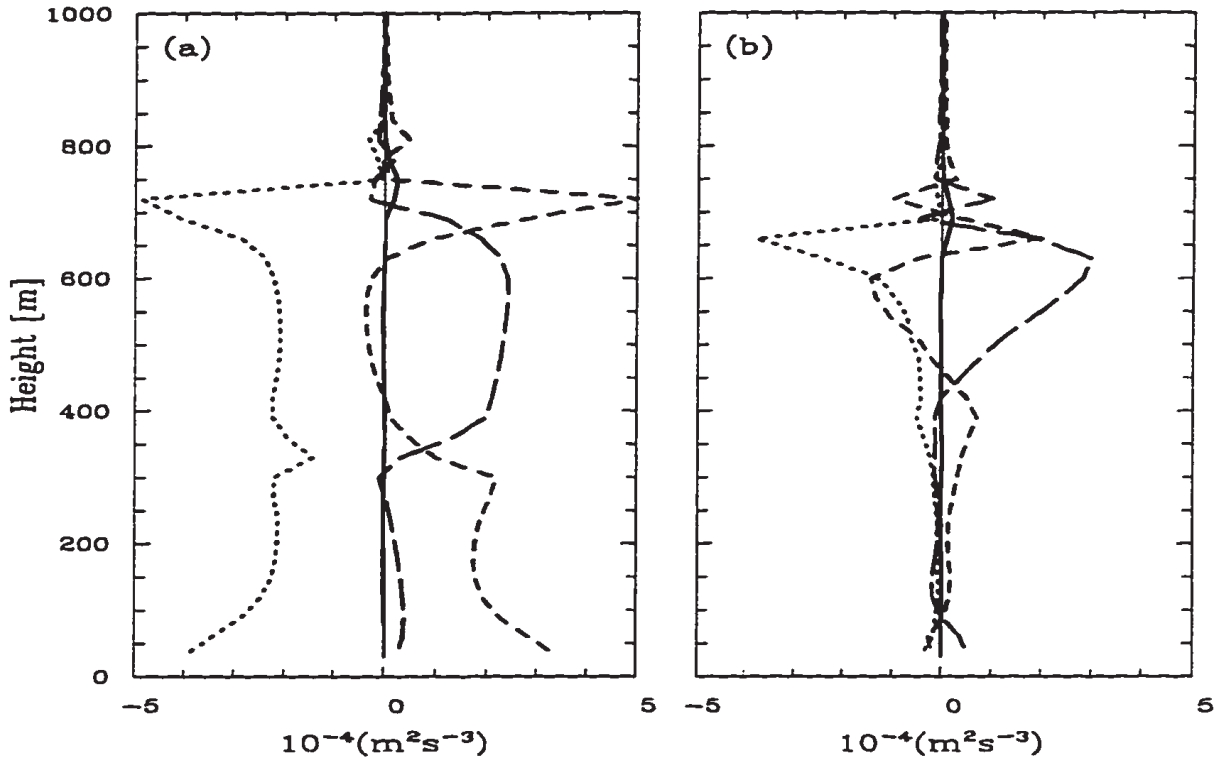


Figure 4.10: TKE budgets LES-NM (a); LES-BM (b). Shear term (solid), buoyancy (long-dash), transport (short-dash), dissipation (dotted).

The absence of TKE production by mechanical means is illustrated by the TKE budgets plotted for the two simulations in Fig. 4.10. The precipitating solution shows a smaller region of production of TKE through buoyancy, largely reflective of the thinner cloud. Although there is some evidence of more production of TKE below 100m, this region is poorly resolved, and the sub-cloud layer as a whole is much more quiescent, with much less dissipation reflecting the lack of turbulence below 300m. Nonetheless, if our results capture important aspects of reality the significant reduction of TKE in heavily precipitating boundary layers with small mean winds should be evident in the observations.

Another result, evident in both sets of LES, is the tendency for the buoyancy flux profile in the precipitating integration to be better approximated by a linearly increasing

function of height in the cloud layer, than is the case for the non-precipitating solutions. If the liquid-water flux is divergent over a parcel the buoyancy of the parcel should increase. Given that the precipitation flux is flat between 500 and 550 m, divergent above and convergent below we expect the buoyancy flux profile to be increased above this level and decreased below, something in accord with the plotted buoyancy flux. Overall we expect the generation of precipitation to marginally increase the buoyancy of parcels; nevertheless this effect appears to be a second order one with the dominant effect being that the sub-cloud layer is stabilized with respect to the cloud layer. These arguments are all heuristic; more work needs to be done before the characteristics of the buoyancy flux profile and its relation to the $\overline{w'w'}$ is clearly explained.

4.5.2 Large mean wind

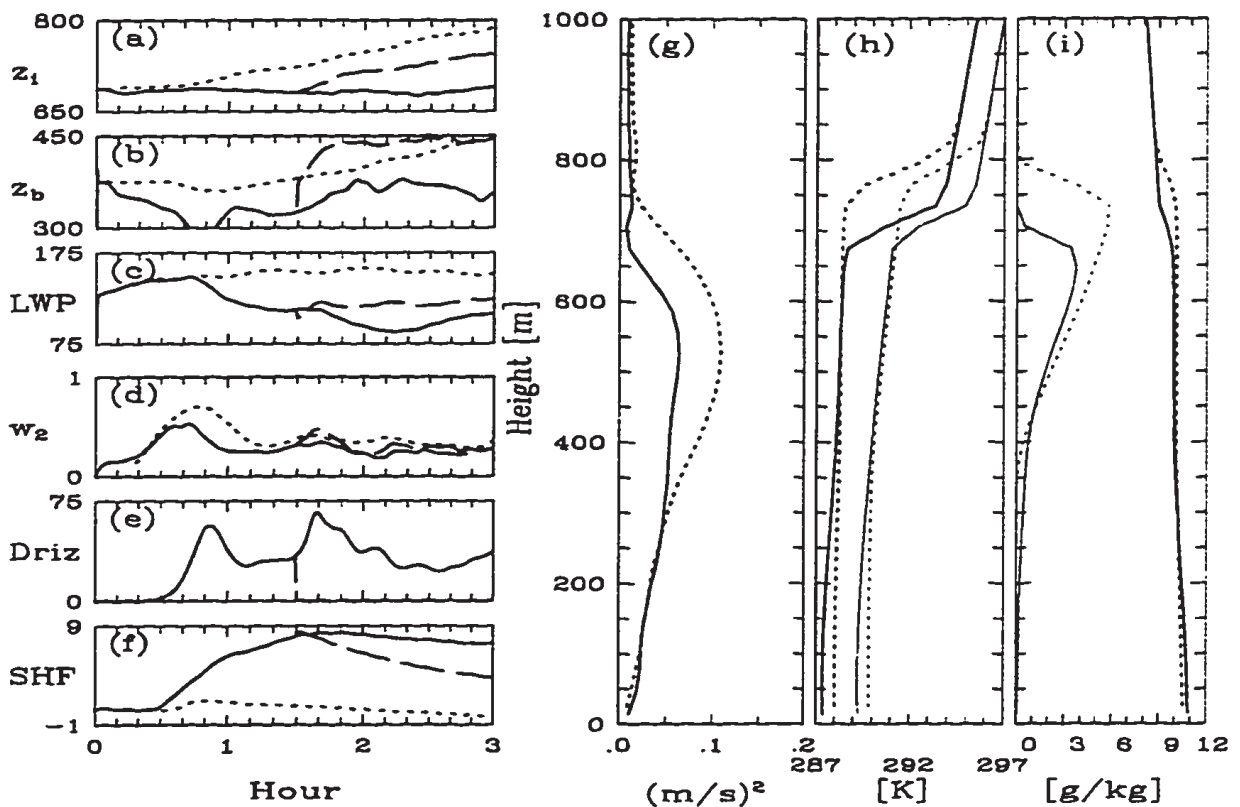


Figure 4.11: Time-sequence data as in Fig. 4.8 except for simulations with strong mean wind and here the dashed line shows an LES-NM integration spawned from the 90 minute mark of the LES-BM.

A few more integrations were performed with the meridional mean wind set back to 10 ms^{-1} , and will be briefly discussed here. Fig. 4.11 illustrates the mean structure and

time evolution of a non-precipitating and precipitating integration with significant mean shear. In these simulations precipitation does generate significant stratification, although the strong mean winds better ventilate the surface (note the more dramatic difference in surface sensible heat fluxes between the precipitating and non-precipitating solutions) and maintain more turbulent kinetic energy in the sub-cloud layer. In these simulations, because buoyancy is not the sole source of turbulent kinetic energy, the effects of drizzle, while still substantial and of the same nature, are mitigated.

If drizzle portends stratocumulus breakup, the changes it induces in the boundary layer should be irreversible. In other words, if drizzle is halted the boundary layer should not return to a state similar to what would be expected had it never drizzled. To test this idea on short time-scales we spawned an LES-NM integration from the 90 minute mark of the LES-BM, as after 90 minutes the characteristics of the sub-cloud layer have been well established. The transition is sudden, as the model is adjusted to saturation in one time-step, leading to significant condensation in cloud and evaporation below cloud; nonetheless, we believe the results illustrate important elements of the dynamics. The time-sequence data from this integration is plotted by the long dashed lines in Fig. 4.8 (a)-(f). Here we see that the entrainment rates immediately become commensurate with the original LES-NM integration. LWP is slowly building, and the sensible heat fluxes are exponentially approaching those of the original LES-NM with an e-folding time of approximately 120 minutes. These results reaffirm the idea that the stratified precipitating boundary layer seen here are forced solutions; moreover, these solutions relax back to conditions expected of non-precipitating boundary layers on time-scales of order three hours immediately after the forcing (i.e., the precipitation) is removed. While this effect was only demonstrated for the integration with significant shear production of TKE we expect it to hold for more buoyancy driven integrations, although the time-constants for relaxation back to equilibrium may well be increased.

4.6 Summary

In Chapter 1 we asked two questions: First, “what processes regulate drizzle production in stratocumulus layers,” and second, “how does the structure of stratocumulus-

topped boundary layers depend on drizzle?” In regard to the first questions, clearly drizzle is sensitive to a number of numerical factors in two-dimensional integrations of our boundary layer model, where most of these sensitivities are stated as hypothesized sensitivities in the previous section. As one would expect the microphysical processes represented by the collection kernel also significantly regulates drizzle production, as does the available number of drops for water to condense on. Drizzle production is also strongly regulated by liquid water content, as a small moistening of the sounding, or enhanced drying through the specification of a drier inversion, is seen to significantly impact drizzle production. In addition to the above, our results suggest that if drop concentrations are reduced sufficiently, drizzle formation becomes so efficient that deep clouds do not form and net precipitation is reduced.

With respect to the second question we find that, consistent with our results of the previous chapter and the Pincus and Baker hypothesis, enhanced drizzle production does, in some instances, reduce cloud-liquid-water path. But the dynamics of the system is complicated. In some cases, particularly those where further entrainment leads to a thinning of the cloud strong precipitation does not easily develop, and the light drizzle that actually does develop leads to an enhancement in cloud LWP. Moreover, in those cases where drizzle leads to a reduction in LWP, a significant portion of this reduction is due to the redistribution of heat and moisture within the boundary layer and not just in the reduction in the entrainment rate. This points to fundamental aspects of precipitating boundary layers not captured by mixed layer models, and suggests the necessity of using at least two layer models, a possibility that will be pursued further in the next chapter.

Overall, drizzle appears to reduce buoyancy production of TKE leading to smaller values of $\overline{w'w'}$ which results in less entrainment and slow the evolution of the boundary layer. Moreover the reduction in mixing allows more internal stratification to develop which in turn is associated with more cumulus-like circulations as evidenced by a significance increase in the skewness. Exactly what this portends for the future evolution of the cloud depends both on the properties of the free-tropospheric air and on drizzle efficiency. Because drizzle when generated modestly, may just as easily maintain the cloud

deck as help dissipate it, we find it difficult to assess how climatological changes in the precipitation efficiency of stratocumulus will affect their radiative properties.

Chapter 5

SIMPLE MODELS

Results presented in chapters three and four indicate that the behavior of drizzling stratocumulus is not consistent with the suggestions of Pincus and Baker (1994; hereafter PB). In forming their hypothesis, PB used what is perhaps the simplest of all boundary layer models to illustrate their arguments. This model, called a mixed-layer model, assumes that turbulence is at all times sufficient to maintain a well mixed boundary layer, and thus assumes that all conserved variables are independent of height within the boundary layer. PB show that the steady states of their model correspond to deeper clouds as drizzle efficiency is reduced, but they give little physical justification as to why this might be so. Thus we are left with the following unanswered questions: Why do mixed-layer models produce deeper clouds in the absence of drizzle? Is this feature of mixed-layer models sensitive to closure assumptions or ones choice of initial sounding? If mixed-layer models are unable to capture the fundamental physical interactions in precipitating boundary layers what are the prospects for more complicated boundary layer models such as two-layer or higher-order turbulent closure models?

In order to answer these question we construct some simple models and analyze their behavior. Below in §5.1 we look at the dynamics of precipitating mixed-layer models. In §5.2 we develop a look simple two-layer model to see if the separation of the physics into cloud and sub-cloud layers (as suggested by our LES and ERM results) is sufficient to capture the dynamics of precipitating stratocumulus-topped boundary layers.

5.1 Mixed-layer models (MLMs)

Mixed-layer models were introduced for the study of convective atmospheric boundary layers by Lilly (1968), and subsequently a number of investigators have explored their

dynamics. Currently, mixed-layer models are used in at least one family of GCMs and they continue to be used as a framework for answering (asking?) questions about boundary layer dynamics (Pincus and Baker, 1994; Chen, 1996). They are essentially thermodynamic box-models of the ensemble averaged PBL which rely on the following assumptions: (i) The boundary layer is at all times well-mixed in quantities conserved under moist-adiabatic processes. (ii) The expected values of all turbulent quantities are homogeneous in the horizontal directions. (iii) Fluxes vanish at the top of the internal interface separating the boundary layer from the free-troposphere above, and drizzle fluxes vanish as one approaches z_i from above and below. (iv) Fluxes at the base of this interface can be expressed in terms of known variables.

5.1.1 Basic formulation

Because potential density is conserved in single-phase flow only two equations are needed to predict the thermodynamic state of dry boundary layers (one for the boundary-layer height, one for some measure of density). In potentially cloudy boundary layers density is no longer conserved and an additional variable must be predicted to identify the location of cloud base. We follow Schubert and predict the evolution of moist static energy $h = c_p T + gz + L_v q_v$, (here L_v is the energy released by condensing 1kg of water and c_p is the isobaric specific heat per unit mass) and total water mixing ratio $q_t = q_v + q_l$. Both are well conserved for shallow (relative to a scale-height in the atmosphere) moist-adiabatic processes. For a mixed layer as represented by the diagram in Fig. 5.1, which is constrained by the first and second assumptions above, the following equations may be derived to represent the evolution of h_2 and $q_{t,2}$ (the mixed layer values of h and q_t) :

$$\frac{dh_2}{dt} = \frac{-1}{z_i} \left[\mathcal{F}_h(z_i^-) - \mathcal{F}_h(0^+) + \frac{\mathcal{F}_{rad}(z_i^-) - \mathcal{F}_{rad}(0^+)}{\rho} \right] \quad (5.1)$$

$$\frac{dq_{t,2}}{dt} = \frac{-1}{z_i} \left[\mathcal{F}_{q_t}(z_i^-) - \mathcal{F}_{q_t}(0^+) - \frac{\mathcal{F}_{drz}(0^+)}{L_v \rho} \right]. \quad (5.2)$$

Here $\frac{\partial \mathcal{F}_{rad}}{\partial z}$ is the radiative-flux convergence and is a source of moist-static energy $\frac{\partial \mathcal{F}_{drz}}{\partial z}$ is the convergence in the drizzle flux and is a source of total water. The flux, $\overline{w'x'}$, of an arbitrary variable x is denoted by \mathcal{F}_x .

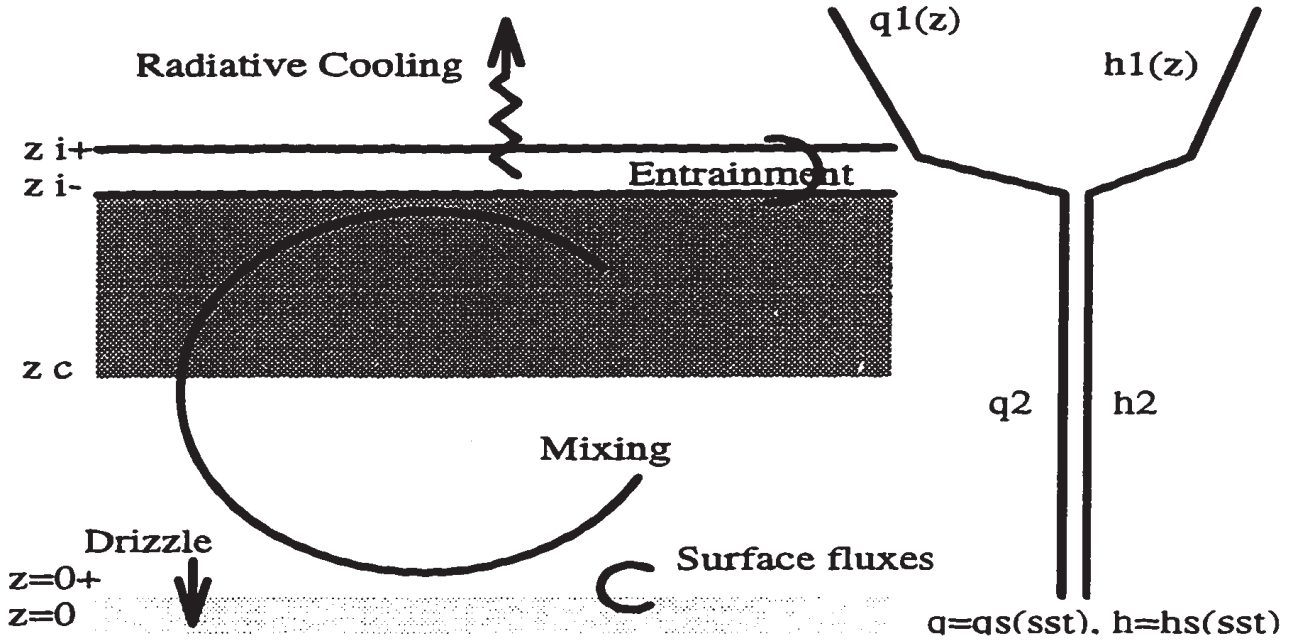


Figure 5.1: Diagram of mixed layer model.

Integrating the budget equations for h and q_t over the vanishingly thin interfacial layer separating the boundary layer from the free-troposphere and using assumption (iii) results in the following relations:

$$\frac{dz_i}{dt} = w_D + w_e, \quad (5.3)$$

where

$$w_e = -\frac{1}{h_1 - h_2} \left\{ \mathcal{F}_h(z_i^-) + \frac{1}{\rho} \left[\mathcal{F}_{rad}(z_i^-) - \mathcal{F}_{rad}(z_i^+) \right] \right\} = -\frac{\mathcal{F}_{q_t}(z_i^-)}{q_{t,1} - q_{t,2}}, \quad (5.4)$$

where h_1 and $q_{t,1}$ refer to the thermodynamic state of the free troposphere at $z = z_i^+$ and are given through the specification of a fixed in time, but height-dependent basic state. For future reference we have also introduced w_e , the entrainment velocity.

This leaves three equations and nine unknowns. Assuming a known sea-surface temperature (T_{sst}) and sea-level pressure (p_{00}) eliminates two unknowns as the surface-fluxes may be derived from bulk aerodynamic formulas:

$$\mathcal{F}_h(0^+) = \overline{w'h'}|_{0^+} = C_T v_2 [h_2 - c_p T_{sst} - L_v q_s(T_{sst}, p_{00})] \quad (5.5)$$

$$\mathcal{F}_{q_t}(0^+) = \overline{w'q'_{t,2}}|_{0^+} = C_T v_2 [q_{t,2} - L_v q_s(T_{sst}, p_{00})], \quad (5.6)$$

where C_T is a bulk exchange coefficient, v_2 is the wind-speed in the mixed layer (which we keep fixed) and q_s is the saturation mixing ratio as a function of the surface temperature

and pressure. The large-scale advective velocity, w_D is largely controlled by processes external to the boundary layer and is therefore assumed to be a known parameter of the system. We prescribe it as a linear function of height: $w_D = -zD$, where D , the large-scale divergence, is a prescribed number of order 10^{-6} . Both $\mathcal{F}_{drz}(z)$ and $\mathcal{F}_{rad}(z)$ depend on the internal structure of the cloud layer. Initially we consider the behavior of the model for \mathcal{F}_{drz} fixed, although later we make it a function of the depth of the cloud and sub-cloud layers, as well as the assumed microphysical structure of the cloud layer.

Much effort has been extended toward understanding how the dynamics of mixed-layer models depend on the profile of the radiative flux, and there is some qualitative and quantitative sensitivity to exactly how $\mathcal{F}_{rad}(z)$ is specified. Nonetheless the basic sensitivity of the mixed-layer formulation to drizzle is sufficiently well illustrated by assuming that

$$\mathcal{F}_{rad}(z) = \begin{cases} F_0 & z \geq z_i^+ \\ 0 & \text{otherwise,} \end{cases} \quad (5.7)$$

to warrant not considering more complicated radiative interactions. This assumed profile is justified by the fact that clouds are strong absorbers of long-wave radiation, so radiative profiles vary sharply across cloud top due to the nearly discontinuous flux of downward long-wave radiation as you enter the cloud from above.

5.1.2 *Entrainment closures*

The last remaining quantity which must be specified before our system of equations is closed is w_e (or equivalently the flux of some conserved variable at the top of the mixed layer. Exactly how to specify this term has been the subject of considerable debate and a number of methods have been proposed—most of which are based on the rate at which buoyancy is producing turbulent kinetic energy (TKE). The simplest method is to assume that all or none of the TKE produced through buoyancy is immediately available to drive entrainment—these are respectively called the maximum and minimum entrainment assumptions (Lilly, 1968). Assuming, as is done in the ERM-NM, that the atmosphere is at all times less-than or just saturated (so that condensation time-scales are much less than dynamical time-scales) allows us to write the buoyancy flux (or flux of virtual-dry

static energy \mathcal{F}_{s_v} where $s_v = c_p T_v + gz$) as a function of the fluxes of moist-static energy and total water:

$$\mathcal{F}_{s_v}(z) = \begin{cases} \mathcal{F}_h(z) - (1 - \epsilon\delta)L_v\mathcal{F}_{q_t}(z) & z < z_c \\ \beta\mathcal{F}_h(z) - \epsilon L_v\mathcal{F}_{q_t}(z) & z \geq z_c, \end{cases} \quad (5.8)$$

where $\delta = 0.608$ and $(\beta, \epsilon) \approx (0.5, 0.1)$ are strong functions of temperature, but weak function of height since temperature varies by only a few percent over a 1km well-mixed layer. By our first assumption (conserved thermodynamic variables are independent of height within the boundary layer) and the fact that we require \mathcal{F}_{rad} to vanish in the boundary layer, both F_h and F_{q_t} must be linear functions of height (see discussion in Appendix 1). Given F_h and F_{q_t} at the surface, their values at z_i^- can be uniquely determined so long as \mathcal{F}_{s_v} is suitably constrained. Interpolating between Lilly's (1968) minimum and maximum entrainment assumptions (Schubert et al., 1979):

$$\frac{1}{2}(1 - k)(\mathcal{F}_{s_v})_{min} + \frac{k}{z_i} \int_{0^+}^{z_i^-} \mathcal{F}_{s_v} dz \quad (5.9)$$

allows the system of equations to be closed once the interpolation parameter k is specified. For $k = 0$ Schubert's formulation reduces to the minimum entrainment assumption, while $k = 1$ implies that all the energy being created by buoyancy is being used to do the work of entrainment. PB assume $k = 0$, although $k = 0.2$ is most often chosen. Other investigators have used variants of this flux partitioning scheme for which the negative area of the buoyancy flux profile is constrained to be a fixed fraction of the positive area. An interesting discussion of various flux-partitioning methods is given by Kraus and Schaller (1978).

Nicholls and Turton (1987) argue that

$$w_e = w_* a_1 R_i^{-1} [1 + a_2(1 - \Delta_m/\Delta\theta_v),] \quad (5.10)$$

with a_1 and a_2 constants whose suggested values are 0.2 and 60 respectively. $\Delta\theta_v$ is the virtual temperature difference (include water-loading effects) across the inversion, and Δ_m is the average density difference between fluid in layer 2 and all possible mixtures of fluid at z_i^- with fluid at z_i^+ . Because Δ_m is smaller than $\Delta\theta_v$, this model accounts for the fact

that evaporation in mixing parcels will reduce the density of the mixture thus reducing the effective stratification. R_i is a Richardson number based on the depth of the mixed layer, z_i , and w_* is a scale velocity such that

$$R_i = \frac{gz_i\Delta\theta_v}{w_*^2\theta_0}, \quad \text{and} \quad w_* = \left(\frac{2.5g}{c_p T_0} \int_{0^+}^{z_i^-} \mathcal{F}_{sv} dz \right)^{1/3}. \quad (5.11)$$

Randall (personal communication) and Chen (1996) prefer to predict a value of boundary layer TKE and use this to derive entrainment rates. This type of model is similar to that proposed by Nicholls, but allows for energy to mediate the relationship between entrainment and the buoyancy flux profile. It also allows shear to affect the TKE budget, and thereby influence entrainment. By allowing shear to contribute to the production of TKE in narrow layers centered at the base and top of the mixed-layer the following equation may be derived to describe the evolution of TKE, e_2 , within the mixed layer: (Krasner, 1993)

$$\frac{de_2}{dt} = \frac{1}{z_i} \left[\underbrace{-\int_{0^+}^{z_i^-} \overline{v'w'} \frac{\partial v}{\partial z} dz}_{\text{Shear}} + \underbrace{\frac{g}{c_p T_0} \int_{0^+}^{z_i^-} \mathcal{F}_{sv} dz}_{\text{Buoyancy}} - w_e e_2 - \underbrace{\frac{e_2^{3/2}}{\Lambda}}_{\text{Diss}} \right]. \quad (5.12)$$

This closure requires the specification of a dissipation length scale ratio defined by: $\Lambda = 2^{-5/2} L) \epsilon / z_i$, Where L_ϵ is the integral length-scale which characterizes the dissipation rate. Originally Λ was taken to be 0.066 (Krasner, 1993; Chen, 1996). Changan Zhang (personal communication) suggests that this value of Λ may be an order of magnitude too small. Indeed, LES of the dry-convective boundary layer (Moeng and Sullivan, 1994) indicates that $L_\epsilon = 2.2z_i$ (for the buoyancy driven case) and $L_\epsilon = 2.8z_i$ (for the shear and buoyancy driven case) well describe the data. Taking $L_\epsilon = 2.8z_i$ and noting that by definition $\Lambda = 2^{-5/2} L/z_i$ implies $\Lambda \approx 0.5$. In the shear term the momentum flux, $(\overline{v'w'})_{z=0^+}$, is taken to be $C_M v_2^2$, and while not generally warranted we take $C_M = C_T$ for simplicity. If we confine the region of shear production of TKE to the surface layer this allows us to model the shear term as $C_M v_2^3$. Given a value of TKE at each time-step an entrainment rate may be derived on the basis of simple energy-budgets at the entraining interface (i.e., assuming a certain amount of TKE is available to do work against the

stratification separating the fluid layers). Krasner (1993) adopts Breidenthal and Baker's (1985) suggested closure wherein

$$w_e = e_2^{1/2} \frac{b_1}{1 + b_2 R_i}, \quad \text{where } R_i = \frac{g z_i \Delta \theta_v}{e_2 \theta_0} \quad \text{and } b_1 = 2\Lambda b_2 = 2 \left(\frac{\Lambda^2}{50} \right)^{1/3}, \quad (5.13)$$

where the values for the constants b_1 and b_2 are derived from the $R_i = 0$ and $R_i \gg 1$ limits for the case of a dry-convective boundary layer with an equilibrium between buoyancy forcing and dissipation in Eq. 5.12. $\Lambda = 0.0658$ implies $b_1 = 0.672$ and $b_2 = 0.0885$, while $\Lambda = 0.5$ implies $b_1 = b_2 = 0.342$. Such a closure has the advantage of not implying infinite entrainment in the limit of vanishing stratification, as some work must be done to impart turbulent energy into the entrained fluid; otherwise, the closure is very similar to that proposed by Nicholls and Turton (1987) except that the effect of evaporation on the effective stratification is not included, and the turbulent quantity e_2 is now a predicted, rather than a diagnosed, variable.

To summarize we allow for three different methods of closing the mixed-layer model: (i) The $(\mathcal{F}_{s_v})_{min}$ closure (Schubert et al., 1979); (ii) the Δ_m closure (Nicholls, 1987); (iii) the e_2 closure (Breidenthal and Baker, 1985; Krasner, 1993). All of the closures reduce to the dry convective boundary layer limit such that $\mathcal{F}_{s_v}(z_i^-) = -\frac{1}{5}\mathcal{F}_{s_v}(0^+)$ for equilibrium situations with $R_i \gg 1$. Only the Δ_m closure takes explicit account of moist processes in modifying the effective stability at the inversion. In the absence of any shear contribution to e_2 , the e_2 closure asymptotically approaches the Δ_m closure as $\frac{\partial e_2}{\partial t} \rightarrow 0$. Consequently for cases where $\Delta_m = \Delta\Theta_v$, the e_2 and Δ_m closures produce equivalent steady state solutions. Moreover, steady state solutions for which surface fluxes are independent of TKE will also be independent of the value of Λ chosen in the evolution equation for e_2 .

5.1.3 Numerical methods and integration specifics

The mixed-layer models are integrated using a third-order Adams-Bashforth scheme for all terms except for the dissipation and entrainment terms in the TKE equation, which are integrated using the semi-implicit method that follows from the approximation

$$e_2^{3/2}(t + \frac{1}{2}\Delta t) \approx e_2(t + \Delta t)e_2^{1/2}(t).$$

When the $(\mathcal{F}_{s_v})_{min}$ closure is used, the thermodynamic coefficients (β, ϵ) in the buoyancy flux equation are taken to be constant with height and given in accord with the basic state temperature. For the case of other closures, (β, ϵ) are allowed to vary with height as the cloud and sub-cloud layer are split into 10 intervals over which the buoyancy-flux integral is approximated using a ten-point center-rule Riemman sum.¹ Use of the Δ_m closure requires the specification of Δ_m which requires the integration over mixtures composed of various mixing fractions. We find that 20 equally spaced mixing fractions are sufficient to yield convergent answers. Since liquid water must be diagnosed for each mixing fraction this scheme greatly increases the computational cost of the integration, although I imagine that the cost of this calculation could be mitigated (hopefully with little loss in accuracy) by using linearized equations to derive the liquid water as a function of mixing fraction.

Most integrations are performed using a time-step of 300s and are strongly forced toward an attracting state, so numerical instability and computational modes do not seem to be a problem. We have encountered problems in numerically integrating the model with the Δ_m closure. Over-prediction of w_e results in the buoyancy flux integral being negative on the following time-step which implies $w_e = 0$ which then allows the buoyancy flux integral to again be positive. This oscillation can be eliminated by iteratively solving for values of w_x and w_e which are self-consistent. Doing so, considerably increases the cost of the integration, but improves its behavior of the integration. Steady state solutions are well-approximated by those solutions which correspond to $\frac{dz_i}{dt}$ changing by less than 10^{-5} % over a 48 hour period. Most integrations satisfy this condition after 10-15 days, a result consistent with that found by Schubert et al. (1979). The results of our model were checked for physical consistency and compared to previously published results to minimize the ever present possibility of coding or conceptual errors.

¹Bretherton and Wyant (1996), who use the Δ_m closure, calculate buoyancy integrals over a fixed grid. This requires that the trapezoidal rule be used in order to have a smooth evolution in z_i across the fixed grid. Defining our discretization relative to z_i and z_c avoids this problem.

Table 5.1: Basic state configuration used in mixed-layer model integrations. Units are as follows h [kJ kg⁻¹], z [km], q_t [gkg⁻¹], T [K], p_{00} [hPa], D [10⁻⁶ s⁻¹], v_2 [ms⁻¹]

Sounding	$h_1(z)$	$q_{t,1}(z)$	T_{sst}	p_{00}	D	v_2
Oakland	$314.4 + 1.87z$	$4.38 - 0.614z$	286.16	1020	5	7.00
GCSS-3	$320.5 - 1.07z$	$11.1 - 2.800z$	290.40	1029	5	7.00
Bretherton	$307.9 + 3.37z$	$3.50 + 0.000z$	290.00	1020	3	7.10

Unless otherwise indicated integrations are performed using one of the soundings specified in Table 5.1. The GCSS-3 and Oakland soundings will predominantly be analyzed; the former is derived from the same sounding used to initialize the integrations of Chapter 4 and is considerably moister than the latter which is taken from the climatology (i.e., 30 year averages) of the Oakland soundings (Schubert et al., 1979). The Bretherton sounding is also based on climatology off the coast of California, and was primarily used to test the implementation of the Δ_m closure by comparing to previously derived results (Bretherton and Wyant, 1996). Because $q_{t,1,Oakland} < q_{t,1,gc3s3}$ for $z < 3$ km, the Oakland sounding will be referred to as the dry sounding. In all simulations we fix $C_T = 0.0015$.

5.1.4 Sensitivity of models to specified drizzle

By now the solution space of mixed-layer models in the absence of drizzle has been well mapped out. Here we present results illustrating (see Fig. 5.2) the behavior of a mixed-layer model with various closures as a function of drizzle rate and sounding. For now the drizzle rate is imposed as a constant parameter. The results using the $(\mathcal{F}_{sv})_{min}$ closure are most fruitfully compared to PB, since they used a similar closure, except with $k = 0$. The nature of the sensitivity of the mixed-layer model to drizzle is not altered by changing the value of k , although changes in the actual steady state values of various variables are commensurate with their changes in non-drizzling integrations. Consistent with what was found by PB the cloud-depth (and hence liquid-water path) decreases with increasing drizzle.² Most of the change is associated with changes in z_i , although the

²More drizzle implies larger negative values of the drizzle flux.

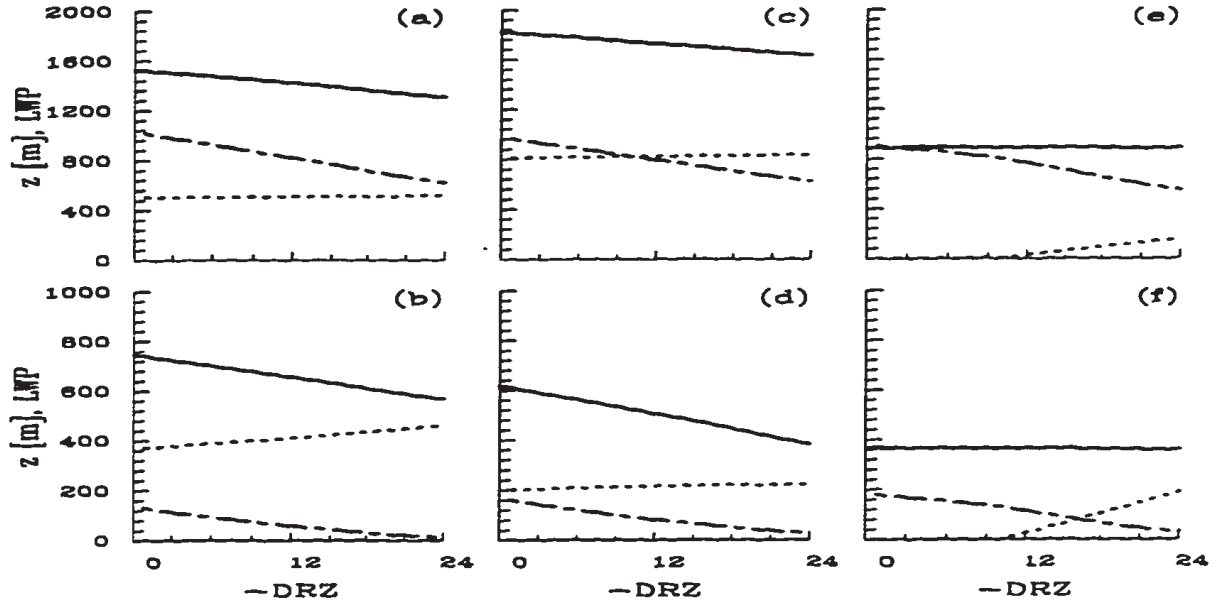


Figure 5.2: Steady states of mixed-layer model with GCSS-3 sounding (upper panels) and Oakland sounding (lower panels). Results plotted for $F_{rad} = 75 \text{ Wm}^{-2}$ as a function of specified value of \mathcal{F}_{drz} . Note that 24 Wm^{-2} of drizzle is approximately 0.8 mm day^{-1} . First column is for $(\mathcal{F}_{sv})_{min}$ closure with $k = 0.2$, second is for the Δ_m closure, third column uses e_2 closure with $\Lambda = 0.5$. Plotted are cloud top (solid lines), cloud base (dotted lines), and LWP in gm^{-2} (dashed lines).

reduction in z_c with less drizzle makes a small contribution to changes in cloud optical depth—more so for the drier sounding. Our results in which cloud-base is lower in a non-drizzling integration mimic the behavior illustrated in PBs Fig. 1. Consequently the general mixed-layer dynamics for precipitating boundary layers appears to be robust to major changes in the sounding, a result not consistent with our ERM integrations.

Integrating the model with a different closure scheme produces different answers, but essentially the same sensitivity: LWP is an approximately linearly decreasing function of drizzle. Comparing the Δ_m closure with the $(\mathcal{F}_{sv})_{min}$ closure illustrates that for the moister sounding the former predicts a deeper boundary layer, but with similar values of LWP. For the drier boundary layer the Δ_m closure actually produces a shallower boundary layer. This is predominantly a result of $a_2 \neq 0$, as when evaporative effects are not allowed to modify the effective stability the boundary layer is always shallower, and for both cases tends toward a fog layer. The e_2 closure produces interesting results. Here again we see that LWP is a monotonically decreasing function of \mathcal{F}_{drz} , however this time for a different reason. This closure tends to want to maintain a fixed value of z_i and adjust z_c

to accommodate the specified amount of drizzle. The differences between the steady-states in the third and fourth columns basically reflects the contribution of shear to e_2 , as when this contribution is removed from Eq. 5.12 the steady-states of the model with the Δ_m closure with $a_2 = 0$ are indistinguishable from those produced by the model with the e_2 closure. So while the tendency of mixed-layer models to produce shallower cloud layers for increasing drizzle is robust, the depth of the boundary layer is a strong function of the chosen closure. We hesitate at this point to say which closure is best, although later we offer a suggestion for a hybrid closure which we find to be physically well justified, and we also compare the behavior of the MLMs to solutions produced by the ERM.

5.1.5 Approach to equilibrium

While we have answered the question as to whether the PB result is a robust one, it remains to be shown why they get the result that they do. In steady state the moisture fluxes must satisfy:

$$\mathcal{F}_{q_t}(z_i^-) - \mathcal{F}_{q_t}(0^+) = \frac{\mathcal{F}_{drz}(0^+)}{L_v \rho} = -\mathcal{D}. \quad (5.14)$$

Generally, $\mathcal{F}_{q_t}(z_i^-)$ is positive (since the jumps in q_t across the inversion are negative), and in a non-drizzling steady-state we must have $\mathcal{F}_{q_t}(z_i^-) = \mathcal{F}_{q_t}(0^+)$. With drizzle $\mathcal{D} > 0$, an approach to steady state requires either $\mathcal{F}_{q_t}(z_i^-)$ to increase or $\mathcal{F}_{q_t}(0^+)$ to decrease. The former is controlled by the entrainment rate and thermodynamic jumps, while for a fixed wind the latter depends only on $q_{t,2}$. In the $(\mathcal{F}_{s_v})_{min}$ and Δ_m closures the entrainment rate is directly tied to the instantaneous state of the model, unlike for the e_2 closure for which the prior history affects e_2 and hence w_e .

Eqs. 5.4 and 5.6 may be written:

$$\mathcal{F}_{q_t}(z_i^-) = w_e[q_{t,2} - q_{t,1}(z_i)], \quad (5.15)$$

$$\mathcal{F}_{q_t}(0^+) = w_s(q_s - q_{t,2}), \quad (5.16)$$

where $q_s > q_{t,2} > q_{t,1}(z_i)$, and $w_s = C_T v_2 \approx 1 \text{ cm s}^{-1}$. So doing allows us to express the steady state condition as follows:

$$z_i^2 \cdot D \cdot \frac{dq}{dz} + z_i \cdot D(q_{t,1}(0) - q_{t,2}) - w_s(q_s - q_{t,2}) = -\mathcal{D}, \quad (5.17)$$

where we have used the fact that at steady state $w_e = -w_D = zD > 0$, and free-tropospheric thermodynamic quantities are defined:

$$q_{t,1}(z_i) = q_{t,1}(0) + z_i \frac{dq}{dz}, \quad \text{where generally } \frac{dq}{dz} < 0.$$

A perturbation equation can be formed from our above relation which expresses how prognostic variables must change with changing drizzle in order to preserve a steady-state³

$$\delta \mathcal{D} = -c_1 \delta q_{t,2} - c_2 \delta z_i, \quad (5.18)$$

where $c_1 = w_s + z_i D$ and $c_2 = D[q_{t,2} - q_{t,1}(0) - z_i D \frac{dq}{dz}]$. Generally both D and w_s are positive definite, moreover because $\frac{dq}{dz} < 0$ and $q_{t,2} > q_{t,1}(0)$, both c_1 and c_2 take positive values. Consequently reductions in drizzle must be compensated for by increases in z_i or increases in $q_{t,2}$. Both lead to a deepening of the cloud. Exactly which path the model will take, in finding a new equilibrium, depends on the closure and the nature of the environmental sounding.

Analyzing the model with the $(\mathcal{F}_{s_v})_{min}$ closure shows that with the onset of drizzle $q_{t,2}$ is reduced, but not h_2 thus leading to larger latent-heat fluxes which for constant moist-static energy fluxes imply smaller sensible heat fluxes as well. This, in turn, leads to a smaller entrainment rate (acting un-opposed the increase in the latent-heat flux actually increases the the entrainment rate) which leads to a smaller value of z_i , and larger thermodynamic jumps. $\mathcal{F}_{q_t}(z_i^-)$ decreases, since Δq_t increases and w_e decreases (see Eq. 5.2) while $\mathcal{F}_{q_t}(z_i^-)$ increases. However so long as the relative increase and decrease in $\mathcal{F}_{q_t}(z_i^-)$ and $\mathcal{F}_{q_t}(0^+)$ isn't sufficient to balance the imposed drizzle rate $q_{t,2}$ will continue to be reduced. Hence we see that in those simulations where z_i falls with increasing drizzle, it falls primarily due to the reduction of the buoyancy flux due to a reduction in the sensible-heat flux associated with the heating of the boundary layer implied by an excess of condensation over evaporation. This is the best a mixed-layer model can do as the

³This does not demonstrate that we will achieve a new steady-state when we preserve drizzle rates, but assuming that our system does find a new equilibrium for perturbations in the drizzle parameter \mathcal{D} then this relation shows the character of this new solution.

dynamics of the ERM and LES integrations (wherein the stabilization of the sub-cloud layer actually led to larger surface-sensible heat fluxes—albeit smaller buoyancy fluxes due to the stabilization of the cloud layer with respect to the sub-cloud layer) are inaccessible to it. Interestingly, changes in cloud base account for more of the change (with increasing drizzle) for the Oakland sounding where both dq/dz and z_i are smaller, thus reducing c_2 relative to c_1 .

In summary, reduced drizzle requires steady-states with larger values of z_i and larger values of $q_{t,2}$. How the change in the model is partitioned among these variables depends on both the basic state and the entrainment closure. While it may be straightforward to decipher how a particular entrainment model responds to a perturbation in the drizzle flux, the overall mixed-layer dynamics do not appear sufficiently realistic to warrant further discussion of this point.

5.1.6 Sensitivity of models to parameterized drizzle

Our results considered the case of specified drizzle rates. A more realistic approach would be to specify the drizzle flux as a function of cloud microphysical and thermodynamical properties. Such an approach was taken by PB wherein they parameterized drizzle in accord with Nicholls and Turton (1987):

$$\mathcal{D} = 3 \times 10^{-5} \left(\frac{r_v}{10} \right)^3 \left(\int_{z_c}^{z_i^-} q_l dz \right)^{1/2}, \quad (5.19)$$

where r_v is the volume mean radius of cloud-top drops in microns⁴. Assuming that cloud water varies linearly with height from zero at cloud base to its cloud top value, and allowing for an r_v^n dependence in the drizzle rate results in the following expression:

$$\mathcal{D} = 3 \times 10^{-5} \left(\frac{z_i - z_c}{2} \right)^{1/2} q_l^{\frac{n+1}{2}}(z_i) \left(1.387 \times 10^5 \frac{\rho}{N} \right)^{n/3}, \quad (5.20)$$

where PB take $n=3$ and vary N the number concentration of cloud-drops.

⁴NT use this parameterization for the cloud-drops, and suggest a different criteria be used when the maximum size of cloud-top drops exceeds a certain size. Nonetheless, because the parameterization nicely represents the first order effects of cloud-depth and drop concentration we shall use the suggested form irrespective of the maximum cloud-top drop size, as did Pincus and Baker.

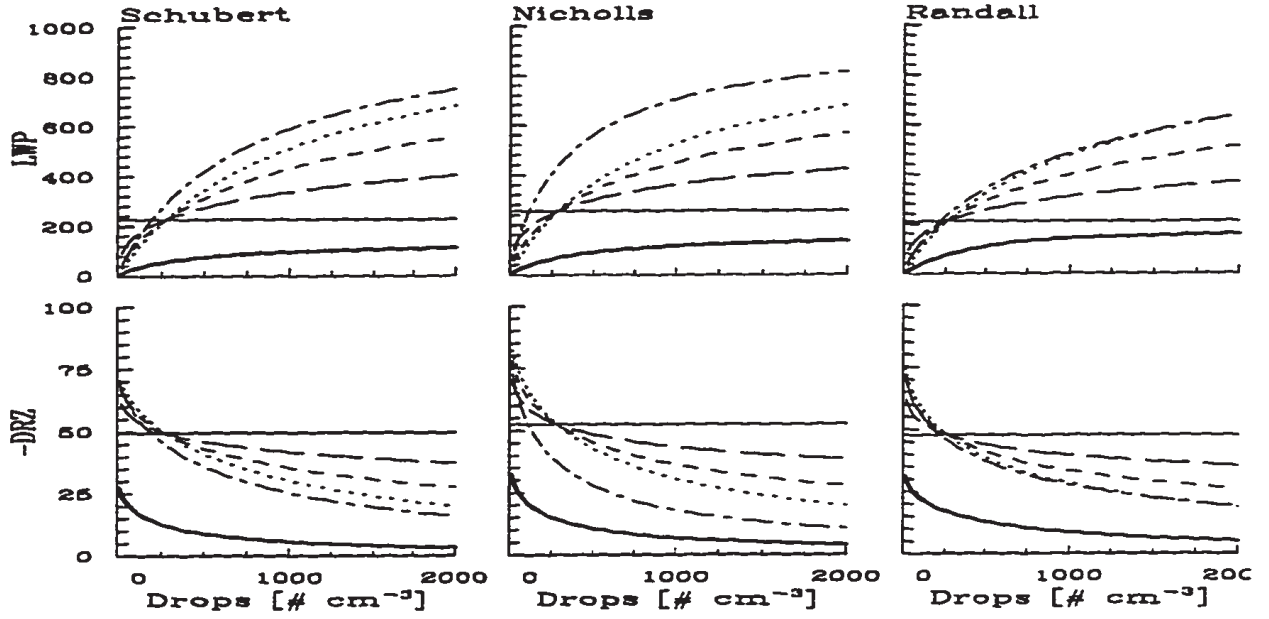


Figure 5.3: Drizzle production and LWP from steady state solutions of mixed layer models with different closures: (a) $(\mathcal{F}_{sv})_{min}$ closure; (b) Δ_m closure; (c) e_2 closure. Oakland sounding with $n = 3$ (thick solid line); GCSS-3 sounding with $n = 0$ (solid line); GCSS-3 sounding with $n = 1$ (long-dashed line); GCSS-3 sounding with $n = 2$ (short-dashed line); GCSS-3 sounding with $n = 3$ (dotted line); GCSS-3 sounding with $n = 3$ and sub-cloud evaporation (dash-dot line).

Evaporation of drizzle below cloud base can also be included in the model (Chen, 1996), wherein if we assume that

$$\frac{dq_r}{dt} = -\frac{[q_s(z) - q_{t,2}]q_r}{\tau_{evap}} \quad (5.21)$$

where $q_s(z)$ is the saturation mixing ratio of air at height z , q_r is the rain mixing-ratio (given by \mathcal{F}_{drz}/w_t where w_t is an assumed settling velocity for the drops) and τ_{evap} is an evaporative time-scale taken to be 2.5 s. The total evaporation can be found by integrating this expression over the time the drops spend in the sub-cloud layer (i.e., z_c/w_t) which allows for the expression of the rain mixing ratio at the surface as a function of the mixing ratio at cloud base, the height of cloud base and an assumed settling velocity:

$$q_r(0) = q_r(z_c) \exp \left[-\left(q_s(z_c/2) - q_{t,2} \right) \frac{z_c}{\tau_{evap} w_t} \right]. \quad (5.22)$$

Using expressions such as the ones above, Fig. 5.3 illustrates how the different models generate different values of LWP and $\mathcal{F}_{drz}(0)$ as a function of sounding, drop number N , drizzle-parameterization number n and sub-cloud evaporation. The significant height of

cloud-base is evident for the Δ_m closure as the inclusion of sub-cloud evaporation is shown to have a proportionally larger impact for this integration. Otherwise, the results reveal no interesting dynamics beyond what has already been discussed, except to illustrate that while LWP is nearly a linear function of \mathcal{F}_{drz} it tends to scale more like

$$LWP(N) \approx \frac{LWP(\infty)}{\frac{1}{N} + 1} \quad (5.23)$$

due to the fact fewer larger cloud drops lead to more drizzle which generates thinner clouds.

5.1.7 Comparison to ERM simulations

In Fig. 5.4 we compare time-sequence statistics from integrations of the mixed-layer models (with the three different closures) and the integration of the ERM. The GCSS sounding is used, with a radiative flux divergence of 37 Wm^{-2} . Integrations with and without drizzle are compared. For the mixed layer model integrations, the drop concentrations were set to give drizzle rates at the surface commensurate with what was predicted by the ERM-BM. Integrations are compared over 15 hours. Looking first at the upper panels, which compares the non-drizzling solutions, we note that all the models predict further deepening of the boundary layer, however, only the ERM predicts a reduction in LWP due to a more rapid rise in cloud base associated with a decoupling in the mixed layer. This decoupling is evident by the increasing separation between the actual cloud base, and that associated with the mean thermodynamic properties of the boundary layer. The relatively cooler and moister sub-cloud layer leads to a more dramatic reduction in the latent heat flux, and a mitigation of the negative sensible heat fluxes.

It is not possible for the mixed layer models to capture this behavior. The entrainment coefficients may be changed so that w_e is identical among all models—nonetheless, the integrations will still diverge. If we specify the entrainment rate based on the ERM results, the three mixed layer models become equivalent and all predict the correct evolution in z_i . However, a well mixed state leads to larger latent heat fluxes and more negative sensible heat fluxes than a state with a slightly cooler, moister sub-cloud layer. These changes cooperate to lower cloud base relative to the ERM simulations and over-predict

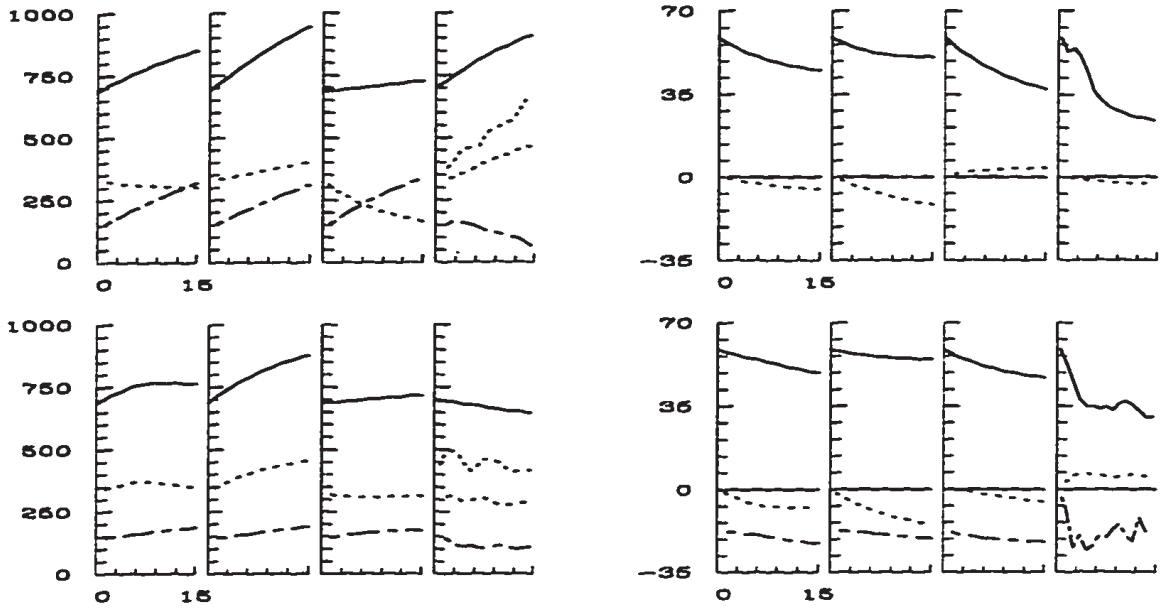


Figure 5.4: Time-sequence of cloud properties and surface fluxes for MLMs and ERM integrations. Four panels are plotted. Each panel contains four plots from left to right these are: MLM with $(\mathcal{F}_{sv})_{min}$ closure; MLM with Δ_m closure, MLM with e_2 closure; ERM integration. No drizzle (upper), drizzle (lower) panel. Left panels plot cloud top (solid line), cloud base (dotted line), LWP (dash dot line). For ERM integrations the second (lower) dotted line refers to the cloud base associated with the mean boundary layer properties. Right panels: Latent heat flux (solid line), sensible heat flux (dotted line), drizzle flux (dash-dot line).

cloud LWP. Consequently LWP is less in the ERM integrations for two reasons: (i) the separation of the boundary layer into cloud and sub-cloud layers raises cloud base from its mixed layer equivalent value; (ii) the mixed layer equivalent value of cloud base is higher due to less moistening and cooling from the surface.

When drizzle is allowed to form there is better agreement in LWP predictions among the models. As we saw in previous sections the natural sensitivity of the MLM is to reduce LWP for more drizzle. More detailed models tend to be more ambiguous in their behavior. For the case of this sounding and this forcing the ERM-BM has a deeper cloud at the end of the simulation when drizzle is allowed to form. Consequently by not representing this sensitivity, the MLMs appear to do a better job. There are however robust differences. The MLMs are incapable of capturing the strong stabilization of the sub-cloud layer (evidenced by the positive surface sensible heat fluxes, the sharp reduction in latent heat fluxes at the surface, and the divergence in the two measures of cloud base)

thereby cooling and strongly moistening the boundary layer, when it should be warmed and moderately moistened as a result of surface interactions.

This is just one case study and it is difficult to say how each mixed layer model will do in each circumstance. However, some of shortcomings are robust. Departures from well mixed states invariably produce cooler moister sub-cloud layers, so to the event that the turbulence is not sufficiently vigorous to maintain a well mixed state, MLMs will over-predict latent heat fluxes and under-predict sensible heat fluxes at the surface. ERM and LES integrations commonly allow some amount of stratification to develop so that this shortcoming of the MLM is often realized. The other shortcoming is that MLMs invariably predict less cloud for more drizzle and rarely predict the positive surface sensible heat fluxes that result from a sub-cloud layer strongly cooled by the evaporation of precipitation.

5.2 Two layer models

The discussion of the previous section motivates an analysis of two layer models. Over the years a number of two-layer models of the atmospheric boundary layer have been proposed. Albrecht et al., (1979) modeled the trade-cumulus boundary layer using a two-layer model. This model was later generalized in to explain the transition of stratocumulus to cumulus and the effect of precipitation on the boundary layer (Wang, 1993). Turton and Nicholls [(1987);hereafter TN] built a two-layer model in order to explain the observed decoupling of the marine stratocumulus topped boundary layer during the day. Krasner (1993) also briefly discusses a two-layer generalization of his second-order bulk boundary layer model.

Because Turton and Nicholl's model appears to be the simplest our original intent was to build this model and examine whether its additional features leads to a more realistic representation of stratocumulus-topped boundary layers. In the course of building this model it was realized that a number of built-in limitations—which we discuss below—make it incapable of dealing with boundary layers in which stratified interfaces develop but fluxes don't vanish. Because of the limitations of the TN model, we suggest a new model. This

model is the simplest model we could think of which is physically justifiable and capable of representing the vertical structure found to be an important element of precipitating boundary layers. It is discussed subsequent to our discussion of the limitations of the TN model.

5.2.1 *The Turton and Nicholls model*

In contrast to flux-partitioning type closures in which the ratio of negative to positive area in the buoyancy flux graph is constrained, Nicholls and Turton (Nicholls, 1987) propose that the entrainment rate be related to the integral of the net area in the graph of the buoyancy flux. Mathematically we can define the positive and negative areas of the buoyancy flux graph as

$$A_n \equiv \frac{1}{2} \int_{0+}^{z_i^+} (|\mathcal{F}_{sv}| - \mathcal{F}_{sv}) dz \quad \text{and} \quad A_p \equiv \frac{1}{2} \int_{0+}^{z_i^+} (|\mathcal{F}_{sv}| + \mathcal{F}_{sv}) dz \quad (5.24)$$

respectively. Flux partitioning schemes restrict the ratio A_n/A_p . In contrast this ratio may vary during the evolution of an integration when the Δ_m or e_2 parameterization is used to model entrainment. For these other parameterizations $A_p + A_n > 0$ is a necessary and sufficient condition for sustaining positive entrainment rates. TN use the added degree of freedom, afforded by a less constricting parameterization of entrainment, to state the following condition for decoupling: "...the rate of working against buoyancy necessary to maintain a single mixed layer, a state of maximum internal potential energy, becomes too great" when A_n/A_p becomes less than a certain threshold value C . Energetic arguments require $C \in (-1, 0)$. NT take $C = -0.4$.

During the course of an integration TN diagnose decoupling on the basis of the above condition (i.e. $A_n/A_p < C$). Once decoupling occurs the level of decoupling is diagnosed by iteratively solving for the level, z_l for which $A'_n/A'_p = C$. Where A'_n and A'_p are defined in analogy to A_n and A_p except that z_l is taken as the lower bound in the integrals of Eq. 5.24. In addition, all fluxes are presumed to vanish at z_l . Because the derivative of the fluxes are discontinuous across z_l two layers with different thermodynamic properties develop. Both are constrained to be well mixed, although they need not share a common interface—as in order to satisfy $A'_n/A'_p = C$ the lower boundary of the upper mixed layer,

z_l , may increase faster than the upper boundary of the lower mixed-layer (z_x). Because $z_c > z_l \geq z_x$, where z_c is the cloud base height, the level of decoupling is guaranteed to be in clear air. Consequently simple entrainment parameterizations (i.e., ones for which density is a linear function of mixing fraction and TKE is produced away from the interface) based on the scale velocity in the lower-mixed layer and the degree of stratification at z_x may be used to predict $\frac{dz_x}{dt}$ (and $\frac{dz_l}{dt}$ for the case when the layers are thermodynamically distinct but $A'_n/A'_p > C$). If after the diagnosis of decoupling $\frac{dz_l}{dt} > \frac{dz_x}{dt}$ then $z_l > z_x$. In this case the thermodynamic properties for $z \in (z_x, z_l)$ are assumed to vary linearly between layers. The boundary layer becomes re-coupled when $z_l = z_x$ and $\Delta\theta_{vx}$, the density difference across the internal interface at z_x , falls below a certain threshold.

The NT formulation for diagnosing and modeling decoupled boundary layers may be suitable for some particular circumstances; however, intrinsic limitations—which we itemize and discuss below—limit a more general application of the model.

- The criteria for decoupling $A_n/A_p < C$ only allows one to diagnose z_l for the special case when $\mathcal{F}_{sv}(0^+) > 0$. However, there are many instances when the model predicts $A_n/A_p < C$ yet the surface buoyancy flux is negative. In such cases $z_l = 0$ minimizes A'_n/A'_p , but generally at a value significantly greater than C . Consequently, while the decoupling condition is necessary to insure that $z_l \in (0, z_c)$ exists, it is not sufficient.
- The condition that fluxes vanish at z_l is too strong. It may be reasonable for fluxes (particularly the buoyancy flux) to vanish at some level when the boundary layer becomes decoupled. However a vanishing buoyancy flux need not imply that the total water flux and the moist-static energy flux also vanish. Moreover, in the case of precipitating boundary layers a large amount of internal stratification may develop, but the fluxes do not necessarily vanish across the region of stratification.
- By setting the fluxes to be zero at z_l and letting the upper mixed layer move away from the lower mixed layer TN implicitly assume that beyond a certain point the cloud layer chooses to mix less with the sub-cloud layer rather than mix less with the free atmosphere. This assumption that the upper-mixed layer would at some

point rather work against buoyancy at the upper interface (rather than at the lower one) doesn't fit with ones intuition that turbulence would prefer to work against buoyancy along the least stratified interface.

- The TN criteria for decoupling is incapable of predicting the development of internal stratification due to drizzle in a mixed layer. In order to do this the model must always recognize different layers within a well-mixed boundary layer so that the drizzle flux can act in opposition to turbulent mixing and promote the development of an internal layer of stratification.

Although the TN model may well be sufficient for special cases, its lack of generality motivates the development of a new model which we discuss below.

The second point itemized above introduces an interesting point. Often the presence of stratification is used as an indicator of decoupling (Martin et al., 1995). TN, however, associate decoupling with the more stringent condition that fluxes vanish somewhere in the boundary layer. To distinguish between the cases we will use TNs definition when talking about decoupling, and will talk about internally stratified boundary layers for the other cases. Clearly the TN model is incapable of dealing with internally stratified but coupled boundary layers. Moreover, the TN condition that fluxes vanish at z_l , may imply instantaneous large changes in the total water and moist-static energy fluxes at the time decoupling is diagnosed—notwithstanding that the associated changes in the buoyancy flux at z_l (and hence the diagnosed entrainment rate) will generally be small.

5.2.2 *A new, simple, two-layer model*

Fig. 5.5 diagrams the geometry of our two-layer model. The model is motivated by the desire to formulate the simplest theory capable of reproducing important elements of the dynamics of precipitating stratocumulus boundary layers. Previous results suggest that at least two layers are necessary to do this. Moreover, the theory should be capable of: (i) reducing to mixed layer theory as a limiting case; (ii) producing a two-layer

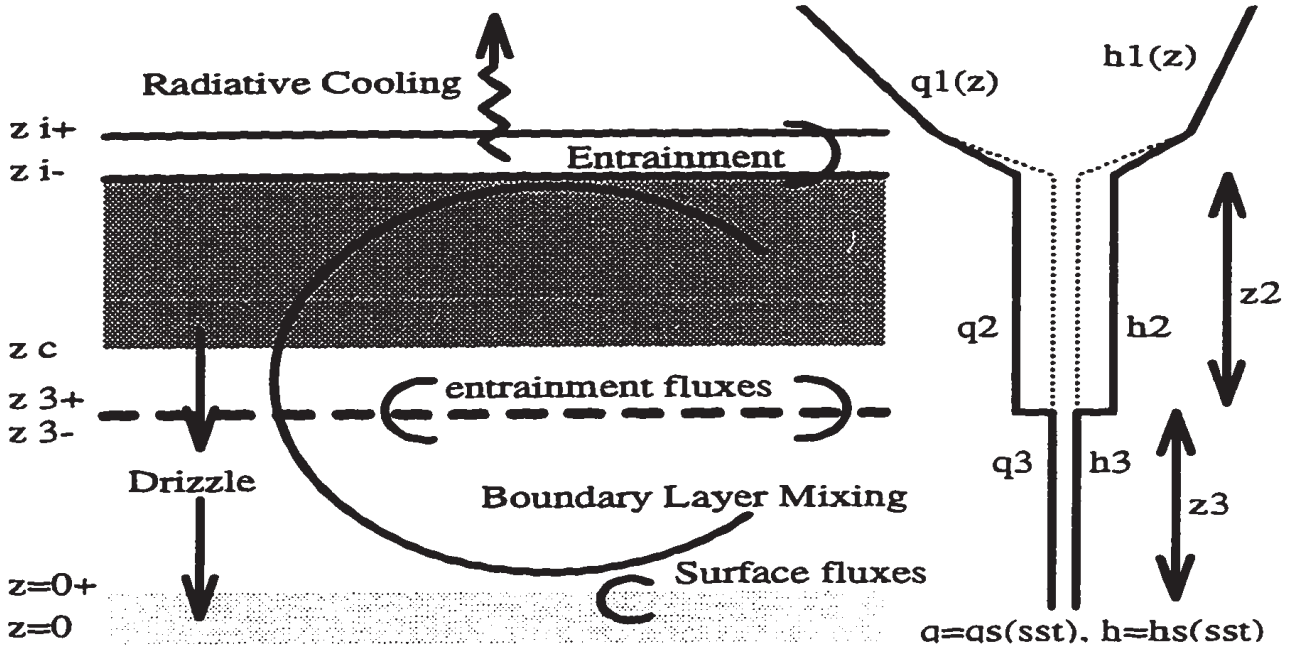


Figure 5.5: Diagram of two layer model.

structure in response to sufficiently strong entrainment or precipitation fluxes; (iii) allowing thermodynamically distinct layers to return to a well mixed state when appropriate. Lastly all elements should be justified on physical grounds⁵, yet be as simple as possible.

The basic framework for the model follows Chen (1996), in that TKE is predicted in each layer, and values of TKE are used in the parameterization of entrainment. The model integrates a total of eight first-order differential equations as it prognosticate three layer-averaged quantities in each layer:

$$\frac{dh_2}{dt} = \frac{-1}{z_2} [\mathcal{F}_h(z_i^-) - \mathcal{F}_h(z_3^+)] \quad (5.25)$$

$$\frac{dh_3}{dt} = \frac{-1}{z_3} [\mathcal{F}_h(z_3^-) - \mathcal{F}_h(z_0^+)] \quad (5.26)$$

$$\frac{dq_{t,2}}{dt} = \frac{-1}{z_2} \left[\mathcal{F}_{q_t}(z_i^-) - \mathcal{F}_{q_t}(z_3^+) - \frac{\mathcal{F}_{drz}(z_3^+)}{L_v \rho} \right] \quad (5.27)$$

$$\frac{dq_{t,3}}{dt} = \frac{-1}{z_3} \left[\mathcal{F}_{q_t}(z_3^-) - \mathcal{F}_{q_t}(z_0^+) + \frac{\mathcal{F}_{drz}(z_3^-)}{L_v \rho} - \frac{\mathcal{F}_{drz}(z_0^+)}{L_v \rho} \right] \quad (5.28)$$

$$\frac{de_2}{dt} = \frac{1}{z_2} \left[S_2 + \frac{g}{c_p T_0} \int_{z_3^+}^{z_i^-} \mathcal{F}_{s_v} dz - \mathcal{F}_e(z_i^-) + \mathcal{F}_e(z_3^+) - \frac{e_2^{3/2}}{\Lambda_2} \right] \quad (5.29)$$

⁵In contrast to non-linear models such as neural networks or genetic algorithms which can “learn” and reproduce the behavior of physical systems with out regard to an explicit statement of the physical processes at work.

$$\frac{de_3}{dt} = \frac{1}{z_3} \left[\mathcal{S}_3 + \frac{g}{c_p T_0} \int_{z_0^+}^{z_3^-} \mathcal{F}_{s_v} dz - \mathcal{F}_e(z_3^-) + \mathcal{F}_e(z_0^+) - \frac{e_3^{3/2}}{\Lambda_3} \right], \quad (5.30)$$

in addition to the position of the layer boundaries:

$$\frac{dz_i}{dt} = w_e + w_D \quad (5.31)$$

$$\frac{dz_3}{dt} = w_{32} + w_{23}. \quad (5.32)$$

In Eq. 5.31 entrainment, w_e is parameterized in a manner which combines the e_2 and Δ_m closures:

$$w_e = a_e e_s^{1/2} R_{i,s}^{-1} [1 + a_2 (1 - \Delta_m / \Delta \theta_v)], \quad (5.33)$$

Here Δ_m , $\Delta \theta_v$ and a_2 retain the same meaning they had in Eq. 5.10. $R_{i,s}$ is again a Richardson number characterizing the relative strength of the stratified interface and the turbulence:

$$R_{i,s} = \frac{gz_s \Delta \theta_v}{e_s \theta_0}, \quad \text{where} \quad e_s = \frac{e_2 z_2 + e_3 z_3}{z_b} + \frac{e_2 R_{i3}}{1 + R_{i3}} \quad \text{and} \quad z_s = \frac{z_b + z_2 R_{i3}}{1 + R_{i3}}. \quad (5.34)$$

Because $R_{i3} = gz_3(\theta_{v2} - \theta_{v3}) / (e_3 \theta_0)$ measures the degree of stratification at the internal interface, $e_s \rightarrow e_2$ and $z_s \rightarrow z_2$ in the limit of strong internal stratification (i.e. as $R_{i3} \rightarrow \infty$) while $e_s \rightarrow (e_2 z_2 + e_3 z_3) / (z_2 + z_3)$ and $z_s \rightarrow z_b$ in the opposite limit. In a study of stratocumulus Chen (1996) questions the validity of using flux partitioning parameterizations because they are based on the dynamics of dry convective boundary layers; nonetheless, she proceeds to use a parameterization which while not a flux partitioning scheme is also derived on the basis of results from dry convective boundary layers (Krasner, 1993) and is nowhere shown to account for cloud effects. Only the Δ_m closure explicitly attempts to account for the influence of phase changes on the density of entraining parcels. For this reason, and the fact that e_2 closure entrains too modestly (see Fig 5.4) we adopt the Δ_m closure. However, so doing requires that we derive the constant a_e in Eq. 5.33. This is done following the approach of Krasner (Krasner, 1993) in that coefficients are chosen to be consistent with the special case of a dry well-mixed steady-state boundary layer where $\mathcal{F}_{s_v}(z_i^-) = -0.2 \mathcal{F}_{s_v}(z_0^+)$. This results in $a_e = \frac{1}{2\Lambda_s}$. Given w_e fluxes of q_i and h_2 at z_i^- are found diagnostically using Eq. 5.4. The entrainment flux of kinetic energy is

found similarly by assuming that there is no source of TKE (except for what already is accounted for in the shear production term) in the interfacial layer, and that the TKE in the free atmosphere, e_1 , vanishes, so that $F_e(z_i^-) = -w_e e_2$.

In the above system of equations surface fluxes $\mathcal{F}_{q_t}(0^+)$ and $\mathcal{F}_h(0^+)$ are given in analogy to Eq. 5.6 and Eq. 5.5. For decoupled boundary layers the shear production term produces TKE in accord with our previous discussion and only in the lowest layer. For now the production of TKE by shear at z_3 or z_i is neglected. Because our model requires $z_3 < z_c$ the lower layer vanishes for the case of fog. In these situations (where cloud base descends toward the surface) the shear production term is distributed over the lowest 100m, and is thus allowed to increasingly contribute to the production of e_2 as $z_3 \rightarrow 0$. For the time being we choose $\Lambda_2 = \Lambda_3 = 0.5$ although an analysis of LES integrations supports $\Lambda_3 > \Lambda_2$ (Changan Zhang, personal communication). Drizzle fluxes are parameterized in accord with our discussion of §5.1.6 in that $\mathcal{D} = -w_t q_r$ where we now take $w_t = -0.65$ ms^{-1} but instead of Eq. 5.22 we use:

$$\begin{aligned} q_r(z_3) &= q_r(z_c) \exp \left\{ - [q_{s,2}(\bar{z}_2) - q_{t,2}] \frac{z_c - z_3}{w_t \tau_{evap}} \right\} \quad \text{where} \quad \bar{z}_2 = \frac{z_c + z_3}{2} \\ q_r(0) &= q_r(z_3) \exp \left\{ - [q_{s,3}(z_3/2) - q_{t,3}] \frac{z_3}{w_t \tau_{evap}} \right\} \end{aligned} \quad (5.35)$$

when solving for q_r at layer edges.. Assuming that all the radiative production of h_2 occurs in the interfacial layer at z_i ; probably overstates the buoyancy production in the cloud layer; nonetheless, our desire for simplicity again motivates the use of Eq. 5.7 to represent radiative fluxes. Note that the use of this equation results in the lack of any radiative contribution to the predictive equations for h_2 and h_3 . Unless otherwise noted all constants are specified in accord with our previous discussion of mixed layer models, SSTs and w_D and the thermodynamic state of the free-troposphere are also retained as prescribed functions representative of the large-scale conditions.

Letting x be any variable not subject to forcing in the interfacial layer at z_3 implies that the fluxes of x ($\mathcal{F}_x = \overline{w'x'}$) satisfy:

$$\mathcal{F}_x(z_3^+) - \mathcal{F}_x(z_3^-) = (x_2 - x_3) \left[\frac{dz_3}{dt} - w_D(z_3) \right]. \quad (5.36)$$

Entrainment is intermittent, a fact which motivates the empirically well supported assumption (Turner, 1968; E and Hopfinger, 1986) that the rate at which fluid in layer 2 entrains fluid in layer 3 is independent of the rate at which fluid in layer 3 entrains fluid in layer 2, i.e.,

$$-\mathcal{F}_x(z_3^-) = (x_2 - x_3)w_{23} \quad (5.37)$$

$$\mathcal{F}_x(z_3^+) = (x_2 - x_3)w_{32}. \quad (5.38)$$

Here w_{ij} is the rate at which layer j entrains layer i it is positive for $i < j$ and negative otherwise. Note also that substitution of Eq. 5.37 and Eq. 5.38 into Eq. 5.36 yields Eq. 5.32.

Given the above assumptions all that remains is to specify the fluxes $\mathcal{F}_x(z_3^+)$ and $\mathcal{F}_x(z_3^-)$. This really is the crux of the problem, as our model is well-posed to the extent that these fluxes can be written as a function of the known variables. After some experimentation we decided to parameterize these fluxes as follows:

$$\mathcal{F}_x(z_3^+) = C_x \left[\left(1 - \frac{z_3}{z_i}\right) \mathcal{F}_x(0^+) + \frac{z_3}{z_i} \mathcal{F}_x(z_i^-) \right] + (x_2 - x_3)w_{32} \quad (5.39)$$

$$\mathcal{F}_x(z_3^-) = C_x \left[\left(1 - \frac{z_3}{z_i}\right) \mathcal{F}_x(0^+) + \frac{z_3}{z_i} \mathcal{F}_x(z_i^-) \right] - (x_2 - x_3)w_{23}, \quad (5.40)$$

where $C_x \in (0, 1)$ is a decoupling coefficient, which we discuss further below, and

$$w_{ij} = \pm e_j^{1/2} \frac{b_1}{1 + b_2 R_{i,j}}, \quad \text{where } R_{i,j} = \frac{gz_j |\theta_{v,i} - \theta_{v,j}|}{e_j \theta_0} \quad \text{and } b_1 = 2\Lambda_j b_2 = 2 \left(\frac{\Lambda_j^2}{50} \right)^{1/3}, \quad (5.41)$$

where the sign is chosen so that $w_{23} < 0$ and $w_{32} > 0$ in accord with the definition of entrainment. Thus we use the e_i closure to predict entrainment rates across any internal interface that develops. This closure is suitable because it does not imply infinite entrainment rates in the presence of vanishing stratification, and because we constrain our interface to be in clear air.

The *a priori* justification for the above closure is as follows:

- It has nice mathematical properties: (i) If \mathcal{F}_x is linear in x at z_i and 0^+ then so long as C_x is independent of x then the above form guarantees that \mathcal{F}_x is linear in x at z_3^\pm ,

i.e., if $x = ay + bz$ and $\mathcal{F}_x(z_i^-) = a\mathcal{F}_y(z_i^-) + b\mathcal{F}_x(z_i^-)$ and $\mathcal{F}_x(0^+) = a\mathcal{F}_y(0^+) + b\mathcal{F}_x(0^+)$ then $\mathcal{F}_x(z_3^\pm) = a\mathcal{F}_y(z_3^\pm) + b\mathcal{F}_x(z_3^\pm)$. (ii) It guarantees that Eq. 5.32, and Eqs. 5.36-5.38 are satisfied.

- It has nice physical properties: (i) For the case of no stratification and $C_x = 1$ the parameterization produces fluxes consistent with a mixed layer layer model (i.e., it linearly interpolates between the surface and cloud-top fluxes). (ii) If the layers become thermodynamically distinct the model will attempt to re-mix the layers so long as C_x is sufficiently large. (iii) For C_x independent of x (i.e., $C_h = C_{q_t}$) the parameterization is guaranteed not to produce unstable states.
- It can be heuristically thought of as a flux partitioning scheme, where the total fluxes at z_3 are composed of boundary layer scale fluxes (the first term) and fluxes on the scale of the individual layers. Mixing from the former is not allowed to directly affect the position or the motion of the internal interface, and at its most efficient it can only maintain a well mixed boundary layer. Mixing associated with the latter, the so-called internal entrainment fluxes, determines the position of the interface.

Clearly the nature of our parameterization is dependent on the specification of C_x . The intuition built up through the course of the detailed numerical experiments analyzed in previous chapters provides some guidance here. For instance by requiring C_x to be a decreasing function of the Richardson number (or e_s , a measure of the energy in the boundary layer as a whole) we are stating that as the boundary layer becomes less energetic, or more stratified, the contribution of boundary-layer scale fluxes is reduced relative to the contribution of entrainment fluxes. Although one could come up with a number of ways to parameterize C_x we explore the consequences of the assumption that $C_e = 0$ and

$$C_h = C_{q_t} = (1 - \lambda) \min \left\{ 1, \sqrt{e_s/e_*} \right\} + \lambda, \quad (5.42)$$

where

$$\lambda \equiv \max \left\{ 0, \min \left[1, \frac{(z_3 - z_{c3}) + \alpha}{\alpha} \right] \right\}. \quad (5.43)$$

This parameterization states that boundary layer fluxes do not mix turbulent kinetic energy.⁶ With respect to thermodynamic fluxes our parameterization states that as e_* decreases below a certain threshold, e_* , the mixing by the boundary layer fluxes becomes less efficient. Counter-balancing the effect whereby less TKE leads to a reduction in fluxes is the fact that as the distance between the lifting condensation level of the lower layer and the top of the lower level approaches α , fluxes are allowed to increase, in the limit as $z_3 \rightarrow z_{c3}$ $C_x \rightarrow 1$. This is a crude way of stating that fluxes are enhanced as the lifting condensation level of the surface layer is reduced relative to the top of the surface layer, presumably by increased cumulus activity. In practice it turns out that the above specification of w_{ij} and $\mathcal{F}_x(z_3^\pm)$ is not sufficient to guarantee that $z_3 < \min(z_{c2}, z_{c3})$. To do this w_{32} is augmented to insure that $z_3 < z_{c3}$, and when necessary a fixed constant is added to both w_{32} and w_{23} to insure that $z_3 < z_{c2}$.

5.2.3 Integrations of the new, simple, two layer model

The behavior of the model is well illustrated by Fig. 5.6. Here are plotted 72 hour integrations of the one and two layer models. The one layer model is identical to the mixed layer model described in §5.1 except that the e_2 closure is replaced with the new hybrid closure described in §5.2. All integrations were of the GCSS sounding, with $\mathcal{F}_{rad} = 37$ Wm^{-2} . In the drizzle parameterization we took $w_t = 0.6$ ms^{-1} , $n = 3$ and $N_{cen} = 100$ cm^{-3} . The numerical integration was done using the third-order Adams-Bashforth scheme with a time-step of 30s.

Looking at the first three columns we note that there is little difference between the one and two layer models in the absence of drizzle. This figure does illustrate however that the model is capable of generating internal stratification in the absence of drizzle, although the effect of this stratification is small. It is interesting that there is very little sensitivity to e_* in the integrations. This may be understood as follows. The model is

⁶This assumption is not strictly justified as the fluxes of e due to boundary layer scale eddies may be considerable, however the lack of a large-scale constraint on the shape of \mathcal{F}_e makes this term difficult to deal with and motivates our choice to neglect it for now.

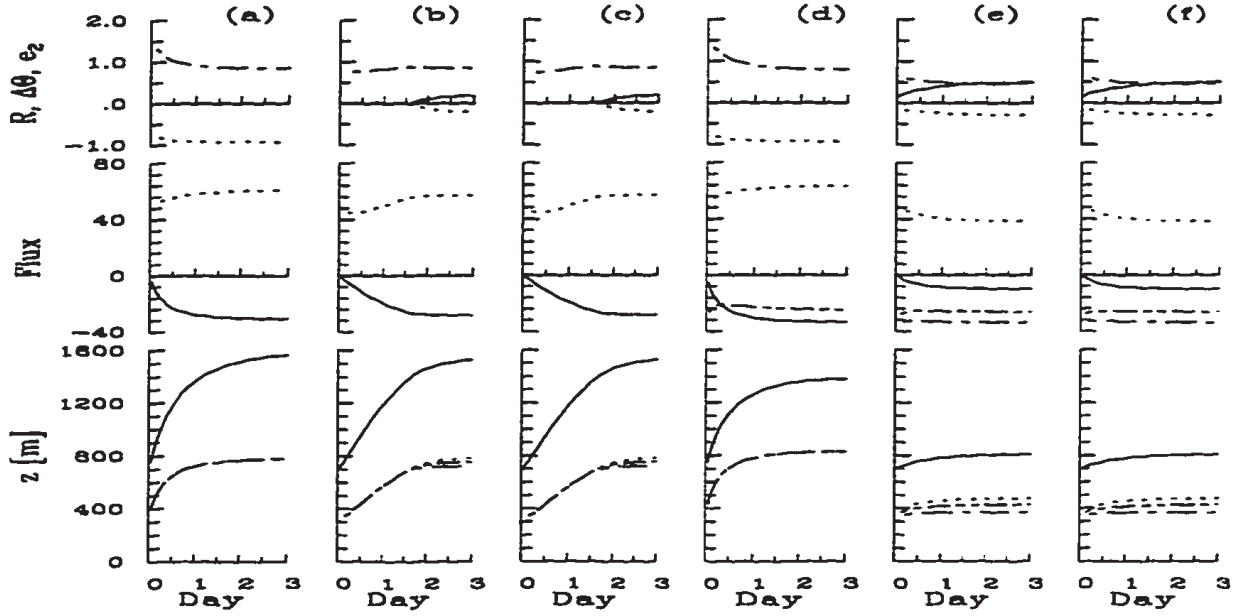


Figure 5.6: 72 hour two layer model integration. GCSS sounding, columns (a)-(c) no drizzle, columns (d)-(f) with drizzle. (a) and (d) are one-layer model. For the two layer mode columns (b) and (e) have $e_* = 0.2$, while columns (c) and (f) have $e_* = 0.5$. First row: $\Delta\theta_v(z_3)$ solid line; A_n/A_p dotted line; e_2 dash-dot line. Second row, fluxes in Wm^{-2} : $\mathcal{F}_\theta(0^+)$ solid; $\mathcal{F}_{q_e}(0^+)$ dotted; $-\mathcal{D}(z_3)$ dash-dot; $-\mathcal{D}(0^+)$ dash-dot-dot. Third row: z_c solid; z_c dotted; z_3 dash-dot. In decoupled layers the equivalent mixed layer cloud depth is also plotted with dash-dot-dot lines

constrained to have $z_3 < z_c$. In the presence of a strong source of TKE at the surface, as is the case in these simulations with significant shear production at low levels, the lower layer tends to be more energetic, causing z_3 to rise as rapidly as z_c . Only when cloud base rises sufficiently high for there to be a significant sink of TKE in the sub-cloud layer will a balance between e_2 and e_3 , at values of $z_3 < z_c$, be found. Only then can the layers begin to decouple. Because e_2 is always small the reduction of C_x from the first term in Eq. 5.43 is immediate, however the layers are not allowed to decouple so rapidly as to allow z_3 to fall below z_{c3} , consequently after decoupling is initiated the rate of decoupling is largely controlled by the λ parameter, and the rate at which the layer energetics allow z_3 to fall.

For the case of the drizzling integrations (last three columns of Fig. 5.6) the generation of an internal interface is much more immediate, and it has a dramatic effect on the evolution of the boundary layer. Fig. 5.6 illustrates that the formation of a moister and warmer lower level inhibits the generation of TKE in the upper level and reduces entrainment. In addition, relative to the non-drizzling two layer solutions, the ratio of

negative to positive area in the upper layer is significantly enhanced in the presence of stratification (see dotted line in first row of figures). This effect is in accord with our previous two and three dimensional simulations. Although the two layer model is not capable of generating a sufficiently shallow surface layer to allow surface sensible heat fluxes to reverse their sign in the presence of strong drizzle, it does exhibit a significant reduction in both total water fluxes and sensible heat fluxes relative to the one-layer model, leading to improved agreement with values expected on the basis of more detailed modeling studies.

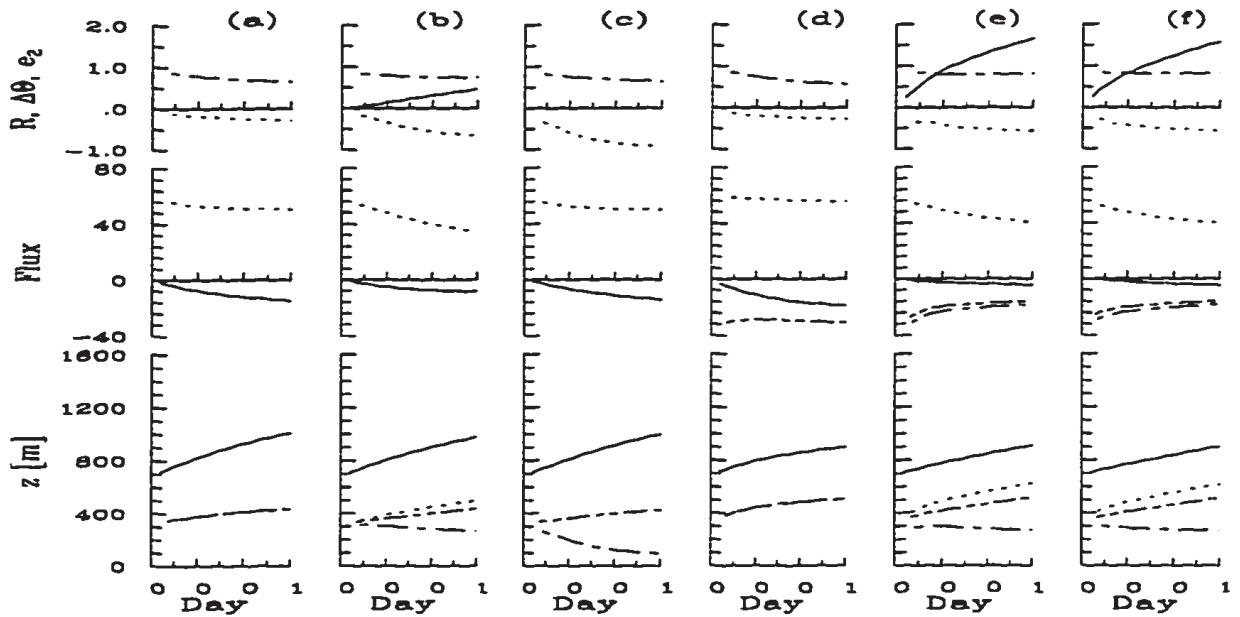


Figure 5.7: Same as previous figure except $C_m = 0.5C_t$

The above discussion illustrates that the level at which entrainment by e_2 balances entrainment by e_3 has a crucial impact on the dynamics of the model. This implies that the energy budget of the individual layers must be accurately predicted if the model is expected to do a good job. Upon closer inspection we found that modeling the shear production term as $C_m v_3^2$ grossly over estimates the amount of shear production. Moeng and Sullivan (1994) suggest that:

$$S = u_* \frac{1 - z/z_i}{kz(1 - 15z/L)^{1/4}} \quad (5.44)$$

well describes the shear production term for weakly convective and shear forced dry planetary boundary layers. If we integrate this form over the depth of our layers, where L is the

Monin-Obukhov length, $k = 0.4$ is von Karman's constant, and u_* is a friction velocity which we derive from similarity theory, we obtain an estimate of the shear production which agrees much better with our LES results. In the two-layer model and mixed layer model integrations, the surface layer often becomes stable, in which case l becomes positive and the shear production term above ceases to be well defined. For this reason we set $L = \min(-100, L)$ in Eq. 5.44 so as to effectively set a lower bound on the amount of shear production.

Results from a 15 hour integration (commensurate with the length of integrations in Fig. 5.4) are plotted in Fig. 5.7. The behavior is substantially different than what was seen in Fig. 5.6, largely because the interfacial layer forms at a lower level. As evidenced by the plots in column (c) choosing $e_* = 0.05$ allows a well-mixed non-drizzling solution to form. In the cases where stratification develops, the reduction in the generation of TKE at low levels puts z_3 at a relatively lower level and so an internally stratified layer develops sooner than in the previous case. Moreover, the amount of stratification is larger (see first row of figures solid line) and the effective reduction in surface fluxes is more pronounced. This is probably the chief advantage of the model. An unrealistic feature of the precipitating two layer model is the relatively large values of TKE in the cloud layer, which allows entrainment to proceed too rapidly for the drizzling case. In this case, the fluxes at z_3 are the mixed layer fluxes, as $\lambda = 1$. However, the effective reduction in the magnitude of the surface fluxes (due to the stratification) leads to less strongly negative buoyancy fluxes at the surface, and commensurately larger TKE production in the cloud. This is despite the fact that the cloud is shallower. Clearly we need a better way to model the response of the fluxes to the lowering of the lifting condensation level in the lower layer needs to be developed.

To recall, our original motivation for developing this model resided in the fact that MLMs could not represent the stratification within the boundary layer due to the presence of drizzle. Because of this fact they predict that clouds would deepen as a result of entrainment when often they would thin, and they were unable to represent the effects of stratification on the buoyancy flux, and surface fluxes (cf. Fig. 5.6). The two layer

model proposed above is successful in allowing internal interfaces of stratification to develop within the boundary layer—both in response to the internal forcing of drizzle, and in response to significant deepening of the boundary layer through entrainment. Although not shown we have done an experiment which illustrates that it can re-mix a formerly stratified boundary layer under appropriate conditions. Once a stratified interface is allowed to develop, it appears to influence the evolution of the cloud and the surface layer in a realistic manner.

The model presented here is still rather crude. Some improvement to it could be generated by considering the following points: First, a critical factor in determining when and where the model will stratify is the relative amount of energy production in the upper and lower layers. If a model of this form is to reach its full potential a more accurate accounting of the energy budget must take place. For instance, our understanding of how boundary layer fluxes of energy effect the distribution of TKE between layers needs to be better incorporated into the model. Second, our method of representing the cumulus convection out of the surface layer (via the λ parameter) is contrived, and overly restricts the behavior of the model by tying the fluxes at z_3 to the surface fluxes. This generates an unrealistic coupling between enhanced surface buoyancy fluxes and buoyancy fluxes at z_3 in the case when $z_{C3} \approx z_3$. A dramatic improvement to the model would hopefully result from a more realistic representation of cumulus convection out of the surface layer. Third, the current model artificially restricts the upper and lower turbulent layers to share a common interface. By relaxing this assumption the model might be able to better represent the case where an entraining cloud layer separates and detaches from the sub-cloud layer due to deepening induced decoupling. In all the above described instances LES results such as those in the previous sections should be used to better inform ones choice of closure.

5.3 Summary

In this chapter we examine the behavior of the Pincus and Baker hypothesis in more detail, in part through a rigorous analysis of the dynamics of precipitating mixed layer

models. We find that their result is qualitatively insensitive to how one specifies the entrainment closure in a mixed layer model. Nor does their hypothesis appear to qualitatively depend on one's choice of initial sounding, so long as it allows cloudy steady states. The dynamics underlying their result is that precipitation leads to an overall warming of the boundary layer which reduces surface sensible heat fluxes and buoyancy production of TKE in the boundary layer. Because all models of stratocumulus topped mixed layers relate, in some fashion, entrainment at cloud top to buoyancy production of TKE within the boundary layer, entrainment is reduced as the surface buoyancy flux is reduced.

We also show that mixed-layer models are unable to capture some fundamental aspect of a precipitating boundary layer, namely that the sub-cloud layer is destabilized with respect to the surface and stabilized with respect to the cloud layer. Because of this they over predict cloudiness in a specified environment, and predict a relationship between surface fluxes and precipitation which is in the wrong sense. To correct for these shortcomings we analyzed the suitability of the Turton and Nicholls two-layer model, but found it ill suited to the case of precipitating boundary layers. As an alternative we propose a new very simple two layer model which despite many limitations does represent a zeroth order illustration of how the two-layer dynamics can improve upon the dynamics of mixed-layer models and begin to capture many elements of the behavior illustrated by LES and ERM integrations.

Chapter 6

CONCLUSIONS

Conclusions are best drawn in the context of previous knowledge or speculation about the dynamics of precipitating stratocumulus. Although this study largely set out to address the hypothesis of Pincus and Baker (1994), our results are relevant to a larger body of work. For this reason we will state our conclusions in relation to a number of previous studies. Following this we offer a brief summary of what our work suggests are the essential ingredients of precipitating stratocumulus. Lastly we review some limitations of our study and offer suggestions for future work. No attempt is made to exhaustively review every result, instead we emphasize how different results combine to form a coherent “picture” of the dynamics of precipitating stratocumulus, and discuss how this picture differs or agrees with those drawn by other investigators.

6.1 Previous studies

6.1.1 *Paluch and Lenschow PL*

Paluch and Lenschow’s (1991) study of stratocumulus and drizzle during FIRE has a number of interesting results. They find that the effects of drizzle are best seen on scales of order 10 km, and that these effects include a significant depression in sub-cloud potential temperature (order 0.6 K) and an elevation in sub-cloud water mixing ratios of order 0.5 gkg⁻¹. We find that precipitation has a similar effect (quantitatively and qualitatively) in our simulations, although the scale selection could not be looked at due to domain size restrictions. In recognizing that precipitation tends to stabilize the sub-cloud layer with respect to the cloud layer PL speculate that this may decouple the layers, where by “decoupling” they mean a reduction or elimination of fluxes within the stabilized interior of

the boundary layer. This is also not in accord with our simulations where the stabilization of the sub-cloud layer leads to equal or more transport of moisture out of the sub-cloud layer (particularly when shear makes a significant contribution to the TKE budget). The nature of the transport is changed, however, as the eddies become more intermittent and cumulus-like with much larger positive skewness. If transport efficiency is defined by considering the ratio of transport to TKE, these narrower more concentrated up-drafts responsible for the transport in the precipitating solutions are much more efficient.

This idea that precipitation, which stabilizes the sub-cloud with respect to the cloud layer, leads to a decoupling of the layers has also been suggested by other authors, e.g., Brost et al., (1982b) and see review in Cotton and Anthes (1989). However, because (as we show) internal stratification need not imply smaller fluxes it does not necessarily portend a drying of the cloud layer and eventual break up of the cloud as suggested by PL. Moreover, for the case of a boundary layer with moderately strong precipitation we show that the characteristics of the sub-cloud layer are established on the order of a few eddy turn-over times, however once these characteristics are established the boundary layer can still revert toward its original characteristics on time-scales of a few hours once precipitation is stopped. In our simulations drizzle does act as a means of temporarily limiting cloud liquid water, and cloud optical path, but most changes in boundary layer structure appear reversible on short time-scales once drizzle stops. Further evidence that drizzle is not the driving force behind the stratus to cumulus transition is provided by simulations of the transition from completely overcast to partly cloudy conditions, which were designed to mimic the evolution of the first ASTEX Lagrangian experiment. These simulations illustrate that changes in sea-surface temperature are the leading order effect and that precipitation plays a secondary role.

6.1.2 *Pincus and Baker*

On the basis of mixed layer model results Pincus and Baker (1994) suggest that stratocumulus optical depth is a monotonically decreasing function of drizzle production. In their discussion cloud base tends to remain moderately constant and cloud top finds a lower level of equilibrium (i.e., less entrainment) as drizzle increases. After a closer

examination of their model, and mixed layer models in general, we find that this hypothesis is not sensitive to ones closure assumptions or ones choice of initial sounding. It is a robust result for mixed layer models, the basic dynamics of which is that greater drizzle production warms the layer as a whole, thereby decreasing surface fluxes. In a mixed layer model where surface buoyancy fluxes are directly connected to fluxes throughout the whole layer this leads to less buoyancy production in the cloud, and hence less entrainment.

In some special cases the LES and ERM produce solutions which are in accord with elements of the Pincus and Baker hypothesis. However, even when the cloud field responds in a way consistent with their hypothesis, it does so for a different reason. Overall precipitation leads to an enhancement in the surface sensible heat fluxes and a reduction in surface latent heat fluxes, exactly opposite of what is predicted by the mixed layer model. In the LES entrainment is generally inhibited through a reduction in the buoyancy flux and less turbulence in cloud. However, this effect is primarily associated with the stabilization of the cloud with respect to the sub-cloud layer, and not a diminishment of the surface buoyancy fluxes. The reduction in entrainment can affect the cloud water field in one of two ways: First, in clouds which deepen with increased entrainment, less entrainment means that there will be less liquid water and shallower clouds. This tends to be the scenario when there are only small jumps in liquid water across cloud top. Second, in cases where more entrainment leads to shallower clouds we find that small or moderate amounts of drizzle, by inhibiting entrainment, can lead to less thinning of the cloud layer (and relatively deeper clouds). Such a possibility is not accounted for in the mixed layer dynamics. Moreover, an additional affect of drizzle is to partition heat and moisture between a warmer drier cloud layer and a cooler moister sub-cloud layer. This leads to a significant reduction in cloud-water from what would be expected if the boundary layer was well mixed. A simple two-level model is proposed, and despite its use of somewhat contrived closures it is able to predict the development of an internal interface of stratification due to drizzle. The development of this internal stratification is also shown to impact the surface fluxes and cloud liquid water path in a manner consistent with what is predicted by the LES and ERM integrations. In this sense it represents an improvement on the mixed-layer model.

6.1.3 *Chen and Cotton*

Chen and Cotton (1987) were among the first to consider the effects of precipitation on stratocumulus dynamics. Using a higher-order turbulence closure model with a simple parameterization of precipitation, they showed that a reduction in precipitation leads to more cloud liquid water, more buoyancy production and a deeper boundary layer. This result is in accord with elements of our integrations, but the underlying dynamics, or interpretation thereof, is different. They attribute their response to an interaction between the radiative forcing and the dynamics because in the presence of more liquid water their model generates significantly more radiative cooling which drives the more vigorous circulations. Because deeper clouds have more liquid water at cloud top, they tend to cool in a shallower layer, so the same amount of radiative-flux divergence drives more intense cooling in a shallower layer. However, we show that the net flux divergence is a more important parameter than the local radiative cooling rate. Regardless, we find that the dominant dynamical effect is not an increase in the amount of excess energy radiated by the cloud layer, but rather the generation of stratification in the interior of the boundary layer. As the cloud layer warms and dries with increased precipitation, the local tendency of precipitation to enhance buoyancy production is overcome and less vigorous circulations result, particularly in the cloud layer. Radiative convective interactions may well be important in actual boundary layers—particularly when very strong drizzle significantly depletes cloud liquid water—but this effect was not needed to explain our results.

6.1.4 *Albrecht*

Using a two-layer model with parameterized precipitation Albrecht (1989) suggests that drizzle production may limit cloud fraction. Although we did not examine his hypothesis as carefully as some others, some of our results bear on his suggestions. In the case of boundary layers with large precipitation efficiencies, cloud fraction can be reduced below unity as the very efficient production of precipitation results in significant warming and drying within the cloud layer which eventually limits the formation of layer clouds. In these strongly (perhaps unrealistically so) forced cases our results are in accord with

Albrecht's hypothesis. However, in the ASTEX Lagrangian 1 case study whose last hours are much more typical of the conditions Albrecht discusses (i.e., a deep trade-cumulus boundary layer out of which cumulus convection intermittently forms) we find different results; integrations with the ERM-NM (no drizzle) generate smaller cloud fractions than do integrations with the ERM-BM (integrations with drizzle).

6.1.5 *Feingold et al.*

Feingold et al., (1996a) primarily studied the influence of boundary layer dynamics on drizzle production and concluded that more vigorous boundary layers support more drizzle production by prolonging the time a collector drops in the cloud layer. Using an ERM to study these effects they also noted that the differences in the level of boundary layer turbulence between strong and weak radiatively forced solutions was mitigated in the presence of drizzle. This effect they attributed to feedbacks whereby they state that "the inclusion of drizzle tends to feedback in a manner that diminishes the boundary layer TKE and cloud liquid water when drizzle is enhanced" (Feingold et al., 1996a). Such a result is very much in accord with our solutions and the mechanism for such a feedback is well addressed in this study.

6.1.6 *Austin et al.*

Lastly, Austin et al. (1995) use a simple dynamical framework to study precipitation formation in the marine boundary layer. They conclude that in the absence of a consideration of the CCN budget, a steady-state balance between turbulence, precipitation and sedimentation can be achieved for periods of 1-2 hours. This result is in accord with our simulations.

6.1.7 *Wang and Wang*

To our knowledge the only previous study which attempts to address in some detail the manner in which drizzle modifies the turbulent structure of the boundary layer is that by Wang and Wang (1994). In this study they used third order closure model with simple parameterization of drizzle to study buoyantly driven precipitating boundary layers. For

weakly precipitating solutions (order 0.1 mm day^{-1}) they found that the the stabilization of the subcloud layer leads to a reduction in the buoyancy flux (particularly near cloud base) which in turn leads to substantially weaker circulations (TKE is reduced by about 30%) particularly in the sub-cloud layer. Their integrations were more strongly forced at the surface, and appear to differ quantitatively from ours (in that given their average drizzle rate at the ground they see what seems to be a quantitatively stronger response); nonetheless, the basic dynamics illustrated by their model is largely consistent with what is shown by the LES. In one of their sensitivity studies the evaporation of drizzle in the sub-cloud layer was neglected, and the dynamics of the simulation reverted back to that of the non-precipitating boundary layer, suggesting that the dominant dynamical effect of drizzle is to cool and moisten the sub-cloud layer. In contrast, Moeng (personal communication 1996) finds that a simple representation of precipitation (for which there is little or no evaporation in the sub-cloud layer) leads to a dynamical response which is very much in accord with the precipitating solutions. Hence the question as to what part of the stabilizing influence of drizzle is dynamically important (sub-cloud cooling, or cloud layer warming) remains an outstanding question—one which we plan to address further in the near future.

For strongly precipitating integrations Wang and Wang interpreted a strong temporal oscillation in cloud fraction and liquid water flux as evidence of cumulus-like activity caused by the evaporation of precipitation in the sub-cloud layer. Because Wang and Wang recognized the inability of their model to properly represent scenarios in which skewness is large (because it assumes zero skewness in using the quasi-normal assumption to close on the fourth moments) they were cautious in their interpretation. Nonetheless, our integrations support their contention that strong precipitation generates a strongly stratified transition layer which in turn favors the creation of a boundary layer with more cumulus like circulations.

6.2 Summary

By this point we hope the reader has become familiar with what we conclude to be some fundamental aspects of precipitating stratocumulus. To summarize, our results

strongly suggest that the primary dynamical consequence of drizzle is to act to alter the mean potential density profile of the boundary layer. Specifically, as suggested by Brost et al., (1982), PL and others, the sub-cloud layer is stabilized with respect to the cloud layer. In addition we find that the cooling of the sub-cloud layer can destabilize it with respect to the surface; to our knowledge this possibility has not previously been recognized. The separation of the boundary layer into a moister and cooler sub-cloud layer and a warmer-drier cloud layer has a number of consequences: (i) Surface sensible heat fluxes are substantially enhanced, although latent heat fluxes are reduced. (ii) Cloud base is higher than would be predicted on the basis of boundary-layer-averaged quantities. (iii) Convective elements emanating from the sub-cloud layer are less buoyant and the rate of buoyancy production of TKE is diminished—although the increased instability at the surface may enhance the shear production term at low levels. This leads to smaller values of $\overline{w'w'}$ in the cloud layer and less entrainment, but larger $\overline{w'w'w'}$ particularly near cloud-base. Depending on the characteristics of the free-troposphere, reduced entrainment may lead to either a deeper or a shallower cloud. (iv) The structure of the boundary layer in the presence of drizzle has the character of a forced solution. The turbulence comes into equilibrium with its forcing after a few eddy turn-over times. Upon cessation of the precipitation, boundary layer structure appears to relax back to the non-drizzling solution on the time-scale of a few hours. (v) Boundary-layer fluxes are maintained, or may actually increase as the boundary layer circulations become more efficient, although more intermittent, transporters of heat and moisture.

The idea that boundary layers decouple (i.e., all turbulent quantities go to zero somewhere in the boundary layer) in the presence of internal stratification is, in the recent literature, often contrasted to mixed-layer in which fluxes are linear and the boundary layer always remains well mixed. Our results suggest a third possibility: *strongly coupled boundary layers in the presence of internal stratification*. To illustrate the differences between coupled but stratified boundary layers and their decoupled and stratified counterparts, it is useful to consider the following two examples.

On the one hand internal stratification may develop as a boundary layer deepens, but fails to generate sufficient kinetic energy to maintain a well mixed layer. Indeed PL

note that only the most turbulent boundary layers tend to be well mixed. We expect this to be the case when the turbulent forcing is diminished, as might be the case of daytime boundary layers in which absorption of solar radiation reduces the production of TKE through cloud top cooling. In such a scenario we expect that the sub-cloud layer will become stabilized with respect to the cloud layer. So long as the surface layer is stable with respect to the surface (as it will be at some point if the SSTs are not changing and the boundary layer is warming due to entrainment) a positive feedback loop will result as the development of an internal layer of stratification means that each subsequent eddy will have to do an increasing amount of work to mix the layer, and is thus increasingly unlikely to succeed. Consequently at some point we expect the upper layer to detach from the lower layer as turbulent fluxes vanish a certain distance below the cloud layer. In this type of boundary layer we expect the cloud layer to thin and dissipate as it is cut off from its supply of moisture below.

On the other hand we believe that the basic dynamics underlying the generation of stratification in the precipitating boundary layer to be different. In this case stratification results because precipitation acts like a forcing on the thermodynamic profile of the boundary layer. Turbulence continually opposes this forcing and attempts to re-mix the boundary layer, but is unable to do so completely. Instead a balance between turbulent mixing from above, surface fluxes from below and the evaporation of precipitation acts to create a cooler moister sub-cloud layer whose characteristics are established on relatively short time-scales. In this type of boundary layer turbulent kinetic energy tends to become more intermittent and cumulus-like in the sub-cloud layer with its magnitude largely dependent on the shear production term at low levels. The stabilization of the sub-cloud layer with respect to the cloud layer tends to lead to less production of TKE in the cloud. If this type of boundary layer were to decouple, the source of precipitation would be eliminated, as would be the forcing on the density profile. In the absence of this forcing the boundary layer tends to return to a well mixed state on time-scales of a few hours, hence boundary layer un-mixing is a forced state, in marked contrast to boundary layers which un-mix due to a deepening or a reduction of buoyancy production at cloud

top. Clearly in the above conceptual model the role of the surface forcing and shear is important. Nonetheless the tendency of precipitation to maintain shallower, cooler, and moister boundary layers does appear to have a largely forced character.

6.3 Limitations, speculation, and future work

This study has numerous limitations. Chief among them is the complete neglect, or poor representation, of many physical processes. Perhaps the primary physical limitation of our study of drizzle formation was the lack of an aerosol model. Real precipitation affects the ambient aerosol concentration, and the suggestion that boundary layers are bi-stable with respect to aerosol production rates (Baker, 1990) may dramatically amplify the effect of precipitation, as weakly precipitating boundary layers may well be a transient state. Also, as discussed at the outset (see Chapter 2), the representation of the entrainment process is also a potential weakness in relatively coarse resolution LES of stratocumulus such as presented here. Consequently, further studies with refined resolution are also warranted.

In addition, the fact that many results were derived on the basis of two-dimensional integrations, leaves many issues ripe for further investigation. Among these are the following:

- Precipitating boundary layers have unstable steady states characterized by a fixed value of precipitation efficiency, surface and radiative forcing and large-scale divergence. A small change in any of these parameters may lead to the break-up of the cloud on long time-scales.
- There is a precipitation rate which maximizes boundary layer integrated $\overline{w'w'}$, as more/less precipitation reduces $\overline{w'w'}$ in the cloud/sub-cloud layer.
- Strongly precipitating solutions prompt up-scale growth in the turbulent circulations.
- Precipitating boundary layers are sensitive to small changes in initial conditions and ones choice of collection kernel, but are relatively insensitive to how sub-grid scale water fluxes are modeled.

- Changes in grid-spacing, which strongly impact the two-dimensional results, are not thought to strongly influence the three-dimensional dynamics.
- In non-precipitating boundary layers in which clouds become thinner due to increased entrainment, moderate increases in precipitation efficiency leads to shallower boundary layers with deeper clouds.

Obviously a fruitful avenue for future work would be the further investigation of these hypotheses.

Lastly, recognizing that we completely neglected to study the drizzle formation process on a microphysical level we believe that further investigation of how drizzle forms and organizes itself with respect to, and locally modifies the ambient turbulent structures would be worthwhile, as would be further study of how exactly precipitation modifies the the TKE budget and other turbulent quantities.

Appendix A

MODEL PARTICULARS

A.1 Continuity Equation

Invariably LES and other detailed atmospheric models approximate the Navier-Stokes equations and the 1st law of thermodynamics by scaling away irrelevant physical processes. Most boundary layer flows use the Boussinesq approximation which drops terms of order d/D except when multiplied by gravity, where d is the depth of the layer and D is a scale height (Spiegel and Veronis, 1960). This approximation produces a continuity equation of the form:

$$\frac{\partial u_i}{\partial x_i} = 0. \quad (\text{A.1})$$

This is a good assumption for shallow flows. For deeper flows the anelastic approximation (Ogura and Phillips, 1962), is better. For this approximation density is allowed to have a height dependence so that $\rho = \rho_0(z)$ and the continuity equation satisfies

$$\frac{\partial(\rho_0 u_i)}{\partial x_i} = 0. \quad (\text{A.2})$$

For deep flows with strong temperature variations a better approximation is obtained by forcing the divergence of the basic-state heat flux to vanish (Durran, 1989). In this case the continuity equation takes the form

$$\frac{\partial(\theta_0 \rho_0 u_i)}{\partial x_i} = 0, \quad (\text{A.3})$$

where θ_0 is a basic-state temperature that is allowed to vary with height. This last continuity equation is often referred to as the pseudo-compressible continuity equation. Generally it is used with models which predict the evolution of pressure in a way which attempts to enforce Eq. A.3. Such is the case for the model from which our LES model is derived.

Unfortunately, this model does not consistently apply its continuity equation, as when the advective terms are cast into flux form they do so using the anelastic continuity equation. To avoid this inconsistency (which for our shallow flows is small to begin with) we generally choose a basic state for which $\theta_0(z)$ is constant, and hence we are justified in our use of the anelastic continuity equation throughout this text. In the cases where an elliptical equation is solved diagnostically for pressure, the elliptic equation is formed by requiring that the anelastic continuity equation is satisfied, and again $\theta_0(z)$ is constrained to be a constant.

A.2 Scalar Budgets & Quasi-Steady states

The equation representing the evolution of an arbitrary scalar on the resolved scale $\bar{\psi}$ subject to an as yet unspecified forcing \mathcal{S}_ψ , may (with the help of the anelastic continuity equation) be written:

$$\frac{\partial \bar{\psi}}{\partial t} = -\frac{1}{\rho_0} \frac{\partial}{\partial x_i} \rho_0 \left(\bar{u}_i \bar{\psi} + \overline{u'_i \psi'} \right) + \mathcal{S}_\psi, \quad (\text{A.4})$$

Here molecular effects are neglected in the explicit formulation of the system because they are much smaller than the correlation of sub-grid-scale motions which ultimately derive their character from the dissipative nature of the flow.

Let us define the operator $\langle \cdot \rangle$:

$$\langle f \rangle = \int_{X,Y} f(x, y) dx dy, \quad (\text{A.5})$$

where the integration is over all x and y and f is an arbitrary function of x and y . Assuming that sub-grid motions are uncorrelated over the spatial extent of the domain implies that $\langle f \rangle = \langle \bar{f} \rangle$; subsequently we will assume this relation is satisfied in the interests of minimizing our notation. Variables that are constant in x and y , such as ρ_0 satisfy: $\langle \rho_0 \rangle = \rho_0$. Applying this operator to Eq. A.4 yields:

$$\frac{\partial \langle \psi \rangle}{\partial t} = -\frac{1}{\rho_0} \frac{\partial}{\partial z} \left(\rho_0 \langle \bar{w} \bar{\psi} \rangle + \rho_0 \langle \overline{w' \psi'} \rangle \right) + \langle \mathcal{S}_\psi \rangle, \quad (\text{A.6})$$

where the horizontal derivatives vanish because our boundary conditions require all variables to be doubly periodic in x and y with a period given by the domain size. Eq. A.6

governs the evolution of the layer mean value of ψ , and shows that it changes due to a divergence in resolved and sub-grid vertical fluxes as well as the layer mean forcing.

Multiplying Eq. A.6 by ρ_0 , differentiating with respect to z while holding time fixed, and interchanging the order of differentiation (assuming that $\langle\psi\rangle$ is suitably well behaved), yields:

$$\frac{\partial}{\partial t} \left[\frac{\partial (\rho_0 \langle\psi\rangle)}{\partial z} \right] = -\frac{\partial^2}{\partial z \partial z} \left(\rho_0 \langle\overline{w\psi}\rangle + \rho_0 \langle\overline{w'\psi'}\rangle \right) + \frac{\partial}{\partial z} (\rho_0 \langle\mathcal{S}_\psi\rangle). \quad (\text{A.7})$$

This equation shows that for the case of a forcing of the form $\mathcal{S}_\psi = \frac{\partial F_{\psi,i}}{\partial x_i}$ the shape of the profile $\rho_0 \langle\overline{\psi}\rangle$ is invariant in time, i.e.,

$$\frac{\partial}{\partial t} \left[\frac{\partial (\rho_0 \langle\psi\rangle)}{\partial z} \right] = 0,$$

so long as

$$F_\Psi = \rho_0 \langle\overline{w\psi}\rangle + \rho_0 \langle\overline{w'\psi'}\rangle + \rho_0 \langle F_{\psi,z} \rangle \quad (\text{A.8})$$

is a linear function of z . When the boundary layer fluxes satisfy this condition the boundary layer is said to be in a quasi-steady state. A true steady state requires F_Ψ to be constant with height so that $\frac{\partial \Psi}{\partial t} = 0$.

The flux F_Ψ completely governs the evolution of the layer averaged variable $\langle\psi\rangle$. In the absence of any external forcing ($\mathcal{S}_\psi = 0$), F_Ψ describes the total evolution of $\langle\psi\rangle$ due to turbulent motions on the resolved, and sub-grid scales. Otherwise, F_Ψ also contains a flux (i.e., $F_{\psi,z}$) associated with the forcing. This is the case for liquid-water potential temperature which is sensitive to spatial changes in the flux of radiation and sedimenting liquid water:

$$\mathcal{S}_{\theta_t} = \frac{1}{\rho_0 c_p} \frac{\partial F_{rad}}{\partial z} - \frac{L}{c_p} \frac{\partial}{\partial z} (w_t q_t)$$

and total water mixing ratio (q_t), whose only source is the divergence of the flux of sedimenting liquid water.

In calculating fluxes, such as those defined above, it is tempting to estimate them from simple finite differences, such as the two point correlations formed by averaging q_t to a w point (recall we use a staggered grid for which w is defined on the edges of grid cells whose centers correspond to the location of q_t). However, when calculating the advective term

the model generally uses higher order polynomial fits (and in the case of the monotonic flux correctors it averages between two estimates of the flux based with weighting based on the nature of the local field). For this reason it is very important to calculate the fluxes in accord with the models finite-difference schemes. Our approach is to accumulate fluxes calculated by the model at certain intervals (i.e., every 15th time-step) for periods on the order of an hour (1800 time-steps) to obtain a robust measure of the average flux over a given period of time. This gives a much more accurate assessment of the model performance than is obtained by analyzing model fields in a post-processing sense.

A.3 TKE Budgets

A.3.1 Continuous Equations

The LES and ERM models attempt to predict the evolution of the resolved velocity field \bar{u}_i using the following equation:

$$\frac{\partial \bar{u}_i}{\partial t} = -\bar{u}_j \frac{\partial \bar{u}_i}{\partial x_j} - \theta_0 \frac{\partial \bar{\pi}_1}{\partial x_i} + \frac{g \bar{\theta}_{v1}}{\theta_0} \delta_{i3} + \epsilon_{ijk} (\bar{u}_j - u_{jg}) f_k + \frac{1}{\rho_0} \frac{\partial (\rho_0 \bar{\tau}_{ij})}{\partial x_j}, \quad (\text{A.9})$$

where the Exner function, $\pi \equiv c_p (p/p_0)^\wedge$, formulation is used in place of pressure since it simplifies treatment of the buoyancy term. The basic state is given by $(\pi_0, \theta_0, \rho_0, u_g, v_g)$, and is chosen to be in hydrostatic as well as geostrophic balance and to satisfy the ideal gas law for a dry atmosphere. Thermodynamic perturbations from this basic state are denoted by subscript “1.”

Here we will consider the equation governing the evolution of the layer averaged turbulent kinetic energy. Our derivation requires the use of the operator $\langle \cdot \rangle$ which we defined in the previous section, as well as the double prime notation: $f'' = f - \langle f \rangle$, which denotes turbulent fluctuations, i.e., deviations from layer averages. By expanding resolved variables:

$$\bar{u}_i = \langle u_i \rangle + \bar{u}_i'' \quad (\text{A.10})$$

Eq. A.9 may be re-written. Subtracting $\langle \text{Eq. A.9} \rangle$ from Eq. A.9 and making use of the anelastic continuity equation (which is satisfied in the layer mean, and therefor also for

the turbulent fluctuations) results in the following equation for the value of the turbulent velocity field:

$$\begin{aligned} \frac{\partial \overline{u_i''}}{\partial t} = & -\frac{1}{\rho_0} \frac{\partial}{\partial x_j} [\rho_0 (\overline{u_j'' u_i''} + \langle u_j \rangle \overline{u_i''} + \langle u_i \rangle \overline{u_j''} - \langle \overline{u_j'' u_i''} \rangle - \overline{\tau_{ij}''})] \\ & -\theta_0 \frac{\partial \overline{\pi_1''}}{\partial x_i} + \frac{g \overline{\theta_{v1}''}}{\theta_0} \delta_{i3} + \epsilon_{ijk} \overline{u_j''} f_k. \end{aligned} \quad (\text{A.11})$$

Contracting this equation with $\overline{u_i''}$, and making judicious use of the continuity equation ($\frac{\partial(\rho_0 \overline{u_i''})}{\partial x_i}$) results in the following equation for the layer averaged turbulent kinetic energy:

$$\begin{aligned} \frac{\partial}{\partial t} \left\langle \frac{\overline{u_i'' u_i''}}{2} \right\rangle = & -\frac{1}{\rho_0} \frac{\partial}{\partial z} \left(\rho_0 \left\langle \frac{\overline{u_i'' u_i''} \overline{w''}}{2} \right\rangle \right) + \langle \overline{w'' u''} \rangle \frac{\partial}{\partial z} \langle u \rangle + \langle \overline{w'' v''} \rangle \frac{\partial}{\partial z} \langle v \rangle \\ & -\theta_0 \frac{\partial}{\partial z} \langle \overline{w'' \pi_1''} \rangle + \frac{g}{\theta_0} \langle \overline{w'' \theta_{v1}''} \rangle + \frac{1}{\rho_0} \left\langle \overline{u_i''} \frac{\partial}{\partial x_j} (\rho_0 \overline{\tau_{ij}''}) \right\rangle. \end{aligned} \quad (\text{A.12})$$

The last term on the RHS of Eq. A.12 may be re-written to illustrate how the sub-grid term has both dissipative and transport qualities:

$$\frac{1}{\rho_0} \left\langle \overline{u_i''} \frac{\partial}{\partial x_j} (\rho_0 \overline{\tau_{ij}''}) \right\rangle = \frac{1}{\rho_0} \frac{\partial}{\partial z} (\rho_0 \langle \overline{u_i'' \tau_{i3}''} \rangle) - \left\langle \overline{\tau_{ij}''} \frac{\partial \overline{u_i''}}{\partial x_j} \right\rangle. \quad (\text{A.13})$$

Taking advantage of this decomposition, and the fact that θ_0 is constant allows us to write the TKE equation in the standard form:

$$\begin{aligned} \frac{\partial}{\partial t} \left\langle \frac{\overline{u_i'' u_i''}}{2} \right\rangle = & \overbrace{-\frac{1}{\rho_0} \frac{\partial}{\partial z} \left(\rho_0 \left\langle \frac{\overline{u_i'' u_i''} \overline{w''}}{2} + \theta_0 \overline{w'' \pi_1''} - \overline{u_i'' \tau_{i3}''} \right\rangle \right)}^{\text{Transport}} \\ & \underbrace{-\langle \overline{w'' u''} \rangle \frac{\partial}{\partial z} \langle u \rangle - \langle \overline{w'' v''} \rangle \frac{\partial}{\partial z} \langle v \rangle + \frac{g}{\theta_0} \langle \overline{w'' \theta_{v1}''} \rangle}_{\text{Production}} \\ & \underbrace{-\left\langle \overline{\tau_{ij}''} \frac{\partial \overline{u_i''}}{\partial x_j} \right\rangle}_{\text{Diss}}. \end{aligned} \quad (\text{A.14})$$

In this form terms have been grouped into production, transport and dissipation terms. The transport terms show how TKE is locally generated through the convergence of a flux which contains TKE transport terms, pressure and sub-grid correlations. TKE is produced by mean shear and buoyancy. The fact that the dissipation terms is positive definite follows from the fact that $\overline{\tau_{ij}}$ is parameterized:

$$\overline{\tau_{ij}} = K D_{ij}, \quad \text{where} \quad D_{ij} = \left(\frac{\partial \overline{u_i}}{\partial x_j} + \frac{\partial \overline{u_j}}{\partial x_i} \right) \quad (\text{A.15})$$

and K is a positive definite constant related to the magnitude of the local deformation, the grid-scale and the local stability. Consequently the dissipation term

$$\epsilon = \left\langle \overline{\tau_{ij}''} \frac{\partial \overline{u_i''}}{\partial x_j} \right\rangle = \frac{1}{2} K \langle D_{ij} D_{ij} \rangle \quad (\text{A.16})$$

is a positive definite function of the resolved velocity field and K .

A.3.2 Discrete approximations

The model actually solves the finite difference analog to Eq. A.9, and an energy equation is only implied by the nature of the finite difference operators. The finite difference analog to Eq. A.14 can be constructed, although spurious terms may arise because the finite difference system is not guaranteed to have an energy principle. The hope is, however, that departures from energy conservation are small—a hope that is partially justified by the fact that the numerical scheme used is stable. Numerical errors tend to have a dissipative nature.

In estimating the TKE budget, it is best to approximate the different terms in a manner which is consistent with the finite difference approximations used in to represent the momentum equation. To illustrate, consider the one-dimensional equation for the evolution of the velocity field under some forcing, written in its continuous form and in terms of a centered-in-time finite difference analog:

$$\frac{\partial u}{\partial t} = S_u \quad \Rightarrow \quad \frac{u_i^{n+1} - u_i^{n-1}}{2\Delta t} = (S_u)_i^n \quad (\text{A.17})$$

The energy analog to this system is formed by multiplying by u :

$$\frac{\partial e}{\partial t} = u S_u. \quad \Rightarrow \quad \frac{e_i^{n+1} - e_i^{n-1}}{2\Delta t} = u_i^n (S_u)_i^n, \quad (\text{A.18})$$

where $e = \frac{1}{2} u^2$, sub-script i denotes spatial location, and super-script n denotes time-level.

Comparing the finite difference analogs in Eqs. A.17 and A.18 illustrates that if we are interested in the energy principle implied by the finite difference analog in Eqs. A.17 we must multiply Eq. A.17 by $\hat{u}_i^n = \frac{1}{2}(u_i^{n+1} + u_i^{n-1})$:

$$\frac{\frac{1}{2}(u_i^{n+1})^2 - \frac{1}{2}(u_i^{n-1})^2}{2\Delta t} = \hat{u}_i^n (S_u)_i^n, \quad (\text{A.19})$$

as so doing yields a form consistent with Eq. A.18.

Terms in the TKE equations are estimated follows. At selected time-steps we collect the local tendencies due to advection, diffusion, pressure gradients and buoyancy. At every grid-point we also solve for the perturbation value of $(\widehat{u}^n)''$, $(\widehat{v}^n)''$, $(\widehat{w}^n)''$ by averaging over time-levels. We then solve for the covariance between the velocity components and tendency terms in the respective momentum equations thus yielding the contribution to the evolution of the TKE from each process. The decomposition of the advection term in to shear and transport terms is discussed below. Pressure correlations and buoyancy production terms can be calculated directly, while the dissipation term is calculated given K and D_{ij} and subtracted from the diffusive contribution to the TKE budget to yield the sub-grid transport term. Each term is calculated at its proper level, and then averaged to a w -point for plotting. This procedure guarantees that the contribution to the energy budgets actually reflect what is happening in the model. If we also calculate the storage of TKE we can calculate a residual, which is an amount of energy not accounted for in our calculations. Ideally this residual should be zero. In our budgets it takes on very small values, which are generally well correlated with the storage term. The source of this residual is two-fold: (i) energy calculations are not done every time-step (mostly because they are time-consuming); (ii) the finite difference analog to the continuous system does not conserve energy exactly.

A potential source of error in our TKE budgets is in our partitioning of the advection term into shear and turbulent transport components. There are two ways to do this, one can estimate the value of the turbulent flux of TKE and subtract it from the advection term, thereby leaving shear behind as a residual, or vica versa. It is difficult to make diagnostic approximations consistent with what is implied by the model solution of the advectin equation. Fortunately the value of the shear production term, which for the u component we approximate as

$$\frac{1}{2} \left\langle \widehat{u}_{i,k} \left[(w_{i,k} + w_{i+1,k}) \frac{\langle u \rangle_{k+1} - \langle u \rangle_k}{(\Delta z)_k} + (w_{i,k-1} + w_{i+1,k-1}) \frac{\langle u \rangle_k - \langle u \rangle_{k-1}}{(\Delta z)_{k-1}} \right] \right\rangle,$$

is not sensitive to the details of how the differences are taken.

Appendix B

MISCELLANEOUS DERIVATIONS

B.1 Saturation pressure level

Here we are interested in calculating how the saturation pressure, p_s , changes as a function of the predictive variables θ_l and q_t . Where the p_s is defined to be the height at which the saturation mixing ratio is equal to the total-water mixing ratio, q_t . The saturation mixing ratio

$$q_s = \frac{\epsilon e_s}{p_s - e_s}$$

where e_s is the saturation vapor pressure and $\epsilon = 0.608$ is the ratio of the molecular weights of water and air. q_s changes with height due to the expansional cooling of the parcel as it is lifted to levels of lower pressure. An implicit relation describing the level at which $q_s = q_t$ is:

$$p_s = e_s(T_s) \left[\frac{\epsilon}{q_t} + 1 \right]. \quad (\text{B.1})$$

Here e_s function of the temperature, T_s , at the saturation level. At the saturation level condensate just begins to form so $q_l = 0$ therefore from the first law of thermodynamics we can write

$$\theta_l = \theta = T_s \left(\frac{p_0}{p_s} \right)^\kappa, \quad (\text{B.2})$$

where $\kappa = 0.287$ is the ratio of the gas constant for air to the isobaric specific heat, and θ is the potential temperature (i.e., the temperature air assumes when adiabatically brought to a reference pressure $p_0 = 1000hPa$). In the limit of infinitesimal perturbations the following equation

$$\delta p_s = \delta e_s \left[\frac{\epsilon}{q_t} + 1 \right] - \frac{e_s \epsilon}{q_t} \frac{\delta q_t}{q_t} \quad (\text{B.3})$$

becomes exact.

Dividing Eq. B.3 by p_s ,

$$\frac{\delta p_s}{p_s} = \frac{\delta e_s}{e_s} - \frac{p_s - e_s}{p_s} \frac{\delta q_t}{q_t} \quad (\text{B.4})$$

using

$$\frac{\delta e_s}{e_s} = \frac{\epsilon L_v}{RT_s^2} e_s \delta T_s, \quad \text{and} \quad \delta T_s = \frac{\delta \theta_l}{\theta_l} T_s + \kappa T_s \frac{\delta p_s}{p_s}, \quad (\text{B.5})$$

which follow from Clausius-Clapeyron and the first-law respectively, results (after some simplification) in the following relation:

$$\frac{\delta p_s}{p_s} = \frac{1}{\frac{\epsilon L_v}{RT_s} \kappa - 1} \left[\frac{\delta q_t}{q_t} - \frac{\epsilon L_v}{RT_s} \frac{\delta \theta_l}{\theta_l} \right]. \quad (\text{B.6})$$

For typical boundary layer conditions (i.e., $T_s = 285$ K) the leading thermodynamic coefficient is approximately 0.25. Thus moistening or cooling leads to a relative raising of the saturation pressure level (i.e., cloud base descends) as is to be expected. Assuming hydrostatic pressure perturbations $\delta p_s = -g\rho\delta z_{lcl}$ and noting, from the discussion in appendix A.2, that $\delta \theta_l = -\frac{\partial F_\Theta}{\partial z} \delta t$ and $\delta q_t = -\frac{\partial F_Q}{\partial z} \delta t$ allows us to write our expression in the desired form:

$$w_{lcl} \approx -C_\Theta \frac{\partial F_\Theta}{\partial z} + C_Q \frac{\partial F_Q}{\partial z}, \quad (\text{B.7})$$

where

$$C_\Theta = \left(\frac{\frac{\epsilon L_v}{RT_s}}{\frac{\epsilon L_v}{RT_s} \kappa - 1} \right) \frac{p_s}{\rho^2 g \theta_l c_p}, \quad \text{and} \quad C_Q = \left(\frac{1}{\frac{\epsilon L_v}{RT_s} \kappa - 1} \right) \frac{p_s}{\rho^2 g q_t L_v}. \quad (\text{B.8})$$

For conditions typical of our experiments $\theta_l = 288$ K, $q_t = 10.2$ gkg⁻¹. This implies $p_s = 989.8$ hPa, $C_\Theta \approx 0.1$ and $C_Q \approx 0.06$.

B.2 Ventilative enhancement of droplet evaporation

Originally we used the analytically integrable form

$$\frac{dm}{dt} = C(p, T) \eta(t) \frac{m^{2/3}}{m^{1/3} + l_0} \quad (\text{B.9})$$

as the basis for describing how drops grow or shrink due to condensation or evaporation. Here $C(p, T)$ is a thermodynamic coefficient dependent on pressure p and temperature T , m is the mass of a drop, and l_0 is a lengthscale introduced to model gas-kinetic effects. The time-dependent function $\eta(t)$ is the difference between the saturation mixing ratio and the

water-vapor mixing ratio, when it is positive the drop mass increases due to condensation, when negative drops evaporate. When drops move relative to the air-stream fluxes of heat and vapor are more efficient and the following equation better describes their evolution in time:

$$\frac{dm}{dt} = C(p, T)\eta(t) \frac{m^{2/3}}{m^{1/3} + l_0} \overline{f_v(m)}, \quad (\text{B.10})$$

where $f_v(m)$ is an empirically determined factor which multiplies the growth equation. Following Pruppacher and Klett (1978) we write

$$\overline{f_v(m)} = \begin{cases} 1.00 + 0.1(N_{sc}^{1/3} N_{re}^{1/2})^2 & N_{re} \leq 2 \\ 0.75 + 0.3(N_{sc}^{1/3} N_{re}^{1/2}) & N_{re} > 2, \end{cases} \quad (\text{B.11})$$

where N_{sc} is the Schmidt number (the ratio of kinematic viscosity to diffusivity) and $N_{re} = \frac{u_\infty d}{\nu}$ is the Reynolds number—here u_∞ is the drop terminal velocity, ν is viscosity and d is drop diameter. Because u_∞ is a function only of mass, $\overline{f_v}$ only has a mass dependence.

In our microphysical parameterization drops are organized into 25 size-categories (or bins), with mass-doubling between bins. The smallest mass represented is 16 pg, and the largest is about 0.5 mg. It turns out that $\overline{f_v}$ doesn't become significantly larger than unity until drops reach bin 15 (approximately 262 ng). Drops rarely reach the upper-size limit for which $\overline{f_v} \approx 6$. Clearly in heavily precipitating situations the inclusion of ventilation effects may be important. For $N_{re} \leq 2$ drop terminal velocities are well described by Stokes flow so that $N_{re} \propto m$, drops larger than this size, but smaller than the largest drop represented by the model are well described by $N_{re} \propto m^{2/3}$, which implies that

$$\overline{f_v(m)} = \begin{cases} c_1 + c_2 m & N_{re} \leq 2 \\ c_3 + c_4 m^{1/3} & N_{re} > 2, \end{cases} \quad (\text{B.12})$$

with c_i being a positive constant. Unfortunately, solutions of Eq. B.10 for $m(t)$ using the above forms for $\overline{f_v(m)}$ taken an implicit form which must be iteratively solved. Alternatively Eq. B.10 may be numerically integrated, or approximated such that its integrals are simple analytic expressions.

The nature of our semi-lagrangian condensation/evaporation scheme (Stevens et al., 1996) requires us to find how large or small drops will grow or evaporate under a given

forcing. Each bin is solved for individually. This means that Eq. B.10 must only be solved locally. Consequently linearizing the integrand, or assuming mass to be constant in part of the expression, may generate approximate expressions for $m(t + \Delta t)$ whose accuracy is reasonably good. After some experimentation¹ it was found that for our purposes Eq. B.10 is well approximated by assuming $\overline{f_v}(m) = \overline{f_v}(m_k)$ for $m \in [m_k, m_{k+1}]$. This means that the analytic form of our solution to the drop growth equation without ventilation effects must only be multiplied by a constant factor which depends on the drop bin in which the drop originally resides.

In other words, sufficiently good accuracy is obtained by neglecting the change in the ventilation effect experienced by a drop during a single timestep. Such an approximation is consistent with the calculation of the mean supersaturation over the timestep, where it is assumed that the integral radius of the droplet spectrum is given by its value at the beginning of the timestep.

¹The work described in the appendix was carried out jointly with Graham Feingold, the experimentation described here was his however.

Bibliography

- Albrecht, B. A., 1989: Aerosols, cloud microphysics and fractional cloudiness. *Science*, **245**, 1227–1230.
- Albrecht, B. A., A. K. Betts, W. H. Schubert, and S. K. Cox, 1979: A model of the thermodynamic structure of the trade-wind boundary layer. Part I: Theoretical formulation and sensitivity tests. *Journal of Atmospheric Sciences*, **36**, 90–98.
- Aldrich, F., 1919: The reflecting power of clouds. *Smithsonian Misc. Coll.*, **69**(10).
- American Meteorological Society, 1952: Bibliography on stratus forecasting. *Meteorological Abstracts and Bibliography*, **3**(6), 575.
- Anderson, J. B., 1931: Observations from airplanes of cloud and fog conditions along the Southern Californian coast. *Monthly Weather Review*, **59**, 264–270.
- Austin, P., Y. Wang, R. Pincus, and V. Kujala, 1995: Precipitation in stratocumulus clouds: Observational and modeling results. *Journal of Atmospheric Sciences*, **52**, 2329–2352.
- Baker, M., 1990: Bistability of ccn concentrations and thermodynamics in the cloud topped boundary layer. *Nature*, **345**, 142–145.
- Blake, D., 1928: Temperature inversions at San Diego, as deduced from aerographical observations by airplane. *Monthly Weather Review*, **56**, 221–224.
- Blake, D., 1933: Remarkably low humidities aloft over San Diego, Calif. *Monthly Weather Review*, **61**, 170.
- Blake, D., 1934: Further conclusions from additional observations in the free air over San Diego, Calif. *Monthly Weather Review*, **62**, 195–199.

- Bougeault, P., 1985: The diurnal cycle of the marine stratocumulus layer: A higher-order model study. *Journal of Atmospheric Sciences*, **42**, 2826–2843.
- Bowen, E. G., 1952: The formation of rain by coalescence. *Australian Journal of Scientific Research, Series A, Physical Sciences*, **3**, 1913–213.
- Bowie, E. H., 1933: The summer nighttime clouds of the Santa Clara valley, Calif. *Monthly Weather Review*, **61**, 40–41.
- Bowman, J. C., 1996: On inertial-range scaling laws. *Journal of Fluid Dynamics*, **306**, 167–181.
- Breidenthal, R. E. and M. B. Baker, 1985: Convection and entrainment across stratified interfaces. *Journal of Geophysical Research*, **90D**, 13055–13062.
- Bretherton, C. S., 1992: A conceptual model of the stratocumulus-trade-cumulus transition in the subtropical oceans. *Proc., 11th Int. Conf. on Clouds and Precipitation, Elsevier Science Publishers*, **50**, 374–377.
- Bretherton, C. S., 1993: Understanding Albrecht's model of trade cumulus cloud fields. *Journal of Atmospheric Sciences*, **50**, 2264–2283.
- Bretherton, C. S. and M. C. Wyant, 1996: Moisture transport, lower tropospheric stability, and decoupling of cloud-topped boundary layers. *Journal of Atmospheric Sciences in press*.
- Bretherton, C. S. and R. Pincus, 1995a: Cloudiness and marine boundary layer dynamics in the ASTEX Lagrangian experiments. part I: Synoptic setting and vertical structure. *Journal of Atmospheric Sciences*, **52**, 2707–2723.
- Bretherton, C. S., P. Austin, and S. T. Siems, 1995b: Cloudiness and marine boundary layer dynamics in the ASTEX lagrangian experiments. part II: Cloudiness, drizzle, surface fluxes, and entrainment. *Journal of Atmospheric Sciences*, **52**, 2724–2735.
- Brost, R. A., D. H. Lenschow, and J. C. Wyngaard, 1982a: Marine stratocumulus layers. Part I: Mean conditions. *Journal of Atmospheric Sciences*, **39**, 800–817.

- Brost, R. A., J. C. Wyngaard, and D. H. Lenschow, 1982b: Marine stratocumulus layers. Part II: Turbulence budgets. *Journal of Atmospheric Sciences*, **39**, 818–836.
- Caughey, S. J., B. A. Crease, and W. T. Roach, 1982: A field study of nocturnal stratocumulus: II. entrainment and turbulence. *Quarterly Journal of the Royal Meteorological Society*, **108**, 125–144.
- Charnock, H., 1955: Wind stress on a water surface. *Quarterly Journal of the Royal Meteorological Society*, **81**, 639.
- Chen, A., 1996: Studies of stratocumulus cloud, drizzle and aerosol interactions. *Atmospheric Science Department Paper*, No. 603, Colorado State University, Ft. Collins, CO 80523 USA, 101 pp.
- Chen, C. and W. R. Cotton, 1987: The physics of the marine stratocumulus-capped mixed layer. *Journal of Atmospheric Sciences*, **44**, 2951–2977.
- Cotton, W. R. and R. A. Anthes, 1989: *Storm and Cloud Dynamics*. Academic Press Inc, San Diego, 883 pp.
- Cotton, W. R., B. Stevens, and S. Nebuda, 1995: A question of balance—simulating microphysics and dynamics. *Proceedings Conference on Cloud Physics, January 15-20 Dallas, Texas* 484–486.
- Deardorff, J. W., 1970: A numerical study of three-dimensional turbulent channel flow at large Reynolds numbers. *Journal of Fluid Dynamics*, **41**, 453–480.
- Deardorff, J. W., 1976: Usefulness of liquid-water-potential temperature in a shallow-cloud model. *Journal of Applied Meteorology*, **15**, 98–102.
- Deardorff, J. W., 1980b: Stratocumulus-capped mixed layers derived from a three-dimensional model. *Boundary Layer Meteorology*, **18**, 495–527.
- Deardorff, J. W., 1980a: Cloud top entrainment instability. *Journal of Atmospheric Sciences*, **37**, 131–147.

- Durran, D. R., 1989: Improving the anelastic approximation. *Journal of Atmospheric Sciences*, **46**, 1453–1461.
- E, X. and E. J. Hopfinger, 1986: On mixing across a interface in stably stratified fluid. *Journal of Fluid Dynamics*, **166**, 227–244.
- Feingold, G., B. Stevens, W. R. Cotton, and A. S. Frisch, 1996a: The relationship between drop in-cloud residence time and drizzle production in numerically simulated stratocumulus clouds. *Journal of Atmospheric Sciences*, **53**, 1108–1122.
- Feingold, G., R. Boers, B. Stevens, and W. R. Cotton, 1996b: A modelling study of the effect of drizzle on cloud optical depth and susceptibility. *Journal of Geophysical Research submitted*.
- Frith, R., 1951: The size of cloud particles in stratocumulus cloud. *Quarterly Journal of the Royal Meteorological Society*, **77**, 441–444.
- Gunn, R. and G. D. Kinzer, 1949: The terminal velocity of fall for water drops in stagnant air. *Journal of Meteorology*, **6**, 243–248.
- Hall, W. D., 1980: A detailed microphysical model within a two-dimensional dynamical framework: Model description and preliminary results. *Journal of Atmospheric Sciences*, **37**, 2486–2507.
- James, D. G., 1955: Nocturnal dissipation of stratocumulus cloud. *Meteorological Magazine*, **8**, 202–208.
- James, D. G., 1959: Observations from aircraft of temperatures and humidities near stratocumulus clouds. *Quarterly Journal of the Royal Meteorological Society*, **85**, 120–130.
- Johnson, D. B., 1982: The role of giant and ultragiant aerosol particles in warm rain initiation. *Journal of Atmospheric Sciences*, **39**, 448–460.
- Jones, R. F., 1951: Rain from non freezing clouds. *Meteorological Magazine*, **80**, 273–274.

- Klein, S. A. and D. L. Hartmann, 1993: The seasonal cycle of low stratiform clouds. *Journal of Climate*, **6**, 1587–1606.
- Krasner, R. D., 1993: The diurnal precipitation change over the sea. *Atmospheric Science Department Paper*, No. 528, Colorado State University, Ft. Collins, CO 80523 USA.
- Kraus, E. B., 1963: The diurnal precipitation change over the sea. *Journal of Atmospheric Sciences*, **20**, 551–556.
- Kraus, H. and E. Schaller, 1978: A note on the closure in Lilly-type inversion models. *Tellus*, **30**, 284–488.
- Krueger, S. K., 1985: *Numerical Simulation of Tropical Cumulus Clouds and Their Interaction with the Subcloud Layer*. Ph.D. dissertation, University of California at Los Angeles, Los Angeles California, USA, 205 pp.
- Krueger, S. K., G. T. McLean, and Q. Fu, 1995a: Numerical simulation of stratus-to-cumulus transition in the subtropical marine boundary layer. Part I: Boundary layer structure. *Journal of Atmospheric Sciences*, **52**, 2839–2850.
- Krueger, S. K., G. T. McLean, and Q. Fu, 1995b: Numerical simulation of stratus-to-cumulus transition in the subtropical marine boundary layer. Part II: Boundary layer circulation. *Journal of Atmospheric Sciences*, **52**, 2851–2868.
- Lilly, D., 1962: On the numerical simulation of buoyant convection. *Tellus*, **14**, 148–172.
- Lilly, D., 1967: The representation of small-scale turbulence in numerical simulation experiments. *Proceedings IBM Scientific Computing Symposium on Environmental Sciences*, H.H. Goldstine Editor, IBM Form No. 320-1951., 195–210.
- Lilly, D. K., 1968: Models of cloud topped mixed layers under a strong inversion. *Quarterly Journal of the Royal Meteorological Society*, **94**, 292–309.
- Long, A. B., 1974: Solutions to the droplet coalescence equation for polynomial kernels. *Journal of Atmospheric Sciences*, **31**, 1040.

- Louis, J. F., 1979: A parametric model of vertical eddy fluxes in the atmosphere. *Boundary Layer Meteorology*, **17**, 187–202.
- Luckiesh, M., 1919: Aerial photometry. *Astrophysical Journal*, **49**, 108–130.
- Martin, G. M., D. W. Johnson, D. P. Rogers, P. R. Jonas, P. Minnis, and D. A. Hegg, 1995: Observations of the interaction between cumulus clouds and warm stratocumulus clouds in the marine boundary layer during astex. *Journal of Atmospheric Sciences*, **52**, 2902–2922.
- Mason, B. J., 1952: Production of rain and drizzle by coalescence in stratiform clouds. *Quarterly Journal of the Royal Meteorological Society*, **78**, 377–386.
- Mason, B. J., 1960: The evolution of droplet spectra in stratus cloud. *Journal of Meteorology*, **17**, 459–462.
- Mason, B. J. and B. P. Howarth, 1952: Some characteristics of stratiform clouds over North Ireland in relation to their precipitation. *Quarterly Journal of the Royal Meteorological Society*, **78**, 226–230.
- Mason, P., 1994: Large eddy simulations: A critical review of the technique. *Quarterly Journal of the Royal Meteorological Society*, **120**, 1–26.
- Moeng, C.-H., 1986: Large eddy simulation of a stratus-topped boundary layer. part i: Structure and budgets. *Journal of Atmospheric Sciences*, **43**, 2886–2900.
- Moeng, C.-H. and A. Arakawa, 1980: A numerical study of a marine subtropical stratus cloud layer and its stability. *Journal of Atmospheric Sciences*, **37**, 2661–2676.
- Moeng, C.-H. and P. P. Sullivan, 1994: A comparison of shear and buoyancy-driven planetary boundary layers. *Journal of Atmospheric Sciences*, **51**, 999–1022.
- Moeng, C.-H., W. R. Cotton, C. S. Bretherton, A. Chlond, M. Khairoutdinov, S. Krueger, W. Lewellan, M. K. MacVean, J. Pasquier, H. A. Rand, A. P. Siebesma, , B. Stevens, and R. I. Sykes, 1996: Simulation of a stratocumulus-topped pbl: Intercomparison

- among different numerical codes. *Bulletine of the American Meteorological Society*, **77**, 261–278.
- Neiburger, M., 1944: Temperature changes during formation and dissipation of west coast stratus. *Journal of Meteorology*, **1**, 29–41.
- Neiburger, M., 1949: Reflection, absorption, and transmission of insolation by stratus cloud. *Journal of Meteorology*, **6**, 98–104.
- Nicholls, S., 1984: The dynamics of stratocumulus: Aircraft observations and comparisons with a mixed layer model. *Quarterly Journal of the Royal Meteorological Society*, **110**, 783–820.
- Nicholls, S., 1987: A model of drizzle growth in warm, turbulent, stratiform clouds. *Quarterly Journal of the Royal Meteorological Society*, **113**, 1141–1170.
- Nicholls, S., B. Brümmer, F. Flenler, A. Grant, T. Hauf, G. Jenkins, C. Readings, and W. Shaw, 1983: The structure of the turbulent atmospheric boundary layer. *Philosophical Transactions of the Royal Society, London A*, **308**, 291–309.
- Noonkester, V. R., 1984: Droplet spectra observed in marine stratus cloud layers. *Journal of Atmospheric Sciences*, **41**, 829–841.
- Ogura, Y. and N. A. Phillips, 1962: Scale analysis of deep and shallow convection in the atmosphere. *Journal of Atmospheric Sciences*, **19**, 173–179.
- Paluch, I. R. and D. H. Lenschow, 1991: Stratiform cloud formation in the marine boundary layer. *Journal of Atmospheric Sciences*, **48**, 2141–2157.
- Pielke, R. A., W. R. Cotton, R. L. Walko, C. J. Tremback, W. A. Lyons, L. D. Grasso, M. E. Nicholls, M. D. Moran, D. A. Wesley, T. J. Lee, and J. H. Copeland, 1992: A comprehensive meteorological modeling system — RAMS. *Meteor. Atmos. Phys.*, **49**, 69–91.
- Pincus, R. and M. B. Baker, 1994: Effect of precipitation on the albedo susceptibility of marine boundary layer clouds. *Nature*, **372**, 250–252.

- Pruppacher, H. R. and J. D. Klett, 1978: *Microphysics of Clouds and Precipitation*. D. Reidel, Dordrecht Holland, 714 pp.
- Randall, D. A., 1980: Conditional instability of the first kind upside-down. *Journal of Atmospheric Sciences*, **37**, 125–130.
- Randall, D. A. and M. J. Suarez, 1984: On the dynamics of stratocumulus formation and dissipation. *Journal of Atmospheric Sciences*, **41**, 3052–3057.
- Randall, D. A., B. A. Albrecht, S. K. Cox, D. Johnson, P. Minnis, W. Rossow, and D. O. Starr, 1996: On FIRE at ten. *Advances in Geophysics*, **38**, 37–177.
- Riehl, H., 1954: *Tropical Meteorology*. McGraw-Hill, New York, 392 pp.
- Roach, W. T., R. Brown, S. J. Caughey, and B. A. C. and A. Slingo, 1982: A field study of nocturnal stratocumulus: I. mean structure and turbulent budgets. *Quarterly Journal of the Royal Meteorological Society*, **108**, 103–123.
- Schubert, W. H., 1976: Experiments with Lilly's cloud-topped mixed layer model. *Journal of Atmospheric Sciences*, **33**, 436–446.
- Schubert, W. H., J. S. Wakefield, E. J. Steiner, and S. K. Cox, 1979: Marine stratocumulus convection. part I: Governing equations and horizontally homogeneous solutions. *Journal of Atmospheric Sciences*, **36**, 1286–1307.
- Shettle, E. P. and R. W. Fenn, 1979: Models for the aerosols of the lower atmosphere and the effects of humidity variations on their optical properties. *Technical Report, Air Force Geophysics Laboratory, AFGL-TR-79-0214*, 94 pp.
- Slingo, A., R. Brown, and C. L. Wrench, 1982: A field study of nocturnal stratocumulus: III. high resolution radiative and microphysical observations. *Quarterly Journal of the Royal Meteorological Society*, **108**, 145–165.
- Smolarkiewicz, P. K. and W. W. Grabowski, 1990: The multi-dimensional positive definite advection transport algorithm: Non-oscillatory option. *Journal of Computational Physics*, **86**, 355–375.

- Spiegel, E. A. and G. Veronis, 1960: On the Boussinesq approximation for a compressible fluid. *Astrophys. J.*, **131**, 442–447.
- Stevens, B., G. Feingold, W. R. Cotton, and R. L. Walko, 1996a: Elements of the microphysical structure of numerically simulated nonprecipitating stratocumulus. *Journal of Atmospheric Sciences*, **53**, 980–1007.
- Stevens, B., R. L. Walko, W. R. Cotton, and G. Feingold, 1996b: The spurious production of cloud-edge supersaturation by eulerian models. *Monthly Weather Review*, **124**, 1034–1041.
- Stull, R., 1976: The energetics of entrainment across a density interface. *Journal of Atmospheric Sciences*, **33**, 1260–1267.
- Tremback, C., J. Powell, W. R. Cotton, and R. A. Pielke, 1987: The forward in time upstream advection scheme: Extension to higher orders. *Monthly Weather Review*, **115**, 3540–555.
- Turner, J. S., 1968: The influence of molecular diffusivity on turbulent entrainment across a density interface. *Journal of Fluid Dynamics*, **33**, 639–656.
- Turton, J. D. and S. Nicholls, 1987: A study of the diurnal variation of stratocumulus using a multiple mixed layer model. *Quarterly Journal of the Royal Meteorological Society*, **113**, 969–1009.
- Tvivion, S., G. Feingold, and Z. Levin, 1987: An efficient numerical solution to the stochastic collection equation. *Journal of Atmospheric Sciences*, **44**, 3139–3149.
- Tvivion, S., G. Feingold, and Z. Levin, 1989: The evolution of rain-drop spectra. part ii: Collisional collection/breakup and evaporation in a rain shaft. *Journal of Atmospheric Sciences*, **46**, 3312–3327.
- Twomey, S. A., 1974: Pollution and the planetary albedo. *Atmospheric Environment*, **8**, 1251–1256.

- Twomey, S. A., 1977: The influence of pollution on the shortwave albedo of clouds. *Journal of Atmospheric Sciences*, **34**, 1149–1152.
- Vernon, E. M., 1936: The diurnal variation in ceiling height beneath stratus clouds. *Monthly Weather Review*, **64**, 14–16.
- Wang, S., 1993: Modeling marine boundary-layer clouds with a two-layer model: A one dimensional simulation. *Journal of Atmospheric Sciences*, **50**, 4001–4021.
- Wang, S. and B. A. Albrecht, 1986: A stratocumulus model with an internal circulation. *Journal of Atmospheric Sciences*, **43**, 2374–2390.
- Wang, S. and Q. Wang, 1994: Roles of drizzle in a one-dimensional third-order turbulence closure model of the nocturnal stratus-topped marine boundary layer. *Journal of Atmospheric Sciences*, **51**, 1559–1576.
- Wyant, M. C., C. S. Bretherton, H. A. Rand, and D. E. Stevens, 1996: Numerical simulations and a conceptual model of the stratocumulus to trade cumulus transition. *Journal of Atmospheric Sciences in press*.
- Zalesak, S. T., 1979: Fully multidimensional flux-corrected transport algorithms for fluids. *Journal of Computational Physics*, **31**, 335–362.